2011

Sensitivity of Neutron Star Properties to the Equation of State

Farrooh Fattoyev

THE FLORIDA STATE UNIVERSITY

COLLEGE OF ARTS AND SCIENCES

SENSITIVITY OF NEUTRON STAR PROPERTIES TO THE EQUATION OF STATE

By

FARROOH FATTOYEV

A Dissertation submitted to the
Department of Physics
in partial fulfillment of the
requirements for the degree of
Doctor of Philosophy

Degree Awarded:
Fall Semester, 2011

Farrooh Fattoyev defended this dissertation on October 18, 2011.

The members of the supervisory committee were:

Jorge Piekarewicz
Professor Directing Dissertation

Paolo Aluffi
University Representative

Simon Capstick
Committee Member

Joseph F. Owens, III
Committee Member

Grigory Rogachev
Committee Member

The Graduate School has verified and approved the above-named committee members, and certifies that the dissertation has been approved in accordance with the university requirements.

To my lovely family

ACKNOWLEDGMENTS

Foremost, I would like to express my deepest gratitude to my advisor, Professor Jorge Piekarewicz, for his guidance and support throughout my PhD studies at the Florida State University. His patience, enthusiasm and immense knowledge has helped me enormously in improving my research skills as a scientist. Whenever I needed a discussion or an advice, he was always ready to offer me thoughtful insights in an articulate manner. I feel very fortunate to have had the opportunity to work with such a wonderful, supportive advisor who cares about the success of his students in research and in life.

Next, my thanks go to my dissertation committee members, Professors Paolo Aluffi, Simon Capstick, Jeff Owens and Grigory Rogachev. I am very much indebted for their careful reading of the original version of this dissertation and for their helpful suggestions and comments.

I am grateful to Karim Hasnaoui and Wei-Chia Chen for numerous discussions we had on my research. A special thanks to Karim for helping me generate figures 6.2 and 6.3.

I am thankful to Professor Bobomurat Ahmedov at the Institute of Nuclear Physics, Tashkent, Uzbekistan for his tremendous encouragement and support in my work for all these years. While visiting my home country, he has always provided me with the scientific environment and the computing facilities to continue my research.

I would like to extend my appreciation to my friends Ben Eakins and Mukesh Saini for providing suggestions and comments on parts of my dissertation.

I am thankful to all of my other friends at FSU, especially to Shaojie Yuan, Daniel Santiago, Melina Avila, Jorge Barreda, Diana Florez, Brendan Diamond, Tiara Diamond, Judy Cherian, Naureen Ahsan, Olga Abramkina, and Ahmet Emin Tatar, for their friendship and support. I could always turn to them whenever there was a need.

Last, and most importantly, I would like to thank my family for all their love and encouragement. I am thankful for my mother who has raised me with a love of poetry and geometry in my early childhood, for my father who brought me into the world of solving puzzles in mathematics and physics, for my brothers and my sisters, who have always believed in me and shared my aspirations. I owe them my gratitude for their whole-hearted support in my pursuits. And most of all, I am much indebted to my dearest wife Zebo for her love, support, and encouragement. Without her love and continued support I could not survive the years of my graduate studies. She has, single-handedly, done so much in raising our kids Aziz and Farid, while constantly encouraged me to work hard to accomplish my projects. I cannot thank her enough!

TABLE OF CONTENTS

LIST OF TABLES

LIST OF FIGURES

LIST OF SYMBOLS

The following is a list of mathematical symbols representing physical constants and physical quantities that are used throughout this dissertation.

$\hbar \cdot c$	Conversion constant, $\hbar \cdot c = 197.3269631(49)$ MeV fm
G	Gravitational constant, $G = 6.67384(80) \times 10^{-11}$ m^3 kg^{-1} s^{-2}
M	Mass of nucleon, $M = 939$ MeV (Same symbols is also used for the total stellar mass)
$M_{\rm Sun}$	One solar mass, $M_{\rm Sun} = 1.98892 \times 10^{30}$ kg
$\boldsymbol{\tau}$	The Pauli matrices
$\mathcal{L}_0$	Free non-interacting Lagrangian density
$\mathcal{L}_{\rm int}$	Interacting Lagrangian density
$g_{\rm s}$	The scalar-isoscalar Yukawa coupling constant
$g_{\rm v}$	The vector-isoscalar Yukawa coupling constant
g_δ	The scalar-isovector Yukawa coupling constant
g_ρ	The vector-isovector Yukawa coupling constant
κ	The cubic nonlinear scalar-isoscalar self interaction coupling constant
λ	The quartic nonlinear scalar-isoscalar self interaction coupling constant
ζ	The quartic nonlinear vector-isoscalar self interaction coupling constant
$\Lambda_{\rm v}$	The quartic mixed isoscalar-isovector interaction coupling constant
ψ	The isodoublet nucleon (proton and neutron) field
ϕ	The scalar-isoscalar meson field
V_μ	The vector-isocalar meson field
$\boldsymbol{\delta}$	The scalar-isovector meson field
$\mathbf{b}_\mu$	The vector-isovector meson field
A	Total number of baryons
Z	Total number of protons
$Y_{\rm p}$	Proton fraction
$\rho_{\rm s}$	The scalar density
$\rho_{\rm v}$	The vector (or the baryon) density
$k_{\rm F}$	Fermi momentum
$T_{\mu\nu}$	Energy-momentum tensor
$g_{\mu\nu}$	Metric tensor
$R_{\mu\nu}$	Riemann tensor
R	Ricci scalar (Same symbol is also used for the stellar radius)
Ω	Stellar frequency
ω	Lense-Thirring frequency

$\mathcal{E}$	Energy density
P	Pressure
μ_i	Chemical potential for species i
M^*	The effective nucleon mass
ϵ_0	Binding energy for symmetric nuclear matter at saturation
K_0	Compression modulus or the incompressibility coefficient for symmetric nuclear matter
Q_0	Skewness parameter for symmetric nuclear matter
α	Asymmetry parameter
S	Symmetry energy
J	Symmetry energy at saturation (Also used rarely as the total angular momentum)
$\tilde{J}$	Symmetry energy at $k_{\mathrm{F}} = 1.15$ fm^{-1}
L	Density slope of the symmetry energy
K_{sym}	The density curvature of the symmetry energy
$R_{1.4}$	The radius of 1.4 solar mass neutron star
M_{max}	Maximum mass of a neutron star
z	Gravitational redshift
I	The moment of inertia
F_{Edd}	Eddington flux
$R_{\mathrm{n,p}}$	Neutron and proton radius of the nucleus
$R_{\mathrm{n}} - R_{\mathrm{p}}$	Neutron skin of the nucleus

ABSTRACT

The subject of this doctoral dissertation is to study the equations of state of nuclear and neutron-star matter. We tackle this problem by employing several models of the relativistic effective interactions. The relativistic effective interactions and their applications to the ground-state properties of medium to heavy nuclei have enjoyed enormous success for the past three decades. With just a few model parameters calibrated to the ground state properties of the closed-shell nuclei, these models exhibit and encode a great amount of physics. However, theses models are untested far away from their narrow window of applicability. In particular, while these models tend to agree on the saturation properties of symmetric nuclear matter, they largely disagree on its density and isospin dependence, especially in the region of high densities and large proton-neutron asymmetries. In order to better understand the properties of nuclear matter at these extreme regions of isospin asymmetry and high-densities, we will apply these models to predict several neutron star properties. Since the matter in the neutron stars are very neutron-rich, while the density of matter in neutron stars spans over a wide range of magnitudes, these compact objects remain unique laboratories for probing the equation of state of neutron-rich matter under conditions unattainable by terrestrial experiments. Thus it is expected that at least the following neutron star properties must be sensitive to the underlying equation of state: maximum mass, typical radii, moments of inertia (both total and crustal), redshifts, and cooling mechanism. We present numerical solutions and in some cases also analytical solutions to each of the properties above.

In particular, the sensitivity of the stellar moment of inertia to the neutron-star matter equation of state is examined using accurately-calibrated relativistic mean-field models. We probe this sensitivity by tuning both the density dependence of the symmetry energy and the high density component of the equation of state, properties that are at present poorly

constrained by existing laboratory data. Particularly attractive is the study of the fraction of the moment of inertia contained in the solid crust. Analytic treatments of the crustal moment of inertia reveal a high sensitivity to the transition pressure at the core-crust interface.

Motivated by a recent astrophysical measurement of the pressure of cold matter above nuclear-matter saturation density, we compute the equation of state of neutron-star matter using various accurately calibrated relativistic models. We found the predictions of these models to be in fairly good agreement with the measured equation of state. In the effort to explain the observational data we introduce a new relativistic effective interaction that is simultaneously constrained by the properties of finite nuclei, their collective excitations, and neutron-star properties. By adjusting two of the empirical parameters of the theory, one can efficiently tune the neutron skin thickness of ^{208}Pb and the maximum neutron star mass. The new effective interaction is moderately soft at intermediate densities and relatively stiff at high densities. It is fitted to a neutron skin thickness in ^{208}Pb of only $R_{\rm n} - R_{\rm p} = 0.16$ fm and a moderately large maximum neutron star mass of 1.94 $M_{\rm Sun}$ consistent with the latest observation.

Last, theoretical uncertainties in the predictions of relativistic mean-field models are estimated using a chi-square minimization procedure that is implemented by studying the small oscillations around the chi-square minimum. It is shown that such statistical analysis provides access to a wealth of information that would normally remain hidden. The power of covariance analysis is illustrated in two relativistic mean field models. By performing this analysis one obtains meaningful theoretical uncertainties for both model parameters and predicted observables. Moreover, it is shown, how covariance analysis is able to establish robust correlations between physical observables.

CHAPTER 1

INTRODUCTION

The quest for the Holy Grail of Nuclear Physics, the equation of state of hadronic matter, remains an area of intense activity that cuts across a variety of disciplines. Indeed, the limits of nuclear existence, the dynamics of heavy-ion collisions, the structure of neutron stars, and the collapse of massive stellar cores all depend sensitively on the equation of state. With the advent and commissioning of sophisticated new radioactive beam facilities (HIE-ISOLDE at CERN, SPIRAL-2 at GANIL, TRIUMF in Canada, RIKEN in Japan, FAIR at GSI, and FRIB at MSU), powerful heavy-ion colliders (RHIC at Brookhaven National Lab, LHC at CERN), telescopes operating at a variety of wavelengths (Hubble, Spitzer and Chandra space telescopes at NASA, Subaru telescope in Japan), and more sensitive gravitational wave detectors (LIGO, Virgo, Advanced LIGO), one will be able to probe the nuclear dynamics over a wide range of nucleon asymmetries, temperatures, and densities. In this dissertation work, we focus on the dynamics of cold matter at extreme densities and isospin asymmetries (both small and large), and for this case neutron stars remain the tool of choice [1, 2, 3]. The densities inside neutron stars span orders of magnitudes ranging from a few g cm^{-3} at the surface to more than 10^{15} g cm^{-3} at their deep interior [4]. The pressure at the center of neutron stars is about 10^{36} dyn cm^{-2}, which is 30 orders of magnitude larger than the atmospheric pressure on the surface of the Earth. Being very compact (with a typical radius of $\sim$ 10 km and mass of $\sim$ 1.4 solar masses) and extremely dense, neutron stars are unique laboratories for probing the equation of state of neutron-rich matter under conditions unattainable by terrestrial experiments.

The structure of neutron stars sensitively depends on the equation of state. The physics used to calculate the equation of state changes as one moves from the surface of the neutron

star towards its center. At low densities atomic and plasma physics play an important role, while at the deep interior the nuclear many-body physics becomes essential. The physics at the very center of the neutron stars is still not well known and remains one of the main mysteries even today. We mainly concentrate on the study of the equations of state that describe the core of the neutron stars. At present, the existing *realistic* equations of state for neutron-star matter can be categorized into three classes: (1) non-relativistic many body calculations based on two or three nucleon interactions; (2) relativistic mean-field approximations; (3) the equations of state of strange quark matter. The equations of state from the first and second class can be used to calculate the structure of *neutron stars*—stars that are bound by the gravitational pull. It has been suggested that the strange quark matter could be the ultimate ground state of matter [5, 6], i.e. the binding energy for such matter is lower than that of ^{56}Fe at zero temperature. If this is the case, at high densities the whole star would be virtually converted into strange quark matter through a phase transition. The strange stars formed this way would be self-bound as opposed to the gravitationally bound neutron stars. However in most cases, based on their observational characteristics like their masses, radii, moment of inertia, *etc.*, strange stars are indistinguishable from neutron stars. The third class of the equations of state are motivated based on these assumptions. Moreover, there are several *unrealistic* polytropic equations of state that are widely used to study the effect of the gravitational field on the electrodynamic processes and on the structure of the neutron stars. Although there are numerous equations of state in the literature underlying each of the classes mentioned above, our main focus will be on the relativistic mean field approximations [7, 8, 9, 10]. Our equations of state are based on realistic nucleon-nucleon interactions mediated through meson fields. We do not employ any exotic degrees of freedom such as hyperons, kaon condensates, or quark matter, whose presence in dense matter is currently unknown.

The two most important properties of neutron stars—their typical *radii* and *maximum masses*—are still not well known [3, 11, 12, 13]. The neutron star radius is sensitive to the equation of state near the saturation density. In particular, the radius is very sensitive to the density dependence of the symmetry energy, a property of the nuclear matter that will be one of the central points of the discussions in this dissertation. Despite this sensitivity, the radius

is the least constrained property of the neutron star. Current observational precision for the typical neutron star radii lies in the range of 10 to 12 km [11, 12]. On the other hand, the maximum mass of the neutron star is sensitive to the high density domain of the equation of state. The notion of the maximum mass comes from the application of general relativity and has no counterpart in Newtonian gravity. At the moment of this writing, the most precise measurement for the maximum mass of a neutron star is 1.97 ± 0.04 solar masses [13]. Current accurately-calibrated relativistic mean-field models [14, 15] describe well the binding energies and charge radii of medium to heavy nuclei, however their predictions for the maximum neutron star mass differ by up to one solar mass [16]. The large difference in the prediction is a manifestation of the *stiffness* of the equations of state at high densities. As we will show in this work, the maximum mass of the neutron star is controlled by the stiffness of the equation of state. In Fig. 1.1, we provide the representative set of neutron stars whose masses have been measured with high accuracy. However, for the same neutron stars the radii are not well known. One of the other most important prediction of the equation of state is the mass-radius relation of neutron stars. A set of the equations of state used to generate such a relation is shown in Fig. 1.2. As it is evident from this figure, an accurate, simultaneous mass and radius measurement from even a single neutron star would significantly constrain the equation of state [17].

In addition to the masses and radii, computing the stellar moment of inertia of the neutron stars is also very interesting. This is due to the fact that the moment of inertia scales as the mass of the neutron star times the square of its radius. A full general relativistic expression for the moment of inertia is complicated and it is discussed in detail in Chapter 4. This feature makes it particularly sensitive to the density dependence of the symmetry energy. While the ground state masses and charge radii constrain the symmetry energy near the saturation density, its density dependence is very poorly constrained. Understanding the density dependence of the symmetry energy is of topical interest in both nuclear physics and nuclear astrophysics. The symmetry energy determines the increase in the energy of nuclear matter as one moves away from equal number of protons and neutrons. From the nuclear context, the symmetry energy should play an important role in the properties of nuclei far from the valley of stability. From the astrophysical context, it is the equation of

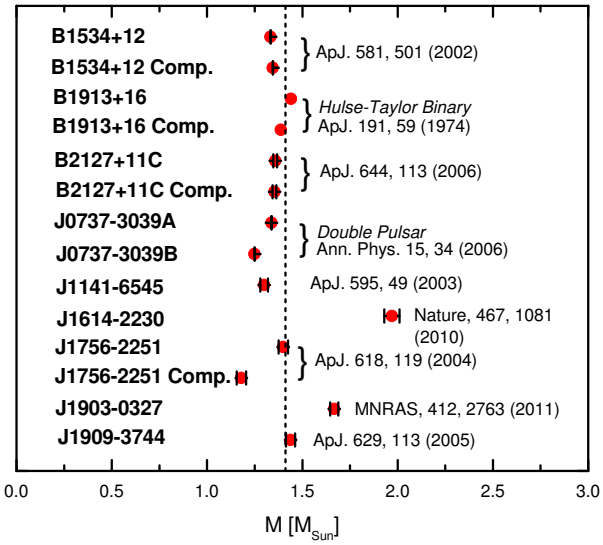

Figure 1.1: The list of most precise neutron star masses measured by different sources. The dashed line corresponds to the average mass for this population of neutron stars.

state of neutron-rich matter that describes the dynamics of core collapse supernovae and the structure of neutron stars. For example, the density slope of the symmetry energy at saturation determines the pressure of pure neutron matter. And it is precisely this pressure that provides the necessary support against gravitational collapse of the neutron star. The moment of inertia is therefore expected to be very sensitive to the symmetry energy. The discovery of binary pulsars in tight orbits, such as the recently discovered pulsars PSR J0737-3039 [18, 19], provides an opportunity to measure the moment of inertia with a good accuracy through timing measurements of the spin-orbit coupling.

Although the geometry of spacetime is strongly curved in the interior of neutron stars, due to the equivalence principle we are guaranteed to have a Lorentz invariant frame at any given spacetime point [20]. Moreover, a relative change of the metric tensor through the entire region of a typical neutron star is in the order of $g_{11}(r = R)/g_{11}(r = 0) \sim 1.7$. However the star is 18 orders of magnitude larger than the dimension of its constituent

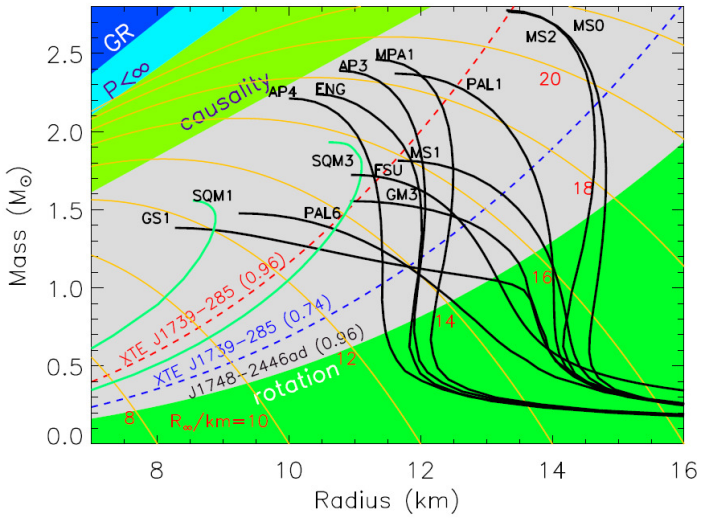

Figure 1.2: The mass-radius relations from a representative set of the equations of state taken from [3]. The black curves correspond to neutron stars, while the green curves correspond to self-bound quark stars. For a detailed description of the equations of state, refer to [3].

particles. Therefore the relative change in the metric over the average spacing of baryons is very small ($\sim 10^{-19}$) [20]. Thus, the nuclear matter at any given density in the star may be treated as infinite nuclear matter. The approximate Lorentz frame established this way is known as the *bulk approximation*, where the energy associated with boundaries is neglected.

Using the equation of state of degenerate Fermi gas for neutrons, Tolman, Oppenheimer and Volkoff (TOV) [21, 22] were the first to compute the structure of neutron stars in 1939. They obtained a limiting maximum neutron star mass of ~ 0.70 solar mass, which is far smaller than the current measured maximum neutron star mass. Of course, the equation of state used by TOV was unrealistic. The correct equation of state should involve all hadronic degrees of freedom. Moreover, a Lorentz covariant theory of nuclear matter is needed to compute the structure of neutron stars. Historically, such Lorentz covariant field theories were first proposed by Johnson and Teller [23], and improved by Duerr [24] in the 1950s, while further developed in a seminal paper by Walecka [7] in the 1970s. In these original field theories the interaction between nucleons were mediated by two isoscalar mesons: the scalar sigma meson and the vector omega meson. Although the original relativistic nuclear

matter theory of Walecka could not describe the properties of nuclear matter as well as non-relativistic nuclear matter in early 1970s, during the past several decades relativistic theories have been vastly improved [8, 10, 14, 15, 16]. In addition to being automatically causal at high densities (which is not always the case in non-relativistic nuclear equations of state), these theories also describe the saturation properties of nuclear matter. Moreover, the spin-orbit interaction arises as a pure relativistic phenomenon. The motivation of the relativistic field theories are further discussed in Chapter 2.

This dissertation is organized as follows. It consists of 7 chapters, 2 appendices and a list of 138 references. It is laid out on 137 pages with 28 figures and 19 tables.

Chapter 2 is devoted to the discussion of relativistic mean-field theories. In Section 2.1, we discuss the motivations for the importance of the relativistic mean-field models in nuclear physics. By introducing a particular form of the Lagrangian density that is widely used at the present time, we discuss the mean-field approximation in detail. In Section 2.2, the nuclear equations of state will be derived and the properties of infinite nuclear matter will be discussed. In particular, we will derive an analytic expression for the incompressibility coefficient of the symmetric nuclear matter at saturation. Applications of relativistic mean-field models to symmetric and asymmetric nuclear matter are presented in Section 2.3.

In Chapter 3, we outline the current knowledge of the structure of neutron stars. Then we present the equations of stellar structure, including the famous Tolman-Oppenheimer-Volkoff (TOV) equation. Following the TOV equation, we introduce the general relativistic expression for the moment of inertia of uniformly rotating, axially symmetric neutron stars in the slow-rotation approximation. In Section 3.3, we give an overview of the current observational status of neutron star properties in detail. In Section 3.4 we obtain the analytic expression for the crustal moment of inertia. The state of matter in a neutron star is determined by the condition of hydrostatic beta equilibrium. This condition is discussed in detail in Section 3.5. Another important section of this chapter is the discussion of the direct Urca process that is responsible for the cooling of neutron stars. We derive the expression for the threshold proton fraction necessary for this process. The chapter is closed by introducing the equation of state of neutron-star matter in relativistic-mean field models.

In Chapter 4, we study the sensitivity of the moment of inertia to the underlying equation of state. Using relativistic mean-field models we generate several families of the equations of state and show that the moment of inertia is sensitive only to the equation of state. We show that the knowledge of the moment of inertia with a 10% percent accuracy discriminates between equations of state that are stiff or soft at high densities. Its sensitivity to the symmetry energy is also discussed in detail. An important section of this chapter is the calculation of the crustal moment of inertia. By obtaining analytic expression for the crustal moment of inertia we will show that it is sensitive to a fundamental nuclear observable—the transition pressure. The correlation between the transition pressure and other nuclear observables, such as the transition density and neutron skin of lead are discussed in detail.

In Chapter 5, we introduce a new relativistic effective interaction that is simultaneously constrained by the nuclear binding energies, charge radii, giant resonances, and neutron star properties. With a detailed overview of state of art relativistic mean-field models, and most updated measurements of neutron star properties, we discuss the motivation for the development of the new interaction. Dubbed as IU-FSU, this relativistic effective interaction reproduces the maximum mass of neutron stars consistent with the latest observation. This new interaction is soft at intermediate densities and is stiff at high densities. We devote a full section to the discussion of giant resonances and the incompressibility of neutron-rich matter. In particular, we discuss why some relativistic-mean field models are not able to reproduce the centroid energies of giant monopole resonances. Further, the equations of state from several relativistic mean-field models will be compared with different theoretical studies.

Chapter 6 explores a new area in the calculations of theoretical uncertainties in the model predictions by implementing a χ^2-minimization procedure. Models fitted to experimental or observational data are often used to extrapolate to the extremes regions of density and isospin asymmetry, therefore it is very important to quantify model uncertainties in theoretical nuclear physics and astrophysics. In Section 6.2.1, we introduce a general class of relativistic mean-field models that are rooted in effective-field-theory concepts. In Section 6.2.2, we present a self-contained derivation of the ideas and formulas required to implement the covariance and correlation analysis. Although the idea of covariance analysis discussed in

this chapter is very general, we concentrate on the relativistic mean-field models and estimate the meaningful theoretical uncertainties. To illustrate the ideas of covariance analysis we use two examples of relativistic mean-field models.

Finally, in Chapter 7 we summarize the main findings of this dissertation work. Throughout the dissertation, we use the system of units in which $\hbar = 1 = c$, Greek indices run from 0 to 3, and isovector fields are denoted using boldface letters.

CHAPTER 2

RELATIVISTIC MEAN-FIELD THEORY

2.1 General Formalism

2.1.1 Lagrangian Density

Relativistic mean field (RMF) models and their applications to the ground-state properties of medium to heavy nuclei have enjoyed enormous success during the past three decades [7, 8, 9, 10, 14, 15, 16, 25, 26, 27, 28, 29, 30]. Having only a handful of model parameters that are calibrated to a few ground state properties of a representative set of closed-shell nuclei, these highly economical descriptions encode a great amount of physics. Historically, traditional nuclear physics is based on non-relativistic quantum mechanics, in which the dynamics is determined by the nucleon-nucleon potential. Despite the success of the nonrelativistic many-body theories, this approach is inadequate in fully understanding many nuclear phenomena. Since the nuclear strong force is mediated by mesons, a more consistent theory of nuclear structure should therefore involve an explicit description of the baryon and meson degrees of freedom in the nuclear system. To maintain the Lorentz transformation properties of the interaction it is also necessary to study the nuclear systems in a relativistic framework. For example, this approach automatically preserves the causality in the propagation of signals in the nuclear medium, which may not be the case in the non-relativistic models. This consideration is very important in the astrophysical applications, where one works at the extreme region of high densities. Since the nuclear binding energy is very small compared to the mass of nucleons, $\epsilon_0/M \approx 0.02$ it is argued that the relativistic effects are not very important and can be considered only as corrections to the nuclear structure calculations. However, it turns out that the small value of the binding energy arises from the *cancelation*

of the large Lorentz scalar and four-vector potentials, which are of the order of the mass of nucleon even at the regular nuclear densities. Moreover, the addition of the the spin-orbit interaction term in the non-relativistic frameworks is also artificial, since it is known to be a purely relativistic phenomena. The strong nuclear spin-orbit interaction arises from the *addition* of these Lorentz scalar and vector potentials [10, 31]. Thus, it is necessary and very important to study the nuclear systems in the relativistic frame. The consistent framework to describe the relativistic many-body problem is therefore the relativistic quantum field theory that is based on local, Lorentz invariant Lagrangian density

$$\mathcal{L} = \mathcal{L}_0 + \mathcal{L}_{int} \ , \tag{2.1}$$

Throughout this work, we will employ the Lagrangian of [15]. That is,

$$\begin{aligned} \mathcal{L}_0 = \quad & \bar{\psi}\left(i\gamma^\mu\partial_\mu - M\right)\psi + \frac{1}{2}\left(\partial_\mu\phi\partial^\mu\phi - m_{\rm s}^2\phi^2\right) + \frac{1}{2}m_{\rm v}^2 V_\mu V^\mu - \\ & -\frac{1}{4}F_{\mu\nu}F^{\mu\nu} + \frac{1}{2}m_\rho^2\mathbf{b}_\mu\cdot\mathbf{b}^\mu - \frac{1}{4}V_{\mu\nu}V^{\mu\nu} - \frac{1}{4}\mathbf{b}_{\mu\nu}\cdot\mathbf{b}^{\mu\nu} \ , \end{aligned} \tag{2.2}$$

$$\begin{aligned} \mathcal{L}_{int} = \quad & \bar{\psi}\left[g_s\phi - \left(g_{\rm v}V_\mu + \frac{g_\rho}{2}\tau\cdot\mathbf{b}_\mu + \frac{e}{2}(1+\tau_3)A_\mu\right)\gamma^\mu\right]\psi - \\ & -\frac{\kappa}{3!}\left(g_{\rm s}\phi\right)^3 - \frac{\lambda}{4!}\left(g_{\rm s}\phi\right)^4 + \frac{\zeta}{4!}\left(g_{\rm v}^2V_\mu V^\mu\right)^2 + \\ & +\Lambda_{\rm v}\left(g_{\rm v}^2V_\mu V^\mu\right)\left(g_\rho^2\mathbf{b}_\mu\cdot\mathbf{b}^\mu\right) \ . \end{aligned} \tag{2.3}$$

The Lagrangian above includes an isodoublet nucleon field

$$\psi = \begin{pmatrix} \psi_{\rm p} \\ \psi_{\rm n} \end{pmatrix} \tag{2.4}$$

interacting via the exchange of a scalar-isoscalar meson field (ϕ for the σ-meson), a vector-isoscalar meson field (V^μ for the ω-meson), a vector-isovector meson field ($\mathbf{b}^\mu$ for the ρ-meson), and a photon field (A^μ). The various tensor fields are defined as follows:

$$F_{\mu\nu} = \partial_\mu A_\nu - \partial_\nu A_\mu \ , \tag{2.5}$$

$$V_{\mu\nu} = \partial_\mu V_\nu - \partial_\nu V_\mu \ , \tag{2.6}$$

$$\mathbf{b}_{\mu\nu} = \partial_\mu \mathbf{b}_\nu - \partial_\nu \mathbf{b}_\mu \ . \tag{2.7}$$

Each of these meson exchange Yukawa couplings ($g_{\rm s}$, $g_{\rm v}$, g_ρ) are responsible for the particular type of interaction: scalar-isoscalar ϕ meson field is responsible for the intermediate attractive interaction among nucleons, vector-isoscalar V^μ field is responsible for the short range

repulsive interaction, and vector-isovector $\mathbf{b}^\mu$ field parameterizes the isospin dependence. In addition to the meson-nucleon interactions, this Lagrangian is supplemented with higher order non-linear meson self interactions. The inclusion of isoscalar meson self-interactions (through κ, λ, and ζ) are used to soften the equation of state of symmetric nuclear matter, while the mixed isoscalar-isovector coupling (Λ_v) modifies the density dependence of the symmetry energy [15, 32]. While power counting suggests that other meson coupling terms could be equally important, their phenomenological impact has been shown to be small [16], so they have not been considered in this work. A detailed analysis of the role of each term in this Lagrangian will be discussed in next sections.

2.1.2 Mean-Field Approximation

Using Lagrange's equations of motion

$$\frac{\partial}{\partial x^\mu}\left(\frac{\partial \mathcal{L}}{\partial \frac{\partial q_i}{\partial x^\mu}}\right) - \frac{\partial \mathcal{L}}{\partial q_i} = 0 \ , \tag{2.8}$$

where q_i are the generalized coordinates, one can obtain the equations of motion for the meson fields,

$$\left(\partial_\mu \partial^\mu + m_\mathrm{s}^2\right)\phi = g_\mathrm{s}\bar{\psi}\psi - \frac{\kappa}{2}g_\mathrm{s}^3\phi^2 - \frac{\lambda}{6}g_\mathrm{s}^4\phi^3 \ , \tag{2.9}$$

$$\partial_\mu V^{\mu\nu} + m_\mathrm{v}^2 V^\nu = g_\mathrm{v}\bar{\psi}\gamma^\nu\psi - \frac{\zeta}{6}g_\mathrm{v}^4\left(V_\mu V^\mu\right)V^\nu - 2\Lambda_\mathrm{v}\left(g_\rho^2\mathbf{b}_\mu\cdot\mathbf{b}^\mu\right)g_\mathrm{v}^2 V^\nu \ , \tag{2.10}$$

$$\partial_\mu \mathbf{b}^{\mu\nu} + m_\rho^2\mathbf{b}^\nu = g_\rho\bar{\psi}\left(\frac{\tau}{2}\gamma^\nu\right)\psi - 2\Lambda_\mathrm{v}\left(g_\mathrm{v}^2 V_\mu V^\mu\right)g_\rho^2\mathbf{b}^\nu \ . \tag{2.11}$$

Similarly, one can obtain the equation of motion for baryon fields, which is known as the Dirac equation:

$$\left[\gamma^\mu\left(i\partial_\mu - g_\mathrm{v}V_\mu - \frac{g_\rho}{2}\tau\cdot\mathbf{b}_\mu\right) - \left(M - g_\mathrm{s}\phi\right)\right]\psi = 0 \ . \tag{2.12}$$

The equations of motion described above are non-linear quantum field equations. Unlike other quantum field theories, such as QCD, the coupling constants for the effective Lagrangian are not small, hence perturbative approach is not relevant. Therefore, the exact solution of the equations of motion is very complicated. However, at medium and high baryon densities the scalar and vector meson field operators can be replaced by their expectation values [10, 20, 31, 33]. Then one can regard meson fields as the classical condensed fields in which the baryons move. Note that the baryon fields, however, remain as operators.

The sole remnant of quantum behavior is therefore in the treatment of the nucleon field which emerges from a solution to the Dirac equation in the presence of appropriate scalar and vector potentials [10, 29].

For a static, spherically symmetric system this implies

$$\phi(x) \rightarrow \langle\phi(x)\rangle = \phi_0(r) \ , \tag{2.13}$$

$$V^{\mu}(x) \rightarrow \langle V^{\mu}(x)\rangle = g^{\mu 0}V_0(r) \ , \tag{2.14}$$

$$b_i^{\mu}(x) \rightarrow \langle b_i^{\mu}(x)\rangle = g^{\mu 0}\delta_{i3}b_0(r) \ , \tag{2.15}$$

$$A^{\mu}(x) \rightarrow \langle A^{\mu}(x)\rangle = g^{\mu 0}A_0(r) \ , \tag{2.16}$$

where we used $\mathbf{x} \equiv r$. Thus, we consider only the ground state expectation values of the meson field operators. Similarly, the baryon sources that are coupled to meson fields are also replaced by their normal ordered expectation values in the mean-field ground state

$$\bar{\psi}\mathbf{1}\psi \rightarrow \langle : \bar{\psi}\mathbf{1}\psi : \rangle = \rho_{\rm s} \ , \tag{2.17}$$

$$\bar{\psi}\gamma^{\mu}\psi \rightarrow \langle : \bar{\psi}\gamma^{\mu}\psi : \rangle = \delta^{\mu 0}\rho_{\rm B} \ , \tag{2.18}$$

$$\bar{\psi}\gamma^{\mu}\tau_a\psi \rightarrow \langle : \bar{\psi}\gamma^{\mu}\tau_a\psi : \rangle = \delta^{\mu 0}\delta_{a3}\rho_3 \ , \tag{2.19}$$

where ρ_s is the scalar number density, $\rho_{\rm B} = \rho_p + \rho_n$, is the baryon number density, and $\rho_3 = \rho_p - \rho_n$. Within this context of the *mean-field approximation*, the field equations may now be solved exactly.

Note that we will mostly be considering uniform systems of infinite nuclear matter, in this work. This type of hypothetical nuclear matter is an idealization that however has very definite properties related to finite nuclei. Moreover, the infinite nuclear matter is applicable to the study of neutron stars, which is the main purpose of this work. For such uniform infinite systems the meson field operators are *constants* independent of x_μ. In addition, we will also neglect the contribution from the photon field A_μ. In general, it is very important to consider all these in studying the properties of finite nuclei. However, since the Coulomb forces are much stronger than the gravitational field, neutron stars are considered to be charge neutral objects [20]. Therefore, in this treatment of infinite nuclear matter, the contribution from the photon fields will be also ignored.

The relativistic mean-field Lagrangian density then simplifies to

$$\begin{aligned}\mathcal{L}_{\rm RMF} &= \bar{\psi}\left(i\gamma^{\mu}\partial_{\mu} - g_{\rm v}\gamma^{0}V_{0} - g_{\rho}\gamma^{0}\frac{\tau_{0}}{2}b_{0} - M^{*}\right)\psi - \\ &- \frac{1}{2}m_{\rm s}^{2}\phi_{0}^{2} + \frac{1}{2}m_{\rm v}^{2}V_{0}^{2} + \frac{1}{2}m_{\rho}^{2}b_{0}^{2} - \frac{\kappa}{3!}\left(g_{\rm s}\phi_{0}\right)^{3} - \\ &- \frac{\lambda}{4!}\left(g_{\rm s}\phi_{o}\right)^{4} + \frac{\zeta}{4!}\left(g_{\rm v}V_{0}\right)^{4} + \Lambda_{\rm v}\left(g_{\rho}b_{0}\right)^{2}\left(g_{\rm v}V_{0}\right)^{2} \ , \end{aligned} \tag{2.20}$$

where, $M^{*} = M - g_{\rm s}\phi_{0}$, is known as the effective nucleon mass.

The equations of motion (2.9-2.11) in the RMF then takes the following form:

$$\frac{1}{c_{\rm s}^{2}}\Phi_{0} + \frac{\kappa}{2}\Phi_{0}^{2} + \frac{\lambda}{6}\Phi_{0}^{3} = \rho_{\rm s} \ , \tag{2.21}$$

$$\frac{1}{c_{\rm v}^{2}}W_{0} + 2\Lambda_{\rm v}R_{0}^{2}W_{0} + \frac{\zeta}{6}W_{0}^{3} = \rho_{\rm B} \ , \tag{2.22}$$

$$\frac{1}{c_{\rho}^{2}}R_{0} + 2\Lambda_{v}W_{0}^{2}R_{0} = \frac{1}{2}\rho_{3} \ , \tag{2.23}$$

where the following definitions have been introduced: $\Phi_{0} = g_{\rm s}\phi_{0}$, $W_{0} = g_{\rm v}V_{0}$, $R_{0} = g_{\rho}b_{0}$, and $c_{i} \equiv \frac{g_{i}}{m_{i}}$.

Performing standard calculations in the Dirac theory [10, 20] we can derive the expressions for the scalar density,

$$\rho_{\rm s} = \frac{1}{\pi^{2}}\int_{0}^{k_{\rm F}^{p}} k^{2}\frac{M^{*}}{\sqrt{k^{2}+M^{*2}}}\,dk + \frac{1}{\pi^{2}}\int_{0}^{k_{\rm F}^{n}} k^{2}\frac{M^{*}}{\sqrt{k^{2}+M^{*2}}}\,dk \ , \tag{2.24}$$

and for the baryon density,

$$\rho_{\rm B} = \rho_{p} + \rho_{n} = \frac{k_{\rm F}^{p\,3} + k_{\rm F}^{n3}}{3\pi^{2}} \ . \tag{2.25}$$

2.2 The Nuclear Equation of State

2.2.1 The Energy-Momentum Tensor

The energy-momentum tensor is defined by

$$T_{\mu\nu} = -g_{\mu\nu}\mathcal{L} + \frac{\partial\psi}{\partial x^{\nu}}\frac{\partial\mathcal{L}}{\partial\frac{\partial\psi}{\partial x_{\mu}}} \ , \tag{2.26}$$

The Euler-Lagrange's equations (2.9-2.12) ensure that this tensor is conserved:

$$\partial^{\mu}T_{\mu\nu} = 0 \ . \tag{2.27}$$

Substituting the (2.20) into (2.26) we find

$$(T_{\mu\nu})_{\rm RMF} = i\bar{\psi}\gamma_\mu\partial_\nu\psi - \Big\{\frac{1}{2}m_{\rm v}^2V_0^2 + \frac{1}{2}m_\rho^2b_0^2 - \frac{1}{2}m_{\rm s}^2\phi_0^2 - \\ -\frac{\kappa}{3!}\left(g_{\rm s}\phi_0\right)^3 - \frac{\lambda}{4!}\left(g_{\rm s}\phi_0\right)^4 + \frac{\zeta}{4!}\left(g_{\rm v}V_0\right)^4 + \Lambda_{\rm v}\left(g_{\rm v}V_0\right)^2\left(g_\rho b_0\right)^2\Big\}g_{\mu\nu} \ . \tag{2.28}$$

For a uniform system of perfect fluid the energy-momentum tensor is given by [20, 34]

$$T_{\mu\nu} = \left(\mathcal{E} + P\right)u_\mu u_\nu - Pg_{\mu\nu} \ , \tag{2.29}$$

where $\mathcal{E}$ is the energy density, P is the pressure, and u_μ is the four-velocity of the fluid. In the local rest frame of the fluid, $u^\mu = (1,0,0,0)$, and the energy-momentum tensor can be written as

$$T_{\mu\nu} = \begin{pmatrix} \mathcal{E} & 0 & 0 & 0 \\ 0 & P & 0 & 0 \\ 0 & 0 & P & 0 \\ 0 & 0 & 0 & P \end{pmatrix} \ . \tag{2.30}$$

Following standard mean-field (MF) practices, the energy density of the system can be derived as:

$$\mathcal{E} = \frac{1}{\pi^2}\int_0^{k_{\rm F}^p} k^2E_k^*\,dk + \frac{1}{\pi^2}\int_0^{k_{\rm F}^n} k^2E_k^*\,dk + g_{\rm v}V_0\rho_{\rm B} + \frac{g_\rho}{2}b_0\rho_3 + U(\phi_0,V_0,b_0) \ , \tag{2.31}$$

where $E_k^* = \sqrt{k^2+M^{*2}}$, $k_{\rm F}^p(k_{\rm F}^n)$ is the proton (neutron) Fermi momentum, $\rho_{\rm B}(\rho_3)$ is the isoscalar (isovector) baryon density, and $U(\phi_0,V_0,b_0)$ is given by the following expression:

$$\begin{aligned} U(\phi_0,V_0,b_0) &= \frac{1}{2}m_{\rm s}^2\phi_0^2 + \frac{\kappa}{3!}(g_{\rm s}\phi_0)^3 + \frac{\lambda}{4!}(g_{\rm s}\phi_0)^4 \\ &- \frac{1}{2}m_v^2V_0^2 - \frac{\zeta}{4!}(g_{\rm v}V_0)^4 - \frac{1}{2}m_\rho^2b_0^2 - \Lambda_{\rm v}(g_{\rm v}V_0)^2(g_\rho b_0)^2 \ . \end{aligned} \tag{2.32}$$

The contribution from each baryon and meson fields can be expressed as following:

$$\mathcal{E} = \mathcal{E}_p + \mathcal{E}_n + \mathcal{E}_\sigma + \mathcal{E}_\omega + \mathcal{E}_\rho + \mathcal{E}_{\omega\rho} \ , \tag{2.33}$$

where

$$\mathcal{E}_p = \frac{1}{\pi^2}\int_0^{k_{\rm F}^p} k^2 E_k^*\, dk + \left(g_{\rm v}V_0 + \frac{g_\rho}{2}b_0\right)\rho_p \ , \tag{2.34}$$

$$\mathcal{E}_n = \frac{1}{\pi^2}\int_0^{k_{\rm F}^n} k^2 E_k^*\, dk + \left(g_{\rm v}V_0 - \frac{g_\rho}{2}b_0\right)\rho_n \ , \tag{2.35}$$

$$\mathcal{E}_\sigma = \frac{1}{2}m_{\rm s}^2\phi_0^2 + \frac{\kappa}{6}\left(g_{\rm s}\phi_0\right)^3 + \frac{\lambda}{24}\left(g_{\rm s}\phi_0\right)^4 \ , \tag{2.36}$$

$$\mathcal{E}_\omega = -\frac{1}{2}m_{\rm v}^2V_0^2 - \frac{\zeta}{24}\left(g_{\rm v}V_0\right)^4 \ , \tag{2.37}$$

$$\mathcal{E}_\rho = -\frac{1}{2}m_\rho^2 b_0^2 \ , \tag{2.38}$$

$$\mathcal{E}_{\omega\rho} = -\Lambda_{\rm v}\left(g_{\rm v}V_0\right)^2\left(g_\rho b_0\right)^2 \ . \tag{2.39}$$

The expression for the energy density may be "simplified" by using the classical equations of motion for the vector fields to express the isoscalar and isovector densities $\rho_{\rm B}$ and ρ_3 in terms of V_0 and b_0. One obtains,

$$\begin{aligned}\mathcal{E} &= \frac{1}{\pi^2}\int_0^{k_{\rm F}^p} k^2 E_k^*\, dk + \frac{1}{\pi^2}\int_0^{k_{\rm F}^n} k^2 E_k^*\, dk \\ &+ \frac{1}{2}m_s^2\phi_0^2 + \frac{\kappa}{3!}(g_{\rm s}\phi_0)^3 + \frac{\lambda}{4!}(g_{\rm s}\phi_0)^4 \\ &+ \frac{1}{2}m_v^2V_0^2 + \frac{\zeta}{8}(g_{\rm v}V_0)^4 + \frac{1}{2}m_\rho^2 b_0^2 + 3\Lambda_{\rm v}(g_{\rm v}V_0)^2(g_\rho b_0)^2 \ .\end{aligned} \tag{2.40}$$

Finally, as the MF approximation is *thermodynamically consistent*, the pressure of the system (at zero temperature) may be obtained either from the energy-momentum tensor or from the energy density and its first derivative with respect to the density [10, 29]. That is,

$$P = \frac{1}{3\pi^2}\int_0^{k_{\rm F}^p}\frac{k^4}{E_k^*}\, dk + \frac{1}{3\pi^2}\int_0^{k_{\rm F}^n}\frac{k^4}{E_k^*}\, dk - U(\phi_0, V_0, b_0) \ , \tag{2.41}$$

The relation between the expressions for the energy density (2.40), and the pressure (2.41) gives us the equation of state of nuclear matter at zero temperature, which is applicable for neutron stars.

2.2.2 The Properties of Infinite Nuclear Matter

Consider an infinite uniform system of nucleons, where the Coulomb forces are switched off. This is an idealized system, whose properties are very essential in the study of the nuclear equations of state. Historically, the notion goes back to Bethe-Weizsäcker mass

formula and the liquid drop model, according to which the energy of a nucleus is related to its atomic mass number, A, and the proton number, Z:

$$E(Z,N) = -a_{\rm v}A + a_{\rm s}A^{2/3} + a_{\rm C}\frac{Z^2}{A^{1/3}} + a_{\rm asym}\frac{(N-Z)^2}{A} + \dots \ , \tag{2.42}$$

where $a_{\rm v}$ is the volume term, $a_{\rm s}$ is the surface term, $a_{\rm C}$ is the Coulomb term, and $a_{\rm asym}$ is the asymmetry term. In this study we will not go into the details of the liquid drop model, rather we concentrate on the infinite nuclear matter. The infinite nuclear matter is then the thermodynamic limit of this model, where Z, N, and V go to infinity. We also turn off the Coulomb term, $a_{\rm C} = 0$, and neglect the surface contribution (as there is no surface for the infinite matter). Introducing the baryon density, proton fraction, and the asymmetry parameter as following:

$$\rho_{\rm B} = \frac{A}{V} \ , \qquad Y_p = \frac{Z}{A} \ , \qquad \alpha = \frac{N-Z}{A} \equiv \frac{\rho_n - \rho_p}{\rho_n + \rho_p} \ , \tag{2.43}$$

we obtain the following expression for the Bethe-Weizsäcker mass formula:

$$E(Z,N)/A = -a_{\rm v} + a_{\rm asym}\alpha^2 + \dots \ , \tag{2.44}$$

The infinite nuclear matter introduced above is incompressible. In general, for a compressible nuclear matter the total energy per nucleon, $E(\rho,\alpha)/A$, can be expanded around $\alpha = 0$:

$$\begin{aligned} E(\rho,\alpha)/A &= E(\rho,\alpha=0)/A + \left(\frac{\partial E(\rho,\alpha)/A}{\partial\alpha}\right)_{\alpha=0}\alpha + \frac{1}{2}\left(\frac{\partial^2 E(\rho,\alpha)/A}{\partial\alpha^2}\right)_{\alpha=0}\alpha^2 + \dots = \\ &= E_{\rm SNM}(\rho) + S(\rho)\alpha^2 + \dots \ . \end{aligned} \tag{2.45}$$

The linear term in α vanishes, because of the charge symmetry of nuclear forces. Substituting $\alpha = 0$ in the above equation, one can see that $E_{\rm SNM}(\rho)$ corresponds to *symmetric nuclear matter*. While, the case $\alpha = 1$ (look at the definition) corresponds to *pure neutron matter*.

The simplest approximation of the bulk nuclear matter for the heavy nuclei is the symmetric nuclear matter, where the number of protons and neutrons are equal. Considering the mass of nucleons to be the same, $M = 939$ MeV, one can view neutrons and protons as one kind of particles with the same Fermi momentum [4]. Then the total baryon density is just the sum of nucleon (proton and neutron) densities:

$$\rho_{\rm B} = \frac{2k_{\rm F}^3}{3\pi^2} \ , \tag{2.46}$$

where $k_{\rm F}$ is the nucleon Fermi momentum. In general, the effect of $\alpha \neq 0$ is very small. For example, in the case of the nucleus of lead ^{208}Pb, this effect is about 4% only: $\alpha^2 \approx 0.0447$. Therefore, in dealing with the terrestrial nuclei, the symmetric nuclear matter (SNM) is a very reasonable approximation. On the other hand, the extreme case of pure neutron matter ($\alpha = 1$) is a good approximation of the nuclear matter in the core of neutron stars. Nevertheless, in the full study of finite nuclei and neutron-star matter, one should treat both neutrons and protons separately.

One characteristic of symmetric nuclear matter is that it *saturates*. This means that there exists a minimum of the total energy per nucleon, where the pressure of the system is zero. The baryon density at which this minimum occurs is called the saturation density, and is denoted by ρ_0. The value of the total energy per nucleon at saturation density is called the binding energy at saturation and is denoted by ϵ_0. Let us expand the total energy per nucleon of SNM around the saturation density:

$$E_{\rm SNM}(x) = \epsilon_0 + \frac{1}{2} K_0 x^2 + \frac{1}{6} Q_0 x^3 + \dots \ , \tag{2.47}$$

where $x \equiv (\rho - \rho_0)/3\rho_0$,

$$K_0 = 9\rho_0^2 \left(\frac{\partial^2 E_{\rm SNM}}{\partial \rho^2} \right)_{\rho=\rho_0} = 9\rho_0^2 \left[\frac{\partial^2}{\partial \rho^2} \left(\frac{\mathcal{E}}{\rho} \right) \right]_{\rho=\rho_0} = 9\rho_0^2 \left[\frac{\partial}{\partial \rho} \left(\frac{P}{\rho^2} \right) \right]_{\rho=\rho_0} \ , \tag{2.48}$$

and

$$Q_0 = 27\rho_0^3 \left(\frac{\partial^3 E_{\rm SNM}}{\partial \rho^3} \right)_{\rho=\rho_0} \ . \tag{2.49}$$

Note that at saturation the first derivative of the total energy per nucleon (i.e., its pressure) vanishes. The quantity K_0 is known as the *compression modulus* or the *incompressibility coefficient* of symmetric nuclear matter. It characterizes the curvature of $E_{\rm SNM}$ at ρ_0, and is very important in the study of equations of state. The high values of K_0 correspond to the *stiff* equations of state, while the small values correspond to the so called *soft* equation of state. In the next sections, we will discuss each of these cases in details. Current estimation of the values of these bulk observables are known to be

$$\rho_0 \simeq 0.16 \text{ fm}^{-3} \ , \tag{2.50}$$

$$\epsilon_0 \simeq -16 \text{ MeV} \ , \tag{2.51}$$

$$K_0 \simeq 230 \text{ MeV} \ . \tag{2.52}$$

The values of ρ_0 and ϵ_0 can be found, for example, by fitting the masses of large number of nuclear isotopes to the liquid drop model [35, 36]. The value of the incompressibility coefficient can be obtained from measuring the giant monopole resonance in nuclei (it is a collective excitation that corresponds to the radial mode) [37, 38]. The uncertainties in its extraction from the experiments however are not free from ambiguities [39].

The quantity $S(\rho)$ in the equation (2.45) is known as the *symmetry energy*. The symmetry energy describes how the energy of nuclear matter rises as one moves away from the equal number of neutrons and protons. This quantity is very important in the study of neutron-rich nuclei. To a good approximation, the symmetry energy can be expressed as the difference between the energies of PNM and SNM:

$$S(\rho) \approx E_{\rm PNM}(\rho) - E_{\rm SNM}(\rho) \ . \tag{2.53}$$

At present the density dependence of the symmetry energy is largely unknown [40, 41, 42, 43]. In this study we will be mostly concentrating on this quantity. Let us expand the symmetry energy around the saturation density:

$$S(x) = J + Lx + \frac{1}{2}K_{\rm sym}x^2 + \dots \ , \tag{2.54}$$

where J is the value of the symmetry energy at saturation,

$$J = \frac{1}{2}\rho\left[\left(\frac{\partial^2\mathcal{E}}{\partial\rho_3^2}\right)_{\rho=\text{fixed}}\right]_{\rho_3=0} = \frac{1}{2\rho}\left[\left(\frac{\partial^2\mathcal{E}}{\partial\alpha^2}\right)_{\rho=\text{fixed}}\right]_{\alpha=0} \ , \tag{2.55}$$

L is the density slope of the symmetry energy,

$$L = 3\left(\rho\frac{\partial S(\rho)}{\partial\rho}\right)_{\rho=\rho_0} \ , \tag{2.56}$$

and $K_{\rm sym}$ defines the curvature of the symmetry energy:

$$K_{\rm sym} = 9\left[\rho^2\frac{\partial^2 S(\rho)}{\partial\rho^2}\right]_{\rho=\rho_0} \ . \tag{2.57}$$

The coefficients L and $K_{\rm sym}$ characterize the density dependence of the nuclear symmetry energy around normal nuclear density ρ_0, and thus carry important information on the properties of nuclear symmetry energy at both high and low densities [44].

Another important property of the nuclear matter is the nucleon effective mass, $M^* = M - g_s\phi_0$. Its value at saturation is one of the least unknown bulk parameters. The RMF

models predict $M^*(\rho_0) \simeq 0.6M$ for the value of the nucleon effective mass at saturation, where M is the nucleon mass. Rewriting the equation of motion (2.21) in terms of M^*, we obtain a transcendental self-consistency equation for the nucleon effective mass:

$$M^* = M + c_{\rm s}^2 \left[\frac{\kappa}{2} \left(M - M^* \right)^2 + \frac{\lambda}{6} \left(M - M^* \right)^3 - \rho_{\rm s} \right] \ , \tag{2.58}$$

where the expression for the scalar density is provided in the equation (2.24). The integral in the scalar density can be calculated analytically:

$$\rho_{\rm s} = \frac{M^*}{2\pi^2} \left[k_{\rm F}^p E_{\rm F}^{p*} + k_{\rm F}^n E_{\rm F}^{n*} - M^{*2} \ln \left(\frac{\left[k_{\rm F}^p + E_{\rm F}^{p*} \right] \left[k_{\rm F}^n + E_{\rm F}^{n*} \right]}{M^{*2}} \right) \right] \ . \tag{2.59}$$

2.2.3 Constraining the RMF parameters

There are seven unknown free parameters (coupling constants) in the Lagrangian density (2.20):

$$c_{\rm s} \ , \quad c_{\rm v} \ , \quad c_\rho \ , \quad \lambda \ , \quad \kappa \ , \quad \zeta \ , \quad \Lambda_{\rm v} \ . \tag{2.60}$$

Five of these coupling constants can be determined using the five properties of infinite nuclear matter: the equilibrium binding energy, ϵ_0, the equilibrium density, ρ_0, the nucleon effective mass at equilibrium, M_0^*, the compression modulus, K_0, and the symmetry energy, J. To fully determine the model we need, at least, two additional constraints.

The enormously successful NL3 parametrization of the relativistic mean-field [14] has indeed only five parameters, where $\zeta = 0$, and $\Lambda_{\rm v} = 0$. This suggests that existing laboratory data is fairly insensitive to the physics encoded in these two parameters. Indeed, it was found possible [16] that one can build different RMF models by varying the value of ζ. Models tuned this way predict the same observed nuclear matter parameters, yet produce maximum mass of neutron stars that differ by almost one solar mass. These results indicate that the only meaningful constraints to the equation of state comes from the observational data on neutron stars, rather than from existing laboratory data. We will see in the next several sections that the empirical parameter ζ provides an efficient tool to control the high-density component of the equation of state. As we noted above, the density dependence of the symmetry energy at present is largely unconstrained. The isoscalar-isovector mixing term, $\Lambda_{\rm v}$, was introduced to modify the poorly known density dependence of symmetry energy [30]. The inclusion of $\Lambda_{\rm v}$ does not affect the well-known ground state properties.

Fixing ζ and $\Lambda_{\rm v}$ at some particular values (usually between $0 < \zeta < 0.06$, and $0 < \Lambda_{\rm v} < 0.06$), one can find algebraic expressions for the coupling constants. Note that to do this we would first need algebraic expressions for the saturation density and the saturation values of the binding energy, the effective nucleon mass, and the incompressibility coefficient for the symmetric nuclear matter. We also need the expression for the symmetry energy at saturation. Since for symmetric nuclear matter protons and neutrons are indistinguishable (they have the same mass and Fermi momentum), one can treat them as one component nucleons. Then the saturation density is

$$\rho_0 = \frac{2{k_{\rm F}^0}^3}{3\pi^2} \ , \tag{2.61}$$

where $k_{\rm F}^0$ is the Fermi momentum of the nucleons at saturation. The binding energy at saturation is simply the total energy per nucleon minus its mass:

$$\epsilon_0 = \frac{E_0}{A_0} = \frac{\mathcal{E}_0}{\rho_0} - M \ . \tag{2.62}$$

The self-consistent expression for the nucleon effective mass, M^* was already derived in (2.58). At saturation it is simply found from the following expression:

$$M_0^* = M + c_{\rm s}^2 \left[\frac{\kappa}{2} \left(M - M_0^*\right)^2 + \frac{\lambda}{6} \left(M - M_0^*\right)^3 - \frac{M_0^*}{\pi^2} \left[k_{\rm F} E_{0{\rm F}}^* - M^{*2} \ln \left(\frac{k_{\rm F} + E_{0{\rm F}}^*}{M^*} \right) \right] \right] \ . \tag{2.63}$$

The derivation of the expression for incompressibility coefficient, K_0, requires some tedious, but straightforward algebra. Here we will provide only some steps. From the definition (2.48),

$$K_0 = 9 \left(\frac{\partial P}{\partial \rho} \right)_{\rho=\rho_0} - 18 \frac{P_0}{\rho_0} = 9 \left(\frac{\partial P}{\partial \rho} \right)_{\rho=\rho_0} \ , \tag{2.64}$$

since at saturation the pressure is zero. We use the fact that for the SNM the isovector field R_0 vanishes. Then the expression for pressure (2.41) takes much simpler form:

$$\begin{aligned} P &= \frac{1}{4\pi^2} \left[k_{\rm F} E_{\rm F}^* \left(\frac{2}{3} k_{\rm F}^2 - M^{*2} \right) - M^{*4} \ln \left(\frac{M^*}{k_{\rm F} + E_{\rm F}^*} \right) \right] + \\ &+ \frac{1}{2c_{\rm v}^2} W_0^2 + \frac{\zeta}{4} W_0^4 - \frac{1}{2c_{\rm c}^2} (M - M^*)^2 - \frac{\kappa}{6} (M - M^*)^3 - \frac{\lambda}{24} (M - M^*)^4 \ . \end{aligned} \tag{2.65}$$

Note that at this point the expressions for M^* and meson field W_0 still depend on the baryon density $\rho_{\rm B}$ (or correspondingly Fermi momentum, $k_{\rm F}$):

$$P = P\left(M^*, W_0; k_{\rm F}\right) \ . \tag{2.66}$$

Then the derivative of the pressure with respect to the baryon density can be written as the sum of three components:

$$\frac{\partial P}{\partial \rho} = \frac{\pi^2}{2k_{\rm F}^2}\left[\frac{\partial P}{\partial k_{\rm F}} + \frac{\partial P}{\partial M^*}\frac{\partial M^*}{\partial k_{\rm F}} + \frac{\partial P}{\partial W_0}\frac{\partial W_0}{\partial k_{\rm F}}\right] \ . \tag{2.67}$$

Each term in this derivative then can be calculated:

$$\frac{\partial P}{\partial k_{\rm F}} = \frac{2}{3\pi^2}\frac{k_{\rm F}^4}{E_{\rm F}^*} \ . \tag{2.68}$$

In calculating $\frac{\partial P}{\partial M^*}$ we use the self-consistency equation (2.63). Straightforward manipulation gives

$$\frac{\partial P}{\partial M^*} = \frac{2M^* k_{\rm F}^3}{3\pi^2 E_{\rm F}^*} \ . \tag{2.69}$$

Taking the derivative of the equation of motion (2.63) with respect to $k_{\rm F}$, and after some manipulation we obtain:

$$\frac{\partial M^*}{\partial k_{\rm F}} = -\frac{2M^* k_{\rm F}^2}{\pi^2 E_{\rm F}^*\,(A+B)} \ , \tag{2.70}$$

where

$$A = \frac{1}{c_{\rm s}^2} + \kappa(M-M^*) + \frac{\lambda}{2}(M-M^*)^2 \ , \tag{2.71}$$

$$B = \frac{3M^{*2}}{\pi^2}\ln\left(\frac{M^*}{k_{\rm F}+E_{\rm F}^*}\right) + \frac{k_{\rm F}}{\pi^2 E_{\rm F}^*}\left(3M^{*2}+k_{\rm F}^2\right) \ . \tag{2.72}$$

Next, it is easy to check that $\frac{\partial P}{\partial W_0} = \rho_{\rm B}$. Performing the derivative of the equation of motion (2.22) with respect to $k_{\rm F}$ one obtains:

$$\frac{\partial W_0}{\partial k_{\rm F}} = \frac{4k_{\rm F}^2 c_{\rm v}^2}{\pi^2\left(2+c_{\rm v}^2\zeta W_0^2\right)} \ . \tag{2.73}$$

Combining all these expressions, and setting $\rho_{\rm B} = \rho_0$, we finally obtain the expression for the incompressibility coefficient:

$$K_0 \ = \ \frac{3k_{0\rm F}^2}{E_{0\rm F}^*} - \left(\frac{M_0^*}{E_{0\rm F}^*}\right)^2 \frac{9\rho_0}{A_0+B_0} + \frac{9\rho_0}{C_0} \ , \tag{2.74}$$

where

$$C = \frac{1}{c_{\rm v}^2} + \frac{\zeta}{2}W_0^2 \ , \tag{2.75}$$

while the index "0" in these expressions stands for the values calculated at saturation density.

Using the equation of motion for scalar field (2.21) it can be shown that the derivative of the energy density at saturation will be equal to the Fermi energy, μ:

$$\frac{\partial \mathcal{E}}{\partial \rho} = W_0 + E^*_{0\mathrm{F}} \equiv \mu \ . \tag{2.76}$$

Since at saturation $\mathcal{E}/\rho$ has a minimum:

$$0 = \frac{\partial(\mathcal{E}/\rho)}{\partial \rho} = \frac{1}{\rho}\left(\frac{\partial \mathcal{E}}{\partial \rho} - \frac{\mathcal{E}}{\rho}\right) \ . \tag{2.77}$$

Combining these expressions we obtain a simple formula for the meson field at saturation:

$$W_0 = \epsilon_0 - E^*_{0\mathrm{F}} + M \ . \tag{2.78}$$

Given the bulk parameters, and employing the equations (2.61), (2.62), and (2.74) we can now invert them to obtain the values of c_{s}^2, κ, and λ. Similarly, using the equation of motion (2.22) and the expression for the meson field at saturation, (2.78), we can find c_{v}^2:

$$c_{\mathrm{v}}^2 = \frac{W_0}{\rho_0 - \frac{\zeta}{6} W_0^3} \ . \tag{2.79}$$

Note the value of c_{v}^2 will vary as one tunes the empirical parameter ζ.

In the previous section we have provided with an expression for the bulk symmetry energy, J. This coefficient can be easily calculated, using the equation of motion (2.23) in the expression for the energy density:

$$J = \frac{k_{0\mathrm{F}}^2}{6E^*_{0\mathrm{F}}} + \frac{\frac{k_{0\mathrm{F}}^3}{12\pi^2}}{\frac{1}{c_\rho^2} + 2\Lambda_{\mathrm{v}} \left(W_0\right)^2} \ . \tag{2.80}$$

Given the value of parameter Λ_{v}, and the bulk symmetry energy, now we are able to calculate the parameter c_ρ^2.

2.3 Applications

2.3.1 Symmetric Nuclear Matter

In this work we will be using several relativistic mean-field models that have been accurately calibrated to the properties of infinite-nuclear matter (MS) [16], to the ground-state properties of finite nuclei (NL3) [14], or to both (FSUGold) [15]. Parameter sets for these three models are listed in Table 2.1 and Table 2.2.

Table 2.1: Parameter sets for the mean-field models used in the text. The parameter κ is given in MeV.

Model	$g_{\rm s}^2$	$g_{\rm v}^2$	g_ρ^2	κ	λ	ζ	$\Lambda_{\rm v}$
NL3	104.3871	165.5854	79.6000	3.8599	−0.01591	0.00	0.00
MS	111.0428	216.8998	70.5941	0.5083	+0.02772	0.06	0.00
FSUGold	112.1996	204.5469	138.4701	1.4203	+0.02376	0.06	0.03

Table 2.2: The σ, ω, and ρ meson masses ($m_{\rm s}$, $m_{\rm v}$, and m_ρ) for each three mean-field models are given in MeV. The nucleon mass has been fixed at $M = 939$ MeV in all the models.

Model	$m_{\rm s}$	$m_{\rm v}$	m_ρ
NL3	508.194	782.501	763.000
MS	485.000	782.500	763.000
FSUGold	491.500	782.500	763.000

As an illustration, we use the FSUGold model to calculate the energy per nucleon in symmetric nuclear matter. The result is given in Fig. 2.1. From the figure one can see that at high densities the system is unbound, i.e. $E/N > M$. This is due to the vector repulsion which is dominated at high densities. At intermediate densities, the attraction force from the scalar field will dominate and the system saturates. For the FSUGold model this corresponds to the Fermi momentum of $k_{\rm F} = 1.30$ fm^{-1}, and binding energy of $\epsilon_0 = -16.30$ MeV. The coupling constants are chosen to reproduce the bulk nuclear parameters: $K_0 = 230.0$ MeV, $M^* = 0.61\ M$, and $J = 32.59$ MeV.

As illustrated in Fig. 2.2, the solution of the self-consistency equation (2.63) for M^* yields a nucleon effective mass that is a decreasing function of density. At low densities it is close to the value of the nucleon mass, while at ordinary nuclear densities the value of the effective mass significantly reduces. This is the consequence of large condensed scalar field Φ_0, which is equal to 366.2 MeV for the FSUGold model at saturation density. This results in a large attractive contribution to the energy per nucleon. Correspondingly, there is a large repulsive contribution to E/N from the vector field ($W_0 = 295.1$ MeV for the FSUGold model). The small nuclear binding energy of $\epsilon_0 = -16.3$ MeV therefore arises from the

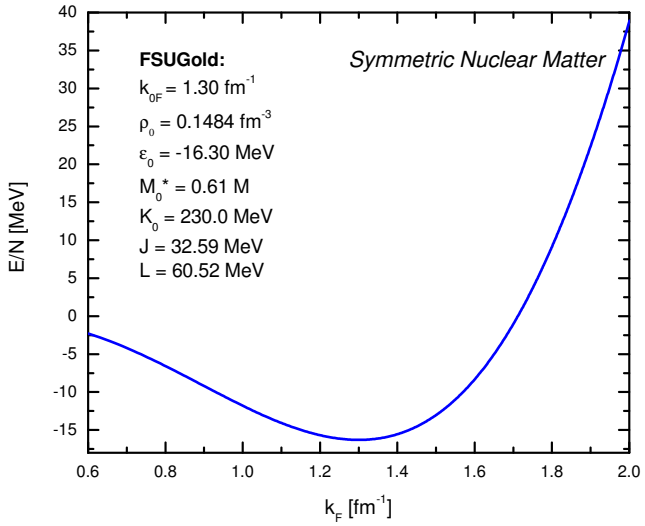

Figure 2.1: Saturation curve for symmetric nuclear matter. The energy per nucleon is calculated in the FSUGold model discussed in the text [15].

cancelation between the large scalar attraction and vector repulsion. This is a particular property of the Lorentz structure that is not present in the non-relativistic calculations.

2.3.2 Asymmetric and Pure Neutron Matter

Decreasing the proton fraction Y_p we obtain the energy per nucleon which is less bound at normal nuclear densities (Fig. 2.3). For the FSUGold model the system is unbound at about $Y_p < 0.085$. In particular, the energy per nucleon for the pure neutron matter is totally unbound. This result is due to the symmetry energy that increases as the neutron-proton asymmetry parameter becomes large.

In Fig. 2.4 we plot the equation of state–the relation between the pressure and the energy density–of the pure neutron matter within the FSUGold model. At very high densities the system approaches the causality limit, $P = \mathcal{E}$, which is the stiffest possible equation of state. A similar equation of state is used in the core of neutron stars that will be discussed in details in next chapter. The neutron-star matter equation of state, however, is not composed of

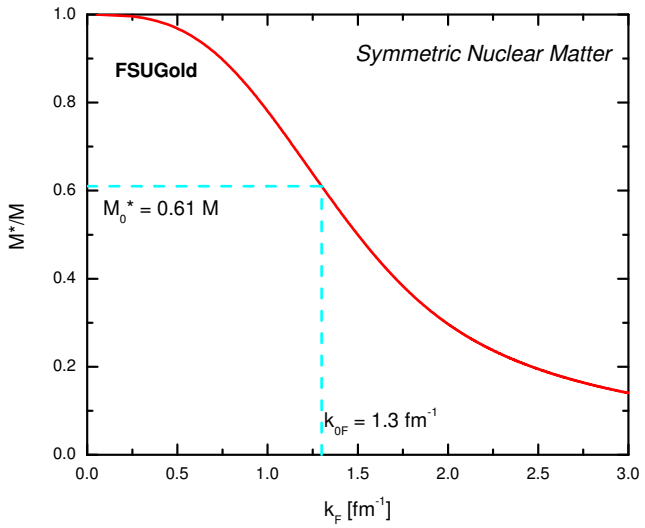

Figure 2.2: The nucleon effective mass as a function of Fermi momentum (or density) for symmetric nuclear matter. The result is calculated using the FSUGold model.

neutrons alone, rather includes other degrees of freedom, such as protons, electrons, and muons.

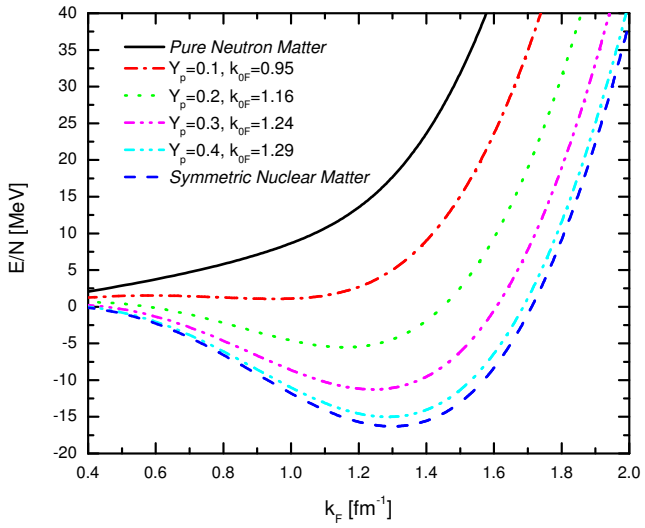

Figure 2.3: Saturation curve for different values of the proton fraction Y_p. For $Y_p < 0.085$, the system is unbound for all densities in the FSUGold model [15].

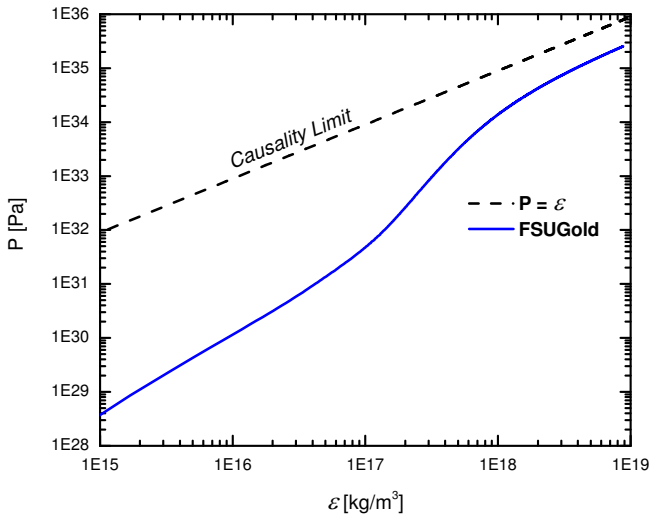

Figure 2.4: Equation of state for pure neutron matter in the FSUGold model [15].

CHAPTER 3

NEUTRON STARS AND THEIR PROPERTIES

3.1 Structure of Neutron Stars

Neutron stars are compact stellar objects that result from the gravitational collapse of massive stars during the supernovae event of type II, type Ib, and type Ic. They have typical masses of $\sim 1.4\ M_{\odot}$ and radii of $\sim 10\ km$. The density inside neutron stars spans many orders of magnitude and may reach values up to 10 times normal nuclear densities ($\rho_0 = 2.4 \cdot 10^{14}\ g/cm^3$) in the core. Neutron stars were originally discovered as *pulsars* (1967) [45], the fast spinning stellar objects that are observed by their electromagnetic dipole radiation. The rotation periods of such compact stars are in the range of milliseconds to few seconds. In addition, neutron stars are the sources of very strong magnetic fields with typical values of $\sim 10^{12}\ Gauss$. Highly magnetized neutron stars, *magnetars*, have also been observed with magnetic field of $B \sim 10^{15}\ Gauss$. Depending on their observable characteristics neutron stars are classified into pulsars, magnetars, *X-ray bursters*, *soft gamma repeaters*, etc.

Current theories of neutron stars suggest that one can subdivide the neutron star into the *atmosphere*, the *outer crust*, the *inner crust*, the *outer core* and the *inner core* [4, 20, 51]. A tomographic picture of a neutron star is shown in figure 3.1. The **atmosphere** of the star is a thin plasma layer of thickness $\sim 10\ cm$, and its dynamics is fully governed by the strong magnetic field. The knowledge of the radiation physics in the atmosphere is very important as it contains valuable information on the surface layer compositions and on the masses and radii of neutron stars.

The **outer crust** is the region of the star, where the density ranges from $\rho \simeq 10^4\ g/cm^3$ to $\rho \simeq 4 \times 10^{11}\ g/cm^3$ [46]. The thickness of this region is about ~ 100 meters. The matter in

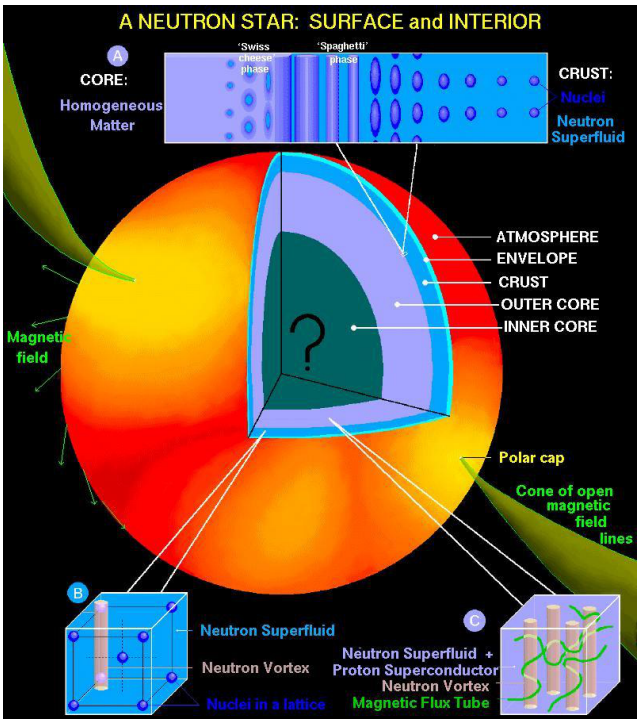

Figure 3.1: A schematic picture of a neutron star. While theoretical models predict the physics of the atmosphere, the crust, and the outer core, the physics of the inner core still remains a mystery as of today (Image credit: Dany Page)

the outer crust consists of ions, electrons, and nuclei. At these densities, the electrons have been pressure ionized and move freely throughout the envelope [47]. This pressure is mainly provided by the degenerate electron gas, which is an ultra-relativistic gas. On the other hand, at these low nuclear densities the uniform matter is unstable against cluster formation. Therefore, the nucleons form clusters of ^{56}Fe nuclei, which in turn arrange themselves in a crystalline face-centered-cubic lattice in order to minimize their overall Coulomb repulsion [48]. This large part of the envelope is solidified, and therefore is known as *crust*. As density increases, the electrons' Fermi energy also increases, and they are captured by the protons through an inverse beta reaction. The excess energy will be carried out by neutrinos, while the nuclei become more neutron-rich. In Chapter 2 we have discussed the nuclear symmetry energy, a quantity that imposes penalty on the system as it departs from the symmetric nuclear matter. At present, the symmetry energy, hence the nuclear masses with large

neutron excess in the outer crust, is poorly understood. The outer crust ends when the neutron-rich nuclei reach the critical density of the neutron drip line, $\rho \simeq 4 \times 10^{11}\ g/cm^3$. At this point the nuclei cannot hold any more neutrons: they drip out.

The density of **inner crust** starts from the neutron drip-line and may reach up to $\simeq 0.5\rho_0$. This region is about one kilometer thick depending on the models of the nuclear equations of state. As the density keeps increasing, the nuclei experience several phase transitions due to the competition between long-range Coulomb potential and short-range nuclear attraction. These phases are known as *nuclear pasta* phases [49, 50]. At present, the transition from a highly ordered crystalline phase to a uniform matter remains one of the main mysteries.

Most of the mass of the neutron star is located in the more dense region known as the *core*. Indeed, making up almost 10 % of the size of neutron stars, the crust has only about 2 % of the total mass. On the other hand, the total mass of the neutron star is intimately related to the equation of state that is governed the core of the star. The cleanest constraint on the high density equation of state (from $0.5\rho_0$ to several nuclear saturation density), will therefore come from the astrophysical measurement of the maximum mass of the neutron star (or the minimum mass of a black hole as a supernovae remnant). The **outer core** is the *theoretically* known region of the star that is several kilometers thick and occupies the region of $0.5\rho_0 < \rho < 2\rho_0$. It mainly consists of neutrons, protons, and electrons. Muons are created when the energy of electrons reach the muon mass threshold. The whole system in the outer core is in the state of beta equilibrium with electrons and muons. The deepest region of the star is known as the **inner core** with $\rho > 2\rho_0$, and it spans over several kilometers. The equation of state for this region is very model dependent. Several hypotheses of the existence of exotic states of new fermion and boson condensates have been put forward, such as, hyperonization of matter, pion condensation, kaon condensation, and quark matter.

3.2 Equations of Stellar Structure

3.2.1 Tolman-Oppenheimer-Volkoff Equation

One of the characteristic properties of neutron stars is their compactness. The Schwarzschild gravitational radius for such stars is very close to their own radius. Therefore, the structure of neutron stars must be studied in a general relativistic framework. The importance of general relativistic effects are usually characterized by the so-called compactness parameter that is defined as

$$\frac{R_g}{R} = \frac{2GM}{c^2 R} = \left(\frac{v_{\rm esc}}{c}\right)^2 , \tag{3.1}$$

where $v_{\rm esc}$ is the escape velocity. For most neutron stars the compactness parameter is of the order of $0.2 < R_g/R < 0.4$, while for regular stars, $R_g/R \ll 1$. For example, for white dwarf stars, $R_g/R \sim 10^{-4}$, and for the Sun, $R_g/R \simeq 4.25 \cdot 10^{-6}$. On the other extreme, stars whose radius is smaller or equal to R_g are known as black holes, and the region R_g is known as an event horizon. Therefore, neutron stars are the most compact known objects without the event horizon, which serve as extraordinary laboratories for general relativity, and dense matter physics. Moreover, neutron stars provide a natural meeting place for nuclear physics and astrophysics.

In order to maintain stability against gravitational collapse the star should be in hydrostatic equilibrium. The hydrostatic configuration of a neutron star is obtained by the compensation of the strong gravitational pressure (inward from the surface of the neutron star) and the outward pressure of the nuclear matter. Once the nuclear equation of state is obtained, one can compute the stellar properties using the framework of general relativity. For a qualitative analysis one could, in principle, use the Newtonian equation for gravity. However, quantitatively, Newtonian gravity is insufficient to fully describe the nature of neutron stars. Indeed, the maximum mass calculated using the Newtonian gravity and the simplest equation of state (the ideal Fermi gas of neutrons), will give a maximum mass of a neutron star, which is equal to about $5.6 M_\odot$. The first general relativistic consideration by Oppenheimer, Volkoff [22], and Tolman [21] showed that this value could be as low as $0.7 M_\odot$. In addition, we will consider several approximate models of neutron-star structure. For example, the star could be approximated by a stationary, spherically-symmetric configuration. However, most neutron stars are spinning objects (pulsars) and therefore a rotating,

axially symmetric spacetime metric may be more realistic. In this study, however we will mostly study slowly rotating neutron stars, where the effect of rotation can be considered only to the first order [52].

The relation between the spacetime geometry and the properties of matter is given by the Einstein field equations,

$$R_{\mu\nu} - \frac{1}{2} g_{\mu\nu} R = 8\pi T_{\mu\nu} \ , \tag{3.2}$$

where $R_{\mu\nu}$ is the Ricci tensor and $R = R^{\mu}{}_{\mu}$ is the Ricci scalar. We treat the neutron star matter as a perfect fluid (the viscous terms and shear stresses are negligibly small compared to the pressure).

The cornerstone of our approach is the *slow-rotation approximation* pioneered by Hartle and Thorne [52, 53]. We assume that the neutron star is rotating uniformly with a stellar frequency Ω that is far smaller than the Kepler frequency at the equator. That is,

$$\Omega \ll \Omega_{\rm max} \approx \sqrt{\frac{GM}{R^3}} \ . \tag{3.3}$$

The space-time metric for such a uniformly rotating axially symmetric compact object is given by Boyer-Lindquist coordinate system $(t,\, r,\, \theta,\, \phi)$ which in the slow-rotation approximation (first order in the angular velocity) [52, 53, 54] can be cast into

$$ds^2 = -e^{2\nu(r)} dt^2 + e^{2\lambda(r)} dr^2 + r^2 d\theta^2 + r^2 \sin^2\theta d\phi^2 - 2\omega(r) r^2 \sin^2\theta dt d\phi \ , \tag{3.4}$$

where $\nu(r)$ and $\lambda(r)$ are the radially varying metric functions governed by

$$e^{-2\lambda(r)} = 1 - \frac{2GM(r)}{r} \ , \tag{3.5}$$

$$\frac{d\nu(r)}{dr} = G \frac{M(r) + 4\pi r^3 P(r)}{r^2 \left(1 - \frac{2GM(r)}{r}\right)} \ , \tag{3.6}$$

with the boundary condition at the surface of the star, $r = R$,

$$\nu(R) = -\lambda(R) \ , \tag{3.7}$$

and $M(r)$ is the total mass within radius r

$$M(r) = \int_0^r 4\pi \mathcal{E}(r) r^2 \ . \tag{3.8}$$

In this approximation the pressure gradient inside the spherically symmetric configuration is then governed by the so-called Tolman-Oppenheimer-Volkoff equation

$$\frac{dP(r)}{dr} = -G\frac{\Big(\mathcal{E}(r)+P(r)\Big)\Big(M(r)+4\pi r^3 P(r)\Big)}{r^2\Big(1-2GM(r)/r\Big)}\,, \tag{3.9}$$

where $\mathcal{E}(r)$ is the energy density at r. These equations should be supplemented by an equation of state, namely, a relation between the pressure P and the energy density $\mathcal{E}$, $P = P(\mathcal{E})$). The above equations then form a closed system of equations, that has to be integrated from the center of the star to the surface with the boundary conditions $M(0) = 0$ and $P(0) = P_c$. Given boundary conditions the TOV equations may be solved once an equation of state is supplied. In particular, the stellar radius R and mass M are determined from the following two conditions: $P(R)=0$ and $M=M(R)$.

3.2.2 Moment of Inertia

The general relativistic formalism—even in the slow-rotation approximation—is subtle, primarily due to the dragging of local inertial frames. The expression for the moment of inertia of an axisymmetric star in hydrostatic equilibrium is derived in great detail in Refs. [51, 52], so we only summarize here some of the most important results. For a more pedagogical discussion one may consult the text by Glendenning [20].

In the slow-rotation (first order in the angular velocity) approximation the moment of inertia of a uniformly rotating, axially symmetric neutron star is given by the following expression:

$$I \equiv \frac{J}{\Omega} = \frac{8\pi}{3}\int_0^R r^4 e^{-\nu(r)}\frac{\bar{\omega}(r)}{\Omega}\frac{\Big(\mathcal{E}(r)+P(r)\Big)}{\sqrt{1-2GM(r)/r}}dr\,, \tag{3.10}$$

where J is the angular momentum,

$$J = \int T^0_\nu \xi^\nu_{(\phi)}\sqrt{-g}d^3x\,, \tag{3.11}$$

$\xi^\nu_{(\phi)}$ is the Killing vector in the azimuthal direction reflecting axisymmetry, g is the determinant of the metric tensor, $\nu(r)$ and $\bar{\omega}(r)$ are radially-dependent metric functions, and $M(r)$, $\mathcal{E}(r)$, and $P(r)$ are the stellar mass, energy density, and pressure profiles, respectively. Perhaps the greatest advantage of the slow-rotation approximation is that all the quantities appearing in Eq. (3.10) may be assumed to remain spherically symmetric.

As alluded earlier, in the slow-rotation approximation the spherically symmetric metric functions $\nu(r)$ and $\lambda(r)$ remain unchanged from their values obtained in the limit of a non-rotating, static, and spherically symmetric neutron star. In particular, $\lambda(r)$ was simply related to the mass profile $M(r)$ by

$$g_{11}(r) = e^{2\lambda(r)} = \Big(1 - 2GM(r)/r\Big)^{-1} \,. \tag{3.12}$$

Further, $\nu(r)$ can be determined from solving a first-order differential equation (3.6) or, equivalently, from evaluating the following integral:

$$\nu(r) = \frac{1}{2}\ln\left(1 - \frac{2GM}{R}\right) - G\int_r^R \frac{\Big(M(x) + 4\pi x^3 P(x)\Big)}{x^2\Big(1 - 2GM(x)/x\Big)}dx \,. \tag{3.13}$$

Finally, one must determine the metric function $\omega(r)$—the one new ingredient that emerges from the slow rotation and which has no counterpart in Newtonian gravity. The frequency $\omega(r)$ appears as a consequence of the dragging of local inertial frames by the rotating star; the so-called Lense-Thirring effect. The *effective* (or relative) frequency $\bar{\omega}(r) \equiv \Omega - \omega(r)$ appearing in Eq. (3.10) represents the angular velocity of the fluid as measured in a local inertial reference frame. In particular, the *dimensionless* relative frequency $\widetilde{\omega}(r) \equiv \bar{\omega}(r)/\Omega$ satisfies the following second-order differential equation:

$$\frac{d}{dr}\left(r^4 j(r)\frac{d\widetilde{\omega}(r)}{dr}\right) + 4r^3\frac{dj(r)}{dr}\widetilde{\omega}(r) = 0 \,, \tag{3.14}$$

where

$$j(r) = e^{-\nu(r)-\lambda(r)} = \begin{cases} e^{-\nu(r)}\sqrt{1 - 2GM(r)/r} & \text{if } r \le R \,, \\ 1 & \text{if } r > R \,. \end{cases} \tag{3.15}$$

Note that $\widetilde{\omega}(r)$ is subject to the following two boundary conditions:

$$\widetilde{\omega}'(0) = 0 \,, \tag{3.16a}$$

$$\widetilde{\omega}(R) + \frac{R}{3}\widetilde{\omega}'(R) = 1 \,. \tag{3.16b}$$

Also note that in the slow-rotation approximation the moment of inertia does not depend on the stellar frequency Ω. In practice, one chooses an arbitrary value for the central frequency $\widetilde{\omega}_c = \widetilde{\omega}(0)$ and numerically integrates Eq. (3.14) up to the edge of the star. In general, the boundary condition at the surface [Eq. (3.16b)] will not be satisfied for an arbitrary choice of

$\widetilde{\omega}_c$, so one must rescale the function and its derivative by an appropriate constant to correct for the mismatch.

The procedure described above provides all the necessary steps to compute the integrand in Eq. (3.10). The moment of inertia is then obtained by performing the one remaining integral using standard numerical techniques. Having solved for both $\widetilde{\omega}(r)$ and I, one could check the consistency of the formalism by ensuring that the following equation is satisfied:

$$\widetilde{\omega}'(R) = \frac{6GI}{R^4} \ . \tag{3.17}$$

3.3 Measurement of the Neutron Star Observables

Presently, the density slope of the symmetry energy at saturation is known with very large error-bars, $L \simeq 60 \pm 30$ MeV. Various nuclear models predict different values of the density slope at high densities that are even more diverse from its saturation value. This results in the density dependence of the symmetry energy that is totally unconstrained in the intermediate and high densities. It is shown that the density slope is highly correlated with the neutron radius of heavy nuclei (See Ref. [55] and references therein). Thus the measurement of the neutron radius of ^{208}Pb in PREx, for example, could significantly constrain the density dependence of the symmetry energy, on terrestrial grounds. On the other hand, the radius of a neutron star is highly correlated with the neutron radius of heavy nuclei. Although they differ by 18 orders of magnitude, it is not surprising that they should be well correlated, since both depend on the same microphysics: the equation of state of neutron-rich matter.

The observational measurement of neutron star radii is therefore very important, not only from the astrophysical point of view, but also in the understanding of nuclear systems with large isospin asymmetry. Observationally, there are only few ways to determine the radius of a neutron star. Let us start with the gravitational redshift, which in the slow-rotation approximation can be written as

$$z \approx \frac{1}{\sqrt{1 - \frac{2GM}{R}}} - 1 \ . \tag{3.18}$$

Here the Doppler effect due to the rotation of the equator has been neglected. It is an extremely difficult task to measure the gravitational redshift of signals emitted from the

surface of neutron stars, mainly due to the strong surface magnetic field. However, there have been some claims of identification of spectral lines. In particular, for the low-mass X-ray binary EXO 0748-676, the gravitational redshift is found to be $z \simeq 0.345$ [63]. However, the identification of the spectral lines is not universally accepted [64]. While the mass of the neutron star can be measured fairly accurately in binary systems, the measurement of its radius is quite complicated. Another reliable way to measure the radius [3] is from the observations of thermal emissions from neutron star surfaces, which yield values for the so-called "radiation radius", $R_\infty = R/\sqrt{1-2GM/R}$. This results from a combination of flux and temperature measurements from the neutron star's surface both redshifted at the Earth. The simultaneous measurement of z and R_∞ would therefore determine the radius and the mass of the neutron star:

$$R = \frac{R_\infty}{1+z} \ , \tag{3.19}$$

$$M = \frac{R_\infty}{2G(1+z)}\left(1 - \frac{1}{(1+z)^2}\right) \ . \tag{3.20}$$

However, there are some major uncertainties involved in the determination of R_∞ such as the distance, interstellar absorption, and details concerning the composition of the atmosphere and its magnetic field strength [3]. In the description above, even though the redshift can be determined, R_∞ would still depend on the interstellar distance, d, which may not be well measured in the near future. Therefore, one will need an additional relation involving M, R and d.

Recently, there have been a great deal of attention to the the X-ray binary sources being as potential sources to the simultaneous determination of the mass and radius of neutron stars [11, 12]. Although these methods of measurement are not free of uncertainties (discussed below), it is a very intriguing possibility, since the simultaneous measurement of mass and radius will pin down the correct equation of state of nuclear matter.

When a neutron star in a binary system accretes matter from its companion star, the temperature of the infalling gas reaches the critical point for thermonuclear fusion. This results in a rapid hydrogen burning with a very high energy release in the X-ray spectra, which is known as the X-ray bursts. There are three important observables whose knowledge, if combined, gives tight, uncorrelated constraints on the masses and the radii of neutron stars.

The first observable is the apparent angular surface area, A, which during the subsequent cooling phase of the bursts can be written as

$$A = \frac{R^2}{d^2 f_c^4} \left(1 - \frac{2GM}{R}\right)^{-1} , \tag{3.21}$$

where $f_c = (T_\infty / T_{\rm eff})$ is a color factor, T_∞ is the observed color (spectral) temperature, $T_{\rm eff}$ is the effective blackbody temperature, and d is the distance to the source. For some subsets of X-ray bursters the flux becomes so high that it exceeds the local Eddington limit (the limit at which the gravitational force equals the continuum radiation force outwards). This further lifts the photosphere of the neutron star to a larger radius. During the subsequent cooling the photosphere returns to the neutron star's surface. The Eddington flux at this "touchdown" point is:

$$F_{\rm Edd} = \frac{GM}{\kappa d^2} \sqrt{1 - \frac{2GM}{R}} , \tag{3.22}$$

where $\kappa = 0.2(1+X)$ cm^2 g^{-1} is the electron scattering opacity in the stellar atmosphere, X is the hydrogen mass function. Combining the measurements of the Eddington flux, $F_{\rm Edd}$, the apparent angular surface area, A, and the distance to the binary sources, d, one can finally obtain both M and R.

With these assumptions, recently Özel et. al. [11] have performed measurements of masses and radii of three X-ray bursters 4U 1608-52, EXO 1745-248, and 4U 1820-30. The results are summarized in Fig. 3.2. Note that even though the high resolution of X-ray spectroscopy with the Chandra X-ray observatory and XMM-Newton has lead to a detailed measurement of the X-ray spectra, the uncertainties are still too large to be ignored. On the other hand, the interstellar distances has still to be known. Steiner et. al. [12] have shown that the photospheric radius at touchdown may, in fact, be a little larger than then the neutron star radius (See Fig. 3.2). This analysis is further confirmed by the independent studies of [65]. Thus different analysis so far give different radii for typical $1.4 M_\odot$ neutron stars: ~ 10 km in [11], ~ 12 km in [12], and ~ 14 km in [65]. Further refinements from the observational front is thus very important.

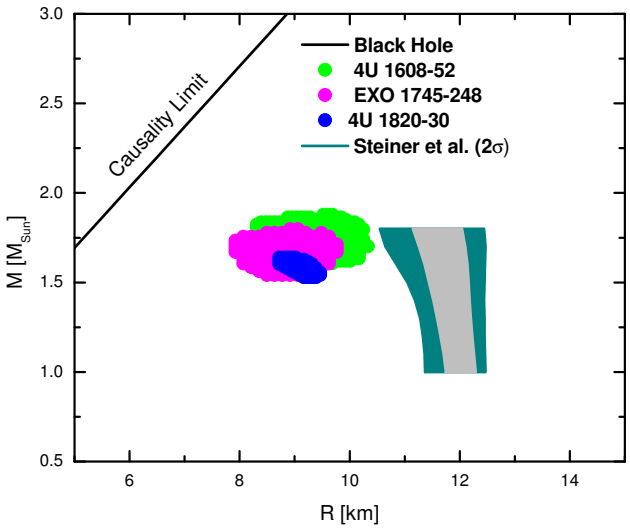

Figure 3.2: 1σ confidence contours for the masses and radii of three neutron stars in binaries 4U 1608-52 (green), EXO 1745-248 (magenta), and 4U 1820-30 (blue) [11]. The 1σ (dashed grey region), and 2σ (the dashed cyan region) confidence contours from the mass-vs-radius analysis of [12]. The solid black line corresponds to the Schwarzschild limit of an event horizon.

3.4 The crustal moment of inertia

It has been suggested that *pulsar glitches*, namely, the sudden increase in the spin rate of pulsars, may place important constraints on the equation of state [1, 56]. In particular, an analysis based on a long time observation of glitches of the Vela pulsar suggests that at least 1.4% of the total moment of inertia must reside in the non-uniform crust [1, 56]. This is interesting as the crustal moment of inertia is particularly sensitive to the transition pressure at the core-crust interface and this observable is believed to be correlated to the density-dependence of the symmetry energy [57, 58, 59, 60]. Thus, it is both interesting and enlightening to obtain analytic expressions for the crustal moment of inertia.

The crustal moment of inertia is defined in terms of the general expression provided in Eq. (3.10) but with the range of the integral now limited from the transition (or core) radius

R_t to the stellar radius R. That is,

$$I_{cr} = \frac{8\pi}{3}\int_{R_t}^{R} r^4 e^{-\nu(r)}\widetilde{\omega}(r)\frac{\Big(\mathcal{E}(r)+P(r)\Big)}{\sqrt{1-2GM(r)/r}}dr\ . \tag{3.23}$$

However, given that the crust is thin and the density within it is low, several approximation have been proposed that help render the integral tractable [1, 3, 56, 61, 62]. The various approximations and details on how to evaluate the integral are left to the appendix. In particular, we show that under those approximations the TOV equation may be solved exactly. Here, however, we simply quote our final result:

$$I_{cr} \approx \frac{16\pi}{3}\frac{R_t^6 P_t}{R_s}\left[1-\left(\frac{R_s}{R}\right)\left(\frac{I}{MR^2}\right)\right]\left[1+\frac{48}{5}(R_t/R_s-1)(P_t/\mathcal{E}_t)+\ldots\right]\ , \tag{3.24}$$

where $R_s=2GM$ is the Schwarzschild radius of the star, and $P_t=P(R_t)$ and $\mathcal{E}_t=\mathcal{E}(R_t)$ are the pressure and energy density at the core-crust interface. The *ellipsis* in the above equation indicates that the derivation was carried out to first order in the small quantity $P_t/\mathcal{E}_t \lesssim 0.01$. A few comments are in order. First, the above expression for the crustal moment of inertia is extremely accurate (of the order of a few percent; see Tables 4.1 and 4.2). Second, the two terms in brackets in Eq. (3.24) provide each a moderate $\sim$10% correction to the leading term, with the corrections being of opposite sign. Third, although the crustal moment of inertia still depends on the total moment of inertia I, one may preserve the accuracy of our result without having to rely on a highly accurate estimate of I. In particular, by using the simple relationship proposed in Ref. [62], namely,

$$\frac{I}{MR^2} = \frac{0.21}{1-R_s/R}\ , \tag{3.25}$$

one obtains

$$I_{cr} \approx \frac{16\pi}{3}\frac{R_t^6 P_t}{R_s}\left[1-\frac{0.21}{(R/R_s-1)}\right]\left[1+\frac{48}{5}(R_t/R_s-1)(P_t/\mathcal{E}_t)+\ldots\right]\ . \tag{3.26}$$

This expression remains extremely accurate, yet has the added appeal that for a neutron star with a given mass M (or R_s) and radius R, the crustal moment of inertia depends exclusively on R_t, P_t, and $\mathcal{E}_t$—all quantities that are expected to be sensitive to the density dependence of the symmetry energy. Note that the approximation for the total moment of inertia given in Eq. (3.25) has been put into question in Ref. [1]. However, for our purposes

such an approximation is adequate as I enters into the expression for the crustal moment of inertia as a small correction. No such approximation will be made for I when reporting the *fractional* moment of inertia I_{cr}/I. Indeed, no approximation for I will be made at all.

For completeness, we include an expression for the crustal mass that was derived in the appendix following similar steps. We obtain,

$$M_{cr} \approx 8\pi R_t^3 P_t (R_t/R_s - 1)\left[1 + \frac{32}{5}(R_t/R_s - 3/4)(P_t/\mathcal{E}_t) + \ldots\right] . \tag{3.27}$$

3.5 Beta Equilibrium with Electrons and Muons

At high densities (inside the neutron stars) the equation of state must be modified. The most important correction to the equation of state comes from the inverse beta decay: $e^- + p \rightarrow n + \nu_e$. Given that neutron-star matter is fully catalyzed, chemical equilibrium must be imposed:

$$n \rightleftharpoons p + e^- + \bar{\nu}_e . \tag{3.28}$$

If the Fermi momentum of electrons is high enough, then the contribution from muons also must be included in the equation of state: $e^- \leftrightharpoons \mu^- + \bar{\nu}_\mu + \nu_e$. Namely, the composition of the star is determined from the equality of the chemical potential of the various species. That is,

$$\mu_n = \mu_p + \mu_e = \mu_p + \mu_\mu . \tag{3.29}$$

Here

$$\mu_n = \sqrt{k_{\rm F}^{n2} + M^{*2}} + W_0 - \frac{1}{2}R_0 , \tag{3.30}$$

$$\mu_p = \sqrt{k_{\rm F}^{p2} + M^{*2}} + W_0 + \frac{1}{2}R_0 . \tag{3.31}$$

Note that electrons and muons are assumed to behave as relativistic free Fermi gases (with $m_e \equiv 0$):

$$\mu_\mu = \sqrt{k_{\rm F}^{\mu 2} + m_\mu^2} , \tag{3.32}$$

$$\mu_e = \sqrt{k_{\rm F}^{e2} + m_e^2} = k_{\rm F}^e . \tag{3.33}$$

Of course, muons appear in the system only after the electronic Fermi momentum becomes equal to the muon rest mass. Neutron stars are also believed to be charge neutral objects, therefore the condition of charge neutrality must be imposed:

$$\rho_p = \rho_e + \rho_\mu \ . \tag{3.34}$$

Then the total energy density and the pressure of a star are simply obtained by adding up the nucleonic and the leptonic contributions. The nucleonic contributions are given as in chapter 2, while the leptonic contributions are:

$$\mathcal{E}_e = \frac{k_{\rm F}^{e4}}{4\pi^2} \ , \tag{3.35}$$

$$\mathcal{E}_\mu = \frac{1}{\pi^2}\int_0^{k_{\rm F}^\mu} k^2\sqrt{k^2+m_\mu^2}\,dk \tag{3.36}$$

Numerically, one can achieve the chemical equilibrium condition through the following steps:

1. Provide the baryon density as an input, $\rho_{\rm B}$;

2. Make an initial guess for the proton fraction, Y_p;

3. Using the following relations,

$$k_{\rm F}^p = (2Y_p)^{1/3}\,k_{\rm F} \ , \tag{3.37}$$

$$k_{\rm F}^n = \left[2\,(1-Y_p)\right]^{1/3}\,k_{\rm F} \ , \tag{3.38}$$

   find the corresponding proton and neutron Fermi momentums. Here $k_{\rm F}$ is defined such that:

$$\rho_{\rm B} = \frac{k_{\rm F}^{p3}}{3\pi^2} + \frac{k_{\rm F}^{n3}}{3\pi^2} = \frac{2k_{\rm F}^3}{3\pi^2} \ ; \tag{3.39}$$

4. Solve the system of equations for charge neutrality and chemical equilibrium,

$$k_{\rm F}^{p3} = k_{\rm F}^{e3} + k_{\rm F}^{\mu 3} \ , \tag{3.40}$$

$$k_{\rm F}^{\mu 2} + m_\mu^2 \equiv k_{\rm F}^{e2} \ , \tag{3.41}$$

   to obtain the electron and the muon Fermi momentums;

5. Having $k_{\rm F}^n$, $k_{\rm F}^p$, $k_{\rm F}^e$, and $k_{\rm F}^\mu$ obtained, use them to calculate the total energy density, $\mathcal{E}$;

6. Now, using the Newton-Raphson or some other numerical technique, find the proton fraction, Y_p, that minimizes the total energy density, $\mathcal{E}$ (the condition for the chemical equilibrium):

$$\frac{\partial \mathcal{E}}{\partial Y_p} = 0 \ ; \tag{3.42}$$

7. Having found the correct proton fraction, we can now compute the total energy density and the total pressure, i.e. the equation of state for stellar matter.

3.6 The Scaling of the Parameters

An important step in the numerical calculations of the neutron star structure equations is the scaling of the parameters. Indeed, we are dealing with two systems that differ 57 order of magnitude in mass scale (mass of the neutron is $m_n = 1.68 \cdot 10^{-27}$ kg, while mass of a typical neutron star is $M_{1.4} = 2.78 \cdot 10^{30}$ kg), and 18 order of magnitude in the length scale (the ~ 5.7 fm of the neutron radius of lead versus the ~ 12 km radius of the neutron star). Without properly scaling the equations, there is almost no hope of dealing with the problem of the neutron star structure, numerically [66].

Recall that we had the following term in the pressure of the infinite nuclear matter (2.41):

$$\begin{aligned} P_n &= \frac{1}{3\pi^2} \int_0^{k_{\rm F}^n} \frac{k^4}{E_k^*} \, dk \ , \\ &= \frac{1}{8\pi^2} \left[M^{*4} \ln \left(\frac{k_{\rm F}^n + E_{n{\rm F}}^*}{M^*} \right) + \left(\frac{2}{3} k_{\rm F}^{n2} - M^{*2} \right) k_{\rm F}^n E_{n{\rm F}}^* \right] \ . \end{aligned} \tag{3.43}$$

Observing this expression, the natural scale for the pressure, therefore would be

$$P_0 = \frac{M^4}{8\pi^2} \equiv \frac{1}{8\pi^2} \frac{\left(Mc^2\right)^4}{(\hbar c)^3} = 1281.48445 \quad \text{MeV fm}^{-3} = 2.05316422 \cdot 10^{35} \quad \text{Pa} \ . \tag{3.44}$$

Note that a typical pressure at the center of neutron stars is about ~ 100 MeV fm^{-3}, which is of the similar order as the natural scale. Therefore the total pressure can be recast as $P = P_0 \overline{P}$, where $\overline{P}$ is a dimensionless pressure used in numerical calculations. Similarly, for the energy density one can use $\mathcal{E} = \mathcal{E}_0 \overline{\mathcal{E}} = P_0 \overline{\mathcal{E}}$ (the central energy density in the neutron stars is about ~ 1000 MeV fm^{-3}). The natural scale for the mass density is

$$\rho_0 = \frac{P_0}{c^2} = 2.28445328 \cdot 10^{18} \quad \text{kg/m}^3 \ . \tag{3.45}$$

Denoting $M = M_0\overline{M}$ and $R = R_0\overline{R}$, we can rewrite the Tolman-Oppenheimer-Volkoff equations as:

$$\frac{d\overline{P}}{d\overline{R}} = -\frac{\overline{M}}{\overline{R}^2}\overline{\mathcal{E}}\left[1+\frac{\overline{P}}{\overline{\mathcal{E}}}\right]\left[1+\frac{\overline{R}^3\overline{P}}{\overline{M}}\right]\left[1-\frac{2\overline{M}}{\overline{R}}\right]^{-1} , \tag{3.46}$$

$$\frac{d\overline{M}}{d\overline{R}} = \overline{R}^2\overline{\mathcal{E}} , \tag{3.47}$$

where $\overline{M}$, $\overline{P}$, and $\overline{\mathcal{E}}$ are functions of $\overline{R}$. With this definition, then we have the following natural scales for the radius and the mass:

$$R_0 = \frac{c^2}{\sqrt{4\pi G P_0}} = 6848.9217 \quad \text{m} = 6.8489217 \quad \text{km} , \tag{3.48}$$

$$M_0 = \frac{R_0 c^2}{G} = 9.22271416 \cdot 10^{30} \quad \text{kg} = 4.63704632 \quad M_\odot . \tag{3.49}$$

3.7 The Direct Urca process

Neutron stars are created as very hot objects at the moment of their birth in supernova explosions, with temperatures as large as 20 MeV [67, 68]. However, within one or two minutes the temperature falls below 1 MeV, and neutron stars become transparent for neutrinos generated in their interiors. Subsequently, neutron stars cool through the neutrino emission process from their volume. In the standard scenario of the neutron star cooling, the neutrinos emission from the interior of the star is dominated by the so-called modified Urca process:

$$\begin{aligned} n + n &\longrightarrow n + p + e^- + \bar{\nu}_e , \\ n + p + e^- &\longrightarrow n + n + \nu_e . \end{aligned} \tag{3.50}$$

This process of cooling is relatively slow, and requires a typical time of $\sim 10^6$ years for a star to cool down below 10^6 K temperatures [69]. The direct Urca process,

$$\begin{aligned} n &\longrightarrow p + e^- + \bar{\nu}_e , \\ e^- + p &\longrightarrow n + \nu_e \end{aligned} \tag{3.51}$$

is usually not considered because it requires a large proton fraction. However, this process of cooling is faster, and the typical cooling time is about ~ 100 years. Recent X-ray observations by Chandra and XMM-Newton suggest that neutron stars may cool very rapidly

([70] and references therein). For example, it was observed that the surface temperatures of pulsars in 3C58 [71], Vela [72], and Geminga [73] are very low. Such low temperatures cannot be explained by the modified Urca process. One needs an enhanced cooling mechanism to explain the observed low surface temperatures. This enhanced cooling may occur via the weak decay of additional hadrons such as pion or kaon condensates, hyperons, or quark matter [70]. However, the direct Urca process is perhaps the most conservative enhanced-cooling mechanism as it does not involve exotic constituent of matters in the interior of neutron stars. Of course, for stars that do not have massive cores (hence with no large proton fraction) the modified Urca process will remain the dominant process for the cooling mechanism.

Consider the direct electron Urca process described in the Eqn. (3.51). This process can proceed when the conditions for momentum and energy conservation can be simultaneously satisfied. That is, the momentum conservation, $\mathbf{p}_n = \mathbf{p}_p + \mathbf{p}_e$, should be satisfied at the Fermi surface:

$$k_{\rm F}^n \leq k_{\rm F}^p + k_{\rm F}^e \ . \tag{3.52}$$

Recalling that $k_{\rm F}^n = [2(1-Y_p)]^{1/3}\, k_{\rm F}$, $k_{\rm F}^p = [2Y_p]^{1/3}\, k_{\rm F}$, and using the charge neutrality condition, $k_{\rm F}^p = k_{\rm F}^e$, we arrive at the following Urca threshold condition:

$$k_{\rm F}^n = 2k_{\rm F}^p \ , \tag{3.53}$$

which is satisfied for $Y_p = 1/9 \approx 0.111$.

Consider now the realistic case when muons are present in the star. Now in addition we have the following expression for the direct Urca process:

$$\begin{aligned} n &\longrightarrow p + \mu^- + \bar{\nu}_\mu \ , \\ \mu^- + p &\longrightarrow n + \nu_\mu \ . \end{aligned} \tag{3.54}$$

From the equation of chemical equilibrium (3.41), one can find the Fermi momentum of the electron, and substitute the result into the equation for the charge neutrality (3.40),

$$[2Y_p\,(1-\alpha)]^{2/3}\, k_{\rm F}^2 = (2\alpha Y_p)^{2/3}\, k_{\rm F}^2 + m_\mu^2 \ , \tag{3.55}$$

where the muon charge fraction $\alpha \equiv Z_\mu/Z$ has been introduced. Obviously, the muon charge fraction is a dynamic function of density, $\alpha = \alpha(k_{\rm F})$. Rearranging the Urca condition, (3.52), we obtain an equation for the proton fraction at the Urca threshold:

$$\left(\frac{1-Y_p}{Y_p}\right)^{1/3} = 1 + (1-\alpha)^{1/3} \ . \tag{3.56}$$

The maximum value of Y_p can be found if one takes the limit $k_{\rm F}^e \gg m_\mu$, which simply occurs at $\alpha = 0.5$, or equivalently, at $Y_p \approx 0.1477$. Thus, the threshold proton fraction must be contained within $0.111 < Y_p < 0.1477$ for all baryon densities.

3.8 The Neutron-Star Matter Equation of State

As alluded earlier, the structure of neutron stars is sensitive to the equation of state of cold, fully catalyzed, neutron-rich matter. Spanning many orders of magnitude in density, neutron stars display rich and exotic phases that await a detailed theoretical understanding. For example, at densities that are about one third of nuclear matter saturation density and below, the uniform ground state becomes unstable against clustering correlations. This non-uniform region constitutes the stellar crust, which itself is divided into an inner and an outer region. In the outer crust the system is organized into a Coulomb lattice of neutron-rich nuclei embedded in a degenerate electron gas [46, 47]. For this region we employ the equation of state of Baym, Pethick, and Sutherland [46]. With increasing density the nuclei become progressively more neutron rich until the neutron drip region is reached; this region defines the boundary between the outer and the inner crust. It has been speculated that the bottom layers of the inner crust consist of complex and exotic structures that are collectively known as nuclear pasta [49, 50, 61]. Whereas significant progress has been made in simulating this exotic region [74, 75, 76], a detailed equation of state is still missing. Hence, we resort to a fairly accurate polytropic EOS to interpolate between the outer solid crust and the uniform liquid interior [56, 77]:

$$P(\mathcal{E}) = A + K\mathcal{E}^\gamma = A + K\mathcal{E}^{4/3} \ , \tag{3.57}$$

where the constants A and K are chosen such that the equation of state is continuous throughout the star. For the uniform liquid core—with densities as low as one-third and as high as ten times nuclear-matter saturation density—we generate the equation of state using

various refinements to the relativistic mean-field model of Serot and Walecka [7, 10, 29]. For consistency, the same models are used to compute the transition density from the liquid core to the solid crust. This is done by searching for the critical density at which the uniform system becomes unstable to small amplitude density oscillations. The stability analysis of the uniform ground state is based on a relativistic random-phase-approximation (RPA) as detailed in Ref. [77].

The equation of state for the uniform liquid core is based on an interacting Lagrangian that has been accurately calibrated to a variety of ground-state properties of both finite nuclei and infinite nuclear matter. The model includes a nucleon field (ψ), two isoscalar mesons (a scalar ϕ and a vector V^{μ}), and one isovector meson (b^{μ}) [10, 29] (the photon field plays no role in the present discussion of infinite nuclear matter at the mean-field level). The free Lagrangian density for this model is given by

$$\begin{aligned}\mathcal{L}_0 = \bar{\psi}\left(i\gamma^{\mu}\partial_{\mu} - M\right)\psi + \frac{1}{2}\partial_{\mu}\phi\partial^{\mu}\phi - \frac{1}{2}m_{\mathrm{s}}^2\phi^2 \\ - \frac{1}{4}V^{\mu\nu}V_{\mu\nu} + \frac{1}{2}m_{\mathrm{v}}^2V^{\mu}V_{\mu} - \frac{1}{4}\mathbf{b}^{\mu\nu}\mathbf{b}_{\mu\nu} + \frac{1}{2}m_{\rho}^2\mathbf{b}^{\mu}\mathbf{b}_{\mu}\ ,\end{aligned} \tag{3.58a}$$

as discussed in Chapter 2, where $V_{\mu\nu}$ and $\mathbf{b}_{\mu\nu}$ are the isoscalar and isovector field tensors, respectively. That is,

$$V_{\mu\nu} = \partial_{\mu}V_{\nu} - \partial_{\nu}V_{\mu}\ , \tag{3.59a}$$

$$\mathbf{b}_{\mu\nu} = \partial_{\mu}\mathbf{b}_{\nu} - \partial_{\nu}\mathbf{b}_{\mu}\ . \tag{3.59b}$$

Further, the parameters M, m_{s}, m_{v}, and m_{ρ} represent the nucleon and meson masses and may be treated (if wished) as empirical constants. The interacting Lagrangian density is given by the following expression (For details, look at the Chapter 2 and references [10, 16, 29]):

$$\mathcal{L}_{\mathrm{int}} = \bar{\psi}\left[g_{\mathrm{s}}\phi - \left(g_{\mathrm{v}}V_{\mu} + \frac{g_{\rho}}{2}\boldsymbol{\tau}\cdot\mathbf{b}_{\mu}\right)\gamma^{\mu}\right]\psi - U(\phi, V^{\mu}, \mathbf{b}^{\mu})\ . \tag{3.60}$$

The model includes Yukawa couplings (g_{s}, g_{v}, and g_{ρ}) between the nucleon and the three meson fields. However, to improve the phenomenological standing of the model—for example, to soften the compressibility of symmetric nuclear matter—the Lagrangian density must be supplemented by nonlinear meson interactions. These are given by

$$U(\phi, V^{\mu}, \mathbf{b}^{\mu}) = \frac{\kappa}{3!}(g_{\mathrm{s}}\phi)^3 + \frac{\lambda}{4!}(g_{\mathrm{s}}\phi)^4 - \frac{\zeta}{4!}\left(g_{\mathrm{v}}^2V_{\mu}V^{\mu}\right)^2 - \Lambda_{\mathrm{v}}\left(g_{\rho}^2\,\mathbf{b}_{\mu}\cdot\mathbf{b}^{\mu}\right)\left(g_{\mathrm{v}}^2V_{\nu}V^{\nu}\right)\ . \tag{3.61}$$

Table 3.1: The central energy densities and central pressures for a 1.4 solar mass neutron star are given in the units of MeV fm^{-3}. The neutron star radius and corresponding thicknesses of each region are given in kilometers.

Model	$\mathcal{E}_{\rm c}$	$P_{\rm c}$	$R_{1.4}$	$R_{\rm core}$	$R_{\rm pasta}$	$R_{\rm BPS}$
NL3	269.7	29.68	15.068	13.379	0.957	0.732
MS	431.3	51.40	13.779	12.436	0.750	0.593
FSUGold	537.3	72.97	12.657	11.340	0.832	0.485

Details on the calibration procedure may be found in Refs. [10, 29, 30, 33] and references therein. Note that additional local terms of the same order in a power-counting scheme could have been included. However, their phenomenological impact has been shown to be small [16], so they have not been included in the calibration procedure. Of particular interest and of critical important to the present study is the isoscalar-isovector coupling term $\Lambda_{\rm v}$ [30, 33]. Such a term has been added to the Lagrangian density to modify the poorly known density dependence of the symmetry energy—a property that is predicted to be stiff (*i.e.,* to increase rapidly with density) in most relativistic mean-field models. The addition of $\Lambda_{\rm v}$ provides a simple—yet efficient and reliable—method of tuning the density dependence of the symmetry energy without sacrificing the success of the model in reproducing experimentally constrained ground-state observables. Because of the sensitivity of the stellar radius to the density dependence of the symmetry energy [78], we also expect a strong correlation between $\Lambda_{\rm v}$ and the stellar moment of inertia.

Whereas the full complexity of the quantum system can not be tackled, the ground-state properties of the system may be computed in the relativistic mean-field approximation discussed in Chapter 2. In the RMF approximation all the meson fields are replaced by their classical expectation values and their solution can be readily obtained by solving the classical Euler-Lagrange equations of motion. The sole remnant of quantum behavior is in the treatment of the nucleon field which emerges from a solution to the Dirac equation in the presence of appropriate scalar and vector potentials [10, 29]. Following standard mean-field practices, one can then find the energy density and the pressure, which make up the equation of state for the core of the neutron star.

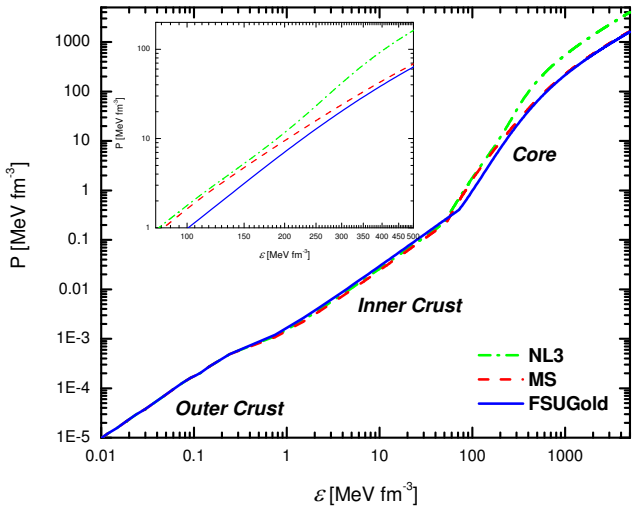

Figure 3.3: The stellar matter equations of state are given for three models discussed in the text: NL3 [14], MS [16], and FSUGold [15]. The BPS equation of state is used [46] for the outer crust, while for the intermediate region between the inner crust the the outer core we use the fairly accurate polytropic equation of state.

In Fig. 3.3 we present three different stellar matter equations of state used to calculate the mass and radius of a 1.4 solar mass neutron star. Corresponding central energy density, central pressure, and the thicknesses of each region are given in Table 3.1. Note that the central density of this star in the NL3 model is twice larger then the nuclear matter density ($\rho_0 = 2.4 \cdot 10^{17}$ kg m^{-3}), while this ratio equals to 3.2 in the MS model, and to 3.99 in the FSUGold model. Similarly, the central pressure is very different in each model. Moreover, these models predict different radii for the 1.4 solar mass neutron star that differ by almost 2.5 km. Thus the properties of the neutron star are very sensitive to the choice of the equation of state.

CHAPTER 4

MOMENT OF INERTIA AS A SENSITIVE PROBE TO THE EOS OF NEUTRON-RICH MATTER

4.1 Introduction

In this chapter we study the sensitivity of the stellar moment of inertia to the underlying equation of state [32]. Although the formalism is general—at least within the *slow-rotation approximation*—we focus on the recently discovered binary pulsar PSR J0737-3039 [18, 19]. Located ten times closer than the celebrated Hulse-Taylor binary system [79] and with the shortest orbital period of its kind (almost three times smaller than the Hulse-Taylor binary), PSR J0737-3039 is the first ever discovered double pulsar. This discovery has resulted in some of the most precise tests of Einstein's general theory of relativity to date. Moreover, it has also enabled the accurate determination of several pulsar properties, such as the orbital period of the binary, both pulsar masses, and both spin periods. However, their individual radii, moments of inertia, gravitational redshifts, or any other property that would allow a simultaneous mass-radius determination—and therefore place important constraints on the equation of state—are still unavailable. Yet the prospects for measuring the moment of inertia of the fastest spinning pulsar in the binary (PSR J0737-3039A) have never been better. Doing so with even a 10% accuracy may provide stringent constraints on the nuclear equations of state [80, 81, 82, 83]. Note, however, that the proposed 10% accuracy has been recently put into question [84]. Yet we trust that the various observational challenges will be met successfully in the near future. With such a view in mind, we focus on a particular feature of the equation of state (EOS) that has a strong impact on the moment of inertia: *the nuclear symmetry energy*.

The nuclear symmetry energy represents the increase in the energy of the system as protons are converted into neutrons (or neutrons into protons). Whereas ground-state masses constrain the symmetry energy near saturation density, they leave its density dependence (slope, curvature, *etc.*) largely undetermined. This is important as the slope of the symmetry energy at saturation density determines the pressure of pure neutron matter (PNM). And it is precisely the pressure of PNM that provides the necessary stellar support against gravitational collapse. Thus, the larger the pressure of PNM the larger the radius of the neutron star (see Table 3.1). Note that it is also the pressure of PNM that accounts for the size of the neutron skin thickness—the difference between the neutron radius and the proton radius—in medium to heavy nuclei. As a result, a strong correlation was uncovered between the neutron skin thickness of ^{208}Pb and the neutron radius of a neutron star [78]. Given that the moment of inertia scales as the square of the stellar radius, the aim of this work is to study the expected correlation between the neutron skin thickness of ^{208}Pb and the stellar moment of inertia. The Parity Radius Experiment ("*PREx*") at the Jefferson Laboratory aims to measure the neutron radius of ^{208}Pb accurately and model independently via parity-violating electron scattering [85, 86]. At the time of this writing the first experimental effort to measure the neutron radius of ^{208}Pb at the Jefferson Laboratory has been performed. The result demonstrated successful control of systematic errors and overcame many technical challenges, but unfortunately ran into difficulties with radiation and the vacuum system that reduced the running efficiency [86]. A follow-up measurement (second run) to PREx-1 is proposed that should provide a unique experimental constraint on the neutron skin thickness of a heavy nucleus and correspondingly on the pressure of pure neutron matter. We should also mention that considerable progress has been achieved on the theoretical front. By building on the universal behavior of dilute Fermi gases with an infinite scattering length, significant theoretical progress has been made in constraining the equation of state of pure neutron matter [82, 83, 84, 85, 86, 87, 88, 89, 90, 91, 92, 93, 94, 95, 96].

While the overall moment of inertia of the neutron star is of great interest, the *fraction* of the moment of inertia contained in the stellar crust may be as useful in constraining the equation of state [3, 56]. Indeed, by studying the sudden and fairly regular spin jumps ("*pulsar glitches*") in the Vela pulsar, it was determined that at least 1.4% of the total moment

of inertia of the star must reside in the solid crust [56]. Pulsar glitches are believed to be the result of angular momentum transfer between the star's solid crust and a more rapidly rotating superfluid component residing in the stellar interior. As the crustal moment of inertia is sensitive to the transition pressure at the core-crust interface [56], the above ($\gtrsim 1.4\%$) limit may place a significant constraint on the EOS of dilute, neutron-rich matter. In this way, the crustal moment of inertia may provide an attractive astrophysical complement to PREx and to the dynamics of dilute Fermi gases in constraining the density dependence of the symmetry energy.

The background material necessary to compute the moment of inertia of a neutron star in the *slow-rotation* approximation [52, 53] is given in Chapter 3. We introduce the families of various accurately-calibrated relativistic mean-field models that will be used to compute the equation of state of the stellar matter [14, 15, 16, 97]. We note that whereas all the models reproduce various experimentally measured properties of finite nuclei, they differ significantly in their predictions for the equation of state at both low and high densities.

4.2 The RMF Equations of State

To study the sensitivity of the stellar moment of inertia to the equation of state we will use relativistic mean-field models that have been accurately calibrated to the properties of infinite-nuclear matter (MS) [16], to the ground-state properties of finite nuclei (NL3) [14, 97], or to both (FSUGold) [15]. Parameter sets for these three models are listed in Table 2.1 and 2.2. The predicted equations of state—pressure *vs* energy density—for the three models are displayed in Fig. 4.1. Given that the equation of state for the solid crust is identical in all three models (as discussed in Chapter 3, and shown in Fig. 3.3), we only present the contribution from the uniform liquid core. The lowest energy density and pressure depicted in the figure—which are different in all three models— signal the transition from the uniform liquid core to the non-uniform solid crust. Note that the uniform core is assumed to consist of nucleons and leptons (electrons and muons) in chemical equilibrium; no exotic degrees of freedom are considered.

The resulting equations of state show a significant model dependence. As the models have been accurately calibrated, this is a clear indication that the existing database of

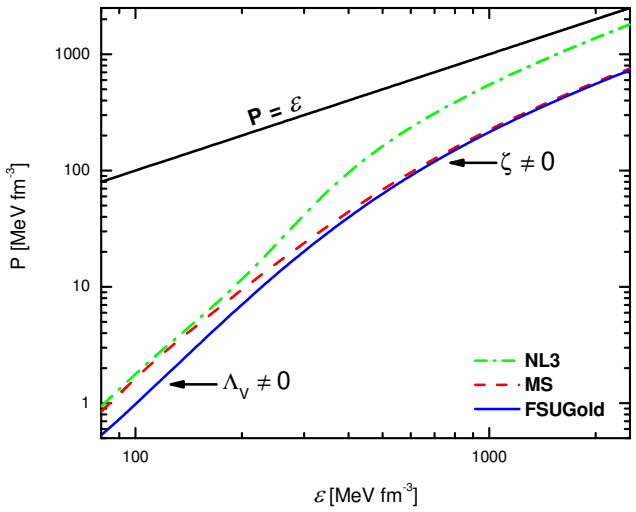

Figure 4.1: Equation of state (*pressure vs energy density*) of neutron-star matter predicted by the three relativistic mean-field models discussed in the text. The solid black line ($P = \mathcal{E}$) denotes the stiffest possible equation of state consistent with causality.

nuclear observables is insensitive to both the low- and high-density behavior of the EOS (the energy density at saturation is about 140 MeV/fm^3). In this contribution we are particularly interested in the sensitivity of the stellar moment of inertia to the two empirical parameters ζ and $\Lambda_{\rm v}$—with the former controlling the high-density behavior of the EOS and the latter the density dependence of the symmetry energy.

The NL3 parameter set [14, 97] provides an excellent description of the ground-state properties of finite nuclei (such as masses and charge radii) without invoking either ζ or $\Lambda_{\rm v}$ (see Table 2.1 and Table 2.2). As a consequence of having set $\zeta = \Lambda_{\rm v} \equiv 0$, NL3 generates a fairly stiff equation of state. At sub-saturation density, this behavior is reflected in the relatively small value of the energy density at the core-crust interface. At the high-density extreme, NL3 approaches the stiffest possible equation of state that is consistent with causality (*i.e.*, $P = \mathcal{E}$). As we shall see below, such a stiff EOS generates neutron stars that are both massive and large (see Fig. 4.2 and Table 4.1).

Table 4.1: Predictions for the maximum neutron star mass and for the radius and central energy density of a 1.4 $M_\odot$ neutron star in the three relativistic mean-field models discussed in the text. The last three quantities represent the transition density, energy density, and pressure at the core-crust interface. The units of the energy density and pressure are given in MeV fm^{-3}.

Model	$M_{\rm max}(M_\odot)$	$R_{1.4}$ (km)	$\mathcal{E}_{1.4}$	ρ_t (fm^{-3})	$\mathcal{E}_t$	P_t
NL3	2.774	15.07	269.7	0.052	48.96	0.212
MS	1.807	13.78	431.3	0.055	51.91	0.216
FSUGold	1.722	12.66	537.3	0.076	71.53	0.402

As far as the MS equation of state is concerned, Müller and Serot were able to build models with a wide range of values for ζ that while reproducing the same observed properties at normal nuclear densities, they produce maximum neutron star masses that differ by almost one solar mass [16]. By selecting a value of $\zeta = 0.06$, the MS model adopted here predicts a softer EOS and consequently a limiting neutron-star mass that is significantly smaller than NL3. Such a softening at high density is clearly evident in Fig. 4.1. Note that the $\zeta = 0.06$ choice appears consistent with the dense-matter equation of state extracted from an analysis of energetic heavy-ion collisions [98, 99]. However, extracting the *zero-temperature* EOS from energetic heavy-ion collisions may be model dependent. Thus, observational data on neutron-star masses may provide the cleanest constraint on the high-density component of the equation of state. Note, however, that since $\Lambda_{\rm v}$ remains equal to zero in this model, the energy density and pressure at the core-crust interface remain largely unchanged from their NL3 values (see Table 4.1).

The FSUGold parameter set is characterized by having both ζ and $\Lambda_{\rm v}$ different from zero [15]. By adding $\Lambda_{\rm v}$ to the model one can soften the EOS—particularly the symmetry energy—at low to intermediate densities. This produces a shift of the core-crust transition energy density and pressure to higher values relative to both NL3 and MS. Moreover, such a softening generates neutron stars of relative small radii (see Fig. 4.2 and Table 4.1). We note that the softening of the symmetry energy is required to describe the isoscalar monopole and isovector dipole modes in medium to heavy nuclei [39]. Further, this softening appears consistent with microscopic descriptions of the equation of state of low-density neutron matter (see Ref. [96] and references therein). On the other hand, the value of $\zeta = 0.06$

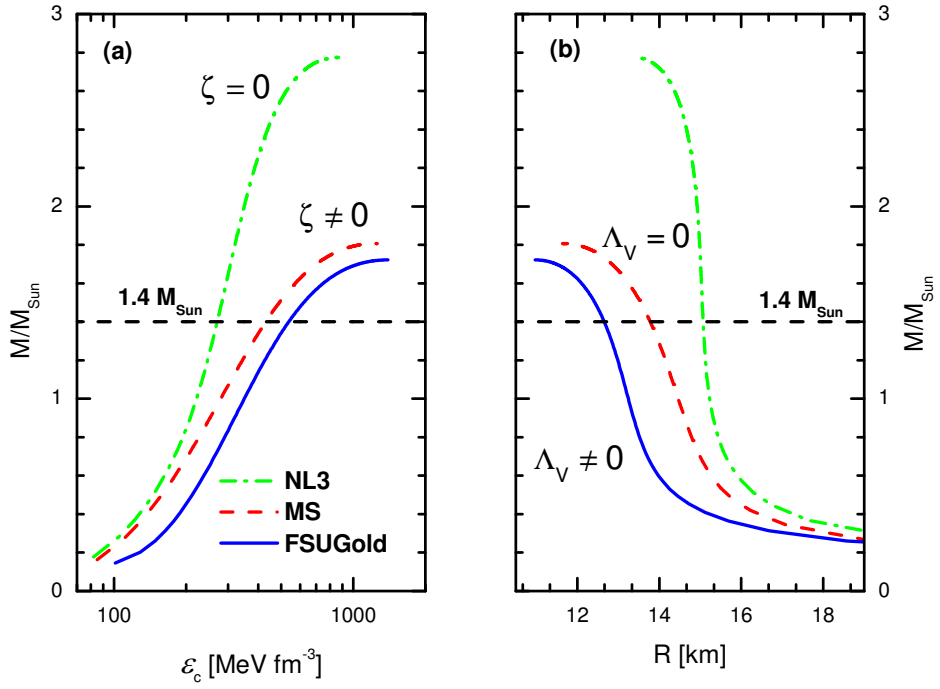

Figure 4.2: Neutron-star mass as a function of the central density (a) and the stellar radius (b) for the three relativistic mean-field models discussed in the text.

adopted here is solely constrained by the dynamics of heavy ions. Yet, the reported errors are large enough to accommodate slightly stiffer equations of state (although not as stiff as NL3) [98, 99].

4.3 Mass-Radius Relation

Having generated an equation of state, one can now proceed to solve the TOV equations [see Eqs. (3.9)]. Once a value for the central energy density $\mathcal{E}_c$ (or pressure P_c) is specified, solutions to the TOV equations are obtained in the form of mass $M(r)$, pressure $P(r)$, and energy density $\mathcal{E}(r)$ profiles. From these, the stellar radius R is extracted from the pressure profile as the point at which the pressure vanishes, namely, $P(R) = 0$. Similarly, the total

stellar mass is obtained from the mass profile as $M = M(R)$. Note that for a given value of the central energy density $\mathcal{E}_c$, a unique point in the M-R diagram is generated.

In Fig. 4.2 we display neutron-star masses as a function of the central energy density (left panel) and the stellar radius (right panel). The imprint of the underlying equation of state is clearly evident on these curves. For example, the stiff behavior of the NL3 equation of state is reflected on its very large limiting mass (of close to 3 solar masses). Also evident is the significant reduction in the maximum stellar mass as one softens the EOS by shifting the value of ζ from 0 to 0.06. Finally, we observe a significant variation in the value of the central energy density required to produce a "canonical" 1.4 $M_\odot$ neutron star. The NL3 equation of state is so stiff (*i.e.*, the pressure gradient is so large) that a central energy density of only twice its value at saturation is sufficient to support the star against gravitational collapse. In contrast, the softer FSUGold equation of state requires a central energy density that is twice as large as NL3 or about 4 times its value at saturation.

Whereas ζ controls the maximum stellar mass, $\Lambda_{\rm v}$ controls the stellar radius. This is illustrated on the right-hand panel of Fig. 4.2. Although the MS and FSUGold equations of state display similar behavior at high density (see Fig. 4.1) the former generates stellar radii that are significantly larger than the latter. For example, for a 1.4 $M_\odot$ neutron star the difference exceeds one kilometer. Note that the stellar radius—although primarily sensitive to the EOS at intermediate densities—is also sensitive to the high-density component of the EOS. Hence, although both NL3 and MS have $\Lambda_{\rm v} = 0$, MS (with $\zeta \neq 0$) produces more compact stars.

4.4 Families of the RMF Models and the Moment of Inertia

Having established the critical role of the two empirical parameters ζ and $\Lambda_{\rm v}$ on the mass-vs-radius relationship of neutron stars, we now return to the central goal of the present chapter: to assess the sensitivity of the stellar moment of inertia—both total and crustal—to the equation of state. To properly address this topic we must build models that, while accurately calibrated, can generate a wide range of values for poorly constrained nuclear observables. To do so, we modify the density dependence of the symmetry energy by resorting to a simple—yet highly robust—procedure first introduced in Ref. [30]. The procedure

Table 4.2: The NL3 and FSUGold *"families"* of mean-field interactions. The isovector parameters $\Lambda_{\rm v}$ and g_ρ were adjusted so that all models have a symmetry energy of ≈ 26 MeV at a density of ≈ 0.1 fm^{-3}. The tuning of the isovector interaction modifies the slope of the symmetry energy L at saturation density. The impact of such a change on the neutron skin thickness of ^{208}Pb and on the transition density, energy density, and pressure at the core-crust interface are displayed in the last four columns. The units of the energy density and pressure are given in MeV fm^{-3}.

Model	$\Lambda_{\rm v}$	g_ρ^2	L (MeV)	R_n-R_p (fm)	ρ_t (fm^{-3})	$\mathcal{E}_t$	P_t
NL3	0.00	79.6000	118.187	0.280	0.052	48.960	0.212
	0.01	90.9000	87.737	0.251	0.061	57.574	0.338
	0.02	106.0000	68.217	0.223	0.746	70.630	0.508
	0.03	127.1000	55.310	0.195	0.085	81.012	0.535
	0.04	158.6000	46.606	0.166	0.090	85.618	0.376
MS	0.00	70.5941	102.382	0.281	0.055	51.911	0.216
FSU	0.00	80.2618	108.764	0.286	0.051	48.458	0.207
	0.01	93.3409	87.276	0.260	0.060	56.330	0.317
	0.02	111.5126	71.833	0.235	0.069	65.387	0.415
	0.03	138.4701	60.515	0.207	0.076	71.534	0.402
	0.04	182.6162	52.091	0.176	0.078	73.924	0.268
	0.05	268.0859	45.742	0.137	0.077	73.206	0.036

consists on modifying the isovector mean-field interaction by simultaneously changing $\Lambda_{\rm v}$ and g_ρ (the $NN\rho$ coupling constant) in such a way that the value of the symmetry energy remains fixed at a specific value of the baryon density. Given that nuclei have a low-density surface, the symmetry energy is best constrained not at nuclear matter saturation density, but at a slightly lower value [100]. In this contribution—as in Ref. [30]—we fixed the symmetry energy at ≈ 26 MeV at a density of ≈ 0.1 fm^{-3} (or exactly at a Fermi momentum of $k_{\rm F} = 1.15$ fm^{-1}). This ensures that well constrained observables (such as masses and charge radii) remain consistent with their experimental values. Moreover, as this procedure involves the tuning of only the isovector interaction, all properties of symmetric nuclear matter remain intact. Yet poorly constrained observables—such as the neutron skin thickness of heavy nuclei and neutron-star radii—can be made to vary over a wide range of values [30, 78]. In Table 4.2 we display the appropriate isovector parameters for the NL3 and FSUGold *"families"* of mean-field interactions. Particularly sensitive to this change is the slope of the symmetry energy L at saturation density. The table illustrates the impact

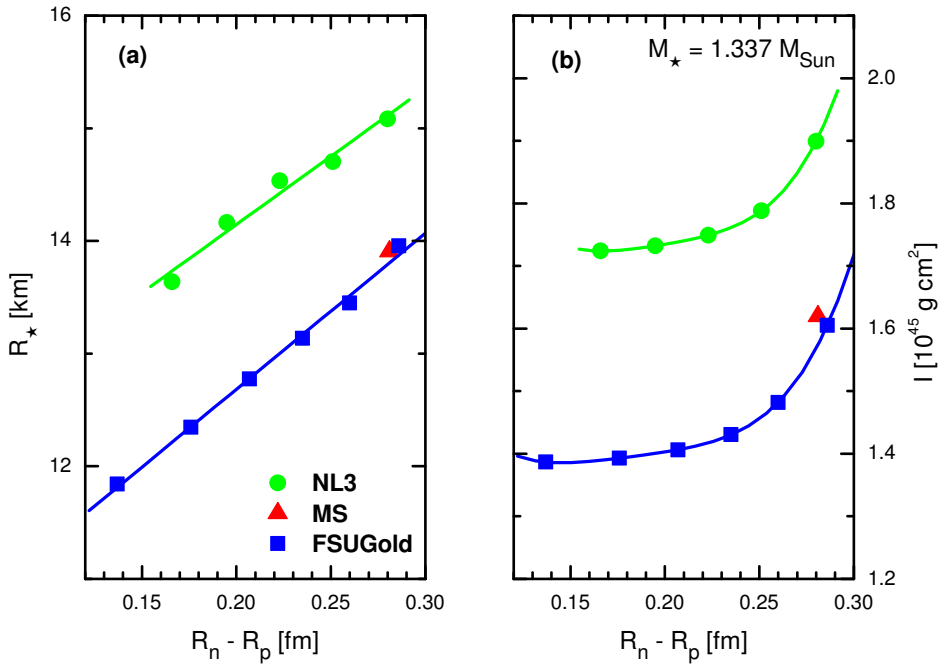

Figure 4.3: Stellar radius (a) and moment of inertia (b) of a 1.337 $M_\odot$ neutron star (J0737-3039 A) as a function of the neutron skin thickness of ^{208}Pb.

of L on the neutron skin thickness of ^{208}Pb and on the transition density, energy density, and pressure at the core-crust interface. Note that there is no need to generate an MS family given that it shares the same value of ζ with FSUGold.

In Fig. 4.3 we display the radius and moment of inertia of a $M = 1.337\ M_\odot$ neutron star (such as J0737-3039 A) as a function of the neutron skin thickness in ^{208}Pb. Although many other observables (such as L) may be used to characterize the density dependence of the symmetry energy, we have selected the neutron-skin of ^{208}Pb because it represents a fundamental nuclear observable that will soon be directly determined from laboratory data. The left-hand panel in the figure is reminiscent of the linear correlation between the neutron skin in ^{208}Pb and the stellar radius uncovered in Ref. [78]. Given that neutron stars and the neutron skin of heavy nuclei are both made of neutron-rich material, the emergence

of such a correlation should not come as a surprise. However, knowledge of the neutron skin is not sufficient to determine the stellar radius. Whereas the neutron skin of heavy nuclei is sensitive to the EOS around saturation density, the stellar radius is also sensitive to its high-density component. Hence, to eliminate the model dependence one must rely on observational data rather than on laboratory experiments. The right-hand panel in Fig. 4.3 displays the corresponding moment of inertia. There is a significant drop in the moment of inertia as the neutron skin departs from its largest value (at $\Lambda_{\rm v}=0$) but then the sensitivity weakens. The same kind of behavior is displayed when I is plotted as a function of the stellar radius (not shown). As in the case of the stellar radius, the total moment of inertia is sensitive to the high-density component of the EOS, so a strong model dependence remains. Note that since both MS and the stiffest member of the FSUGold family have $\Lambda_{\rm v}=0$ and $\zeta=0.06$, their predictions are very close to each other.

4.5 Crustal Properties, the Transition Pressure, and the Neutron Skin

Given the sensitivity of the moment of inertia to the high density component of the EOS, we now shift our attention to its crustal component. Our expectation—based on its high sensitivity to the transition pressure [see Eq. (3.26)]—is that a strong correlation will emerge between the crustal moment of inertia (I_{cr}) and the neutron skin thickness of ^{208}Pb. To our surprise, *no such correlation exists*. We attempt to elucidate this finding in what follows.

The core-crust boundary is determined by identifying the highest baryon density at which the uniform ground state becomes unstable against small amplitude density fluctuations. The stability analysis of the uniform ground state is based on a relativistic random-phase approximation (RPA) that is described in detail in Refs. [30, 77]. As first proposed in Ref. [30]—and confirmed since using various equivalent approaches [57, 58, 59, 93, 101]—a strong correlations emerges between the core-crust transition density (ρ_t) and the neutron skin thickness of ^{208}Pb. The left-hand panel in Fig. 4.4 provides evidence for such a correlation. The figure displays the energy per nucleon as a function of baryon density for uniform, neutron-rich matter in chemical equilibrium. Results are displayed for the various

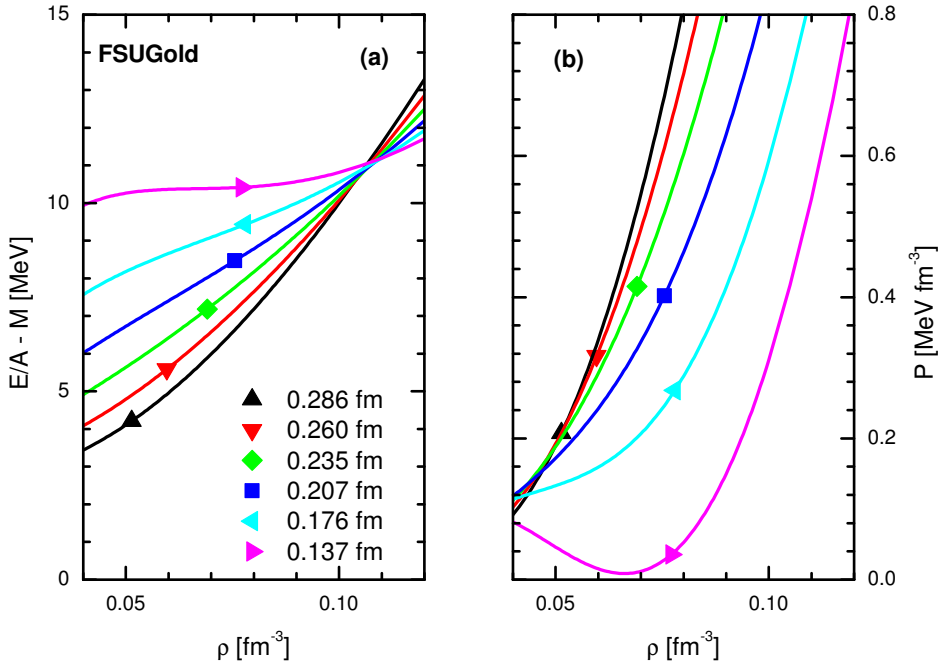

Figure 4.4: Equation of state for uniform, neutron-rich matter in beta equilibrium for the FSUGold family of mean-field interactions (labeled by the value of the neutron skin thickness in ^{208}Pb). The binding energy per nucleon (a) and the pressure (b) are displayed in parametric form in terms of the baryon density. The various symbols indicate the transition density, energy per nucleon, and pressure at which the uniform state becomes unstable against small density fluctuations.

members of the FSUGold family of mean-field interactions. The symbols in the figure are used to denote the transition point and are labeled according to the value of the neutron skin thickness in ^{208}Pb. The behavior displayed in Fig. 4.4(a) is simple to understand given the following facts: (a) all models predict identical properties for symmetric nuclear matter, (b) all models share the same value of the symmetry energy at $\approx$0.1 fm^{-3}, and (c) the softer the symmetry energy the smaller the neutron skin thickness in ^{208}Pb. Based on these fairly general assertions, one concludes that it is energetically expensive for the system to remain uniform if the equation of state is soft. Thus, models with thin neutron skins predict higher transition densities.

However, whereas a clear correlation emerges between the transition density and the neutron skin, *no such correlations is observed in the case of the transition pressure*. The right-hand panel in Fig. 4.4 displays the pressure of neutron-rich matter as a function of the baryon density. As expected, the larger the neutron skin thickness in ^{208}Pb the larger the pressure. That is, at a *fixed given density*, the pressure is larger for models that predict larger neutron skins. However, different models predict different transition densities and this mere fact destroys the correlation between the transition pressure and the neutron skin. For example, for the three stiffest models displayed in the figure, there is a direct correlation between the transition density and the transition pressure (P_t). In this region these three models exhibit relatively little scatter so that an increase in ρ_t is accompanied by a corresponding increase in P_t. However, as the models continue to soften, an inverse correlation develops: models with a soft symmetry energy have large transition densities but small transition pressures. As a result, no correlation between the transition pressure and the neutron skin thickness in ^{208}Pb develops. Note that this result is consistent with the very recent analysis presented in Ref. [101].

We now proceed to examine the correlation between the neutron skin thickness of ^{208}Pb and various quantities defined at the transition region. Before doing so, however, we display in Fig. 4.5 the energy density and pressure at the core-crust boundary as a function of the transition density. As suggested earlier, whereas the energy density is strongly correlated to the density at the interface, the pressure is not. In Fig. 4.6 we plot the value of various observables in the transition region as a function of the neutron skin thickness in ^{208}Pb. In addition to the transition density, energy density, and pressure, the proton fraction is also displayed. Excluding the softest model—which as we shall see below appears in conflict with an observational constraint—there is a clear (inverse) correlation between the transition density ρ_t and R_n-R_p, as originally proposed in Ref. [30]. Not surprisingly [see Fig. 4.5(a)] the transition energy density displays an inverse correlation that is just as strong. In contrast, there is no correlation between the transition pressure and R_n-R_p. Indeed, one can find models that have neutron skins that vary by more than 0.1 fm yet predict identical transition pressures. Finally, the proton fraction at the core-crust interface displays a tight inverse correlation. As mentioned earlier [see Fig 4.4(a)] it is energetically expensive for models

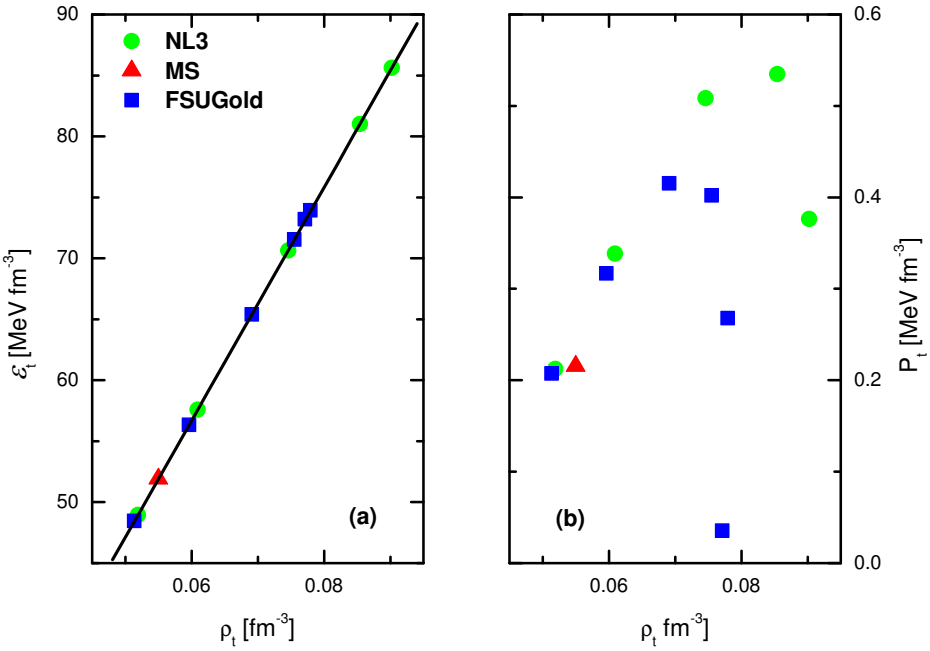

Figure 4.5: Properties of neutron-rich matter at the core-crust interface for the various models discussed in the text. Whereas the transition energy density is strongly correlated to the transition density (a), the transition pressure is not (b).

with a soft-symmetry energy to support a large neutron-proton asymmetry. Thus, the thinner the neutron skin of ^{208}Pb, the larger the proton fraction.

Having explored the correlations (or lack-thereof) between the neutron skin thickness in ^{208}Pb and various properties of the EOS in the transition region, we now proceed to study the sensitivity of several crustal properties to R_n-R_p. In particular, predictions for the crustal mass, thickness, and moment of inertia for a 1.337 $M_\odot$ neutron star (such as J0737-3039 A) are displayed in Fig. 4.7. Note that approximate analytic expressions for the crustal moment of inertia (I_{cr}) and mass (M_{cr}) have been derived in the appendix A and have been collected in Eqs. (3.26) and (3.27). Both of these expressions indicate a high sensitivity to the transition pressure P_t. Indeed, the imprint of the transition pressure is clearly evident in all crustal observables. For example, given that for models with a soft symmetry energy

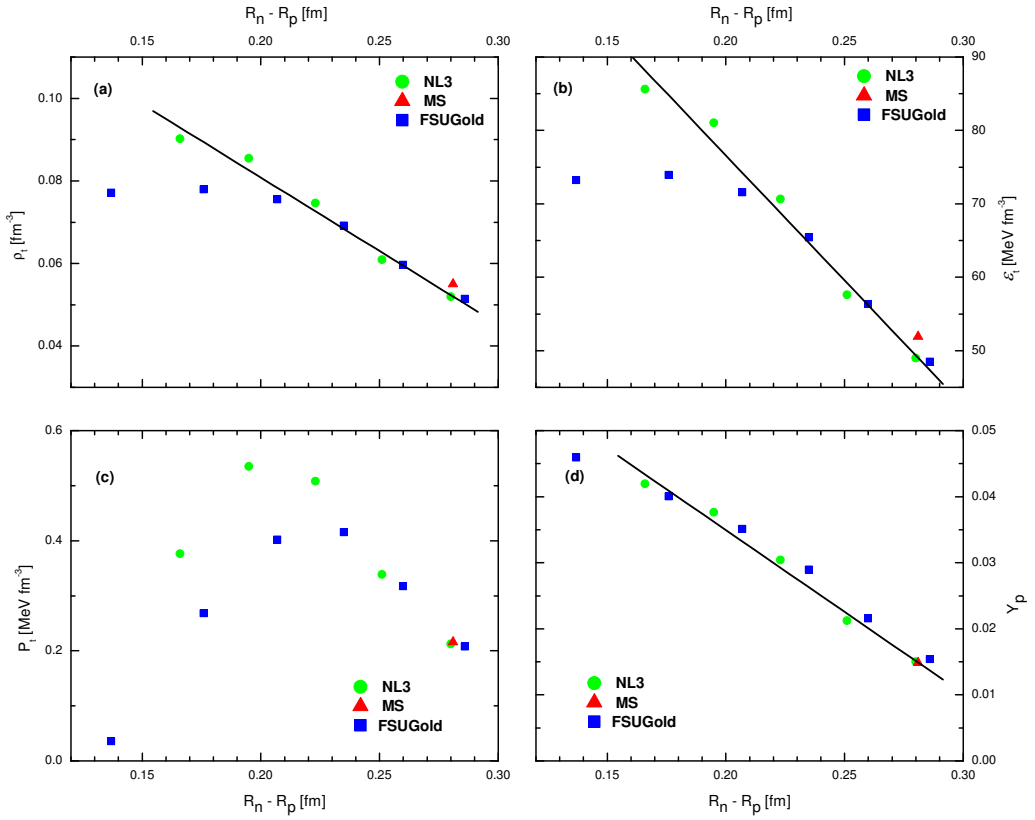

Figure 4.6: Baryon density (a), energy density (b), pressure (c), and proton fraction (d) at the core-crust interface as a function of the neutron skin thickness in ^{208}Pb for the various mean-field interactions discussed in the text.

the transition pressure increases with R_n-R_p, an initial (*i.e.*, for small neutron skins) direct correlation develops between R_n-R_p and all crustal properties. Eventually, however, the transition pressure reaches a maximum and then an inverse correlation ensues. Hence, we conclude that a measurement of the neutron skin thickness in ^{208}Pb will place no significant constraint on the crustal mass, thickness, or moment of inertia. Note that the crustal thickness R_{cr} also follows such a trend due to its dependence on the crustal mass; if a small crustal mass remains, then the crustal thickness will be small.

As mentioned in the section 4.1, the study of pulsar glitches in the Vela pulsar suggests

that at least 1.4% of the total moment of inertia must reside in the solid crust [3, 56]. The results displayed in Fig. 4.8 show how such a constrain may be used to rule out certain equations of state. The figure shows predictions for the fractional moment of inertia (I_{cr}) of the binary pulsar J0737-3039 as a function of the neutron skin thickness in ^{208}Pb. We observe that the softest member of the FSUGold family predicts a fractional moment of inertia of only 0.35%—significantly lower than the 1.4% bound. This suggests that models with such a soft symmetry energy may be in conflict with observation. Ultimately, such a low value for I_{cr} can be traced back to the very small transition pressure predicted by the model. We close this section by mentioning that many of the results presented and discussed in graphical form have been collected in Tables 4.3 and 4.4.

Table 4.3: Predictions for the properties of the J0737-3039 A pulsar with a mass of $M = 1.337 M_{\odot}$ and spin period of $P = 22.7$ ms (or stellar frequency of $\Omega = 276.8$ s^{-1} [19]). The central densities are in units of 10^{14} g/cm^3, the radii in km, the core mass in solar masses and the moments of inertia in 10^{45} g cm^2. The quantities in parenthesis are the analytic results for the fraction of the mass and moment of inertia contained in the solid crust (see text for details).

Model	$\Lambda_{\rm v}$	ρ_c	R	$R_{\rm core}$	$M_{\rm core}$	$M_{\rm cr}/M(\%)$	I	$I_{\rm core}$	$I_{\rm cr}/I(\%)$
NL3	0.00	4.675	15.08	13.29	1.308	2.18(2.13)	1.899	1.810	4.67(4.70)
	0.01	4.980	14.70	12.71	1.298	2.91(2.83)	1.788	1.678	6.17(6.21)
	0.02	5.032	14.53	12.33	1.285	3.91(3.78)	1.749	1.608	8.10(8.10)
	0.03	5.032	14.16	12.17	1.286	3.84(3.72)	1.732	1.597	7.77(7.82)
	0.04	5.019	13.64	12.18	1.302	2.59(2.54)	1.724	1.634	5.19(5.27)
MS	0.00	7.135	13.91	12.45	1.315	1.63(1.61)	1.619	1.560	3.66(3.71)
FSU	0.00	7.329	13.96	12.47	1.316	1.58(1.56)	1.605	1.547	3.61(3.65)
	0.01	8.314	13.45	11.85	1.311	1.96(1.92)	1.482	1.416	4.46(4.52)
	0.02	8.700	13.13	11.50	1.307	2.26(2.22)	1.431	1.358	5.08(5.15)
	0.03	8.856	12.77	11.34	1.310	2.02(1.99)	1.406	1.343	4.49(4.57)
	0.04	8.918	12.35	11.30	1.320	1.28(1.27)	1.393	1.354	2.82(2.87)
	0.05	8.936	11.84	11.33	1.335	0.16(0.16)	1.387	1.382	0.36(0.36)

4.6 Conclusion

In this chapter we have studied the sensitivity of the stellar moment of inertia to the underlying equation of state. In the slow-rotation approximation employed here, the stellar moment of inertia is only sensitive to the equation of state. Several equations of state were

Table 4.4: Predictions for the properties of the J0737-3039 B pulsar with a mass of $M = 1.250 M_{\odot}$ and spin period of $P = 2.77$ ms (or stellar frequency of $\Omega = 2.268$ s^{-1} [19]). The central densities are in units of 10^{14} g/cm^3, the radii in km, the core mass in solar masses and the moments of inertia in 10^{45} g cm^2. The quantities in parenthesis are the analytic results for the fraction of the mass and moment of inertia contained in the solid crust (see text for details).

Model	$\Lambda_{\rm v}$	ρ_c	R	$R_{\rm core}$	$M_{\rm core}$	$M_{\rm cr}/M(\%)$	I	$I_{\rm core}$	$I_{\rm cr}/I(\%)$
NL3	0.00	4.491	15.11	13.16	1.219	2.47(2.41)	1.730	1.639	5.28(5.29)
	0.01	4.808	14.72	12.56	1.209	3.28(3.19)	1.622	1.509	6.94(6.95)
	0.02	4.869	14.54	12.16	1.195	4.39(4.21)	1.582	1.439	9.03(8.97)
	0.03	4.874	14.13	11.99	1.197	4.28(4.12)	1.563	1.428	8.62(8.61)
	0.04	4.864	13.56	11.99	1.214	2.88(2.82)	1.554	1.465	5.73(5.79)
MS	0.00	6.474	14.07	12.44	1.226	1.93(1.90)	1.507	1.443	4.28(4.33)
FSU	0.00	6.631	14.14	12.48	1.226	1.89(1.85)	1.498	1.434	4.25(4.28)
	0.01	7.507	13.65	11.86	1.221	2.34(2.29)	1.381	1.308	5.27(5.31)
	0.02	7.869	13.32	11.49	1.216	2.69(2.63)	1.329	1.249	5.97(6.02)
	0.03	8.023	12.91	11.32	1.220	2.39(2.35)	1.303	1.234	5.24(5.31)
	0.04	8.090	12.43	11.27	1.231	1.51(1.50)	1.288	1.246	3.27(3.33)
	0.05	8.113	11.87	11.31	1.248	0.19(0.19)	1.281	1.275	0.41(0.42)

generated using relativistic mean-field models that have been accurately calibrated to the bulk properties of infinite nuclear matter and finite nuclei. As nuclear observables probe the EOS around nuclear matter saturation density, two aspects of the EOS remain poorly constrained even after the calibration procedure: (a) the density dependence of the symmetry energy and (b) the high-density component of the EOS. The relativistic mean-field models employed here include two empirical parameters—$\Lambda_{\rm v}$ and ζ—that provide an efficient and economical way to modify the EOS. Whereas the former controls the density dependence of the symmetry energy, the latter controls the high density component of the EOS. As such, $\Lambda_{\rm v}$ can be used to tune the pressure of pure neutron matter at saturation density, thereby controlling the neutron radius of objects as diverse as finite nuclei and neutron stars. In contrast ζ—by modifying the high-density component of the EOS—strongly affects the maximum stellar mass that can be supported against gravitational collapse. By tuning these two parameters, one can generate limiting stellar masses that differ by more than one solar mass and radii (for a fixed stellar mass) that may differ by more than 2 km. Note that one can generate these wide range of values without compromising the success of the models in

reproducing a host of well determined nuclear observables.

With several equations of state in hand, we proceeded to compute the moment of inertia of the recently discovered binary pulsar PSR J0737-3039 (with individual masses of $M_A = 1.337\ M_\odot$ and $M_B = 1.250\ M_\odot$). It has been suggested—due to the high sensitivity of the binary to general relativistic effects—that the moment of inertia of the fastest spinning pulsar in the binary (PSR J0737-3039A) may be measured with a 10% accuracy. Our results indicate that knowledge of the pulsar moment of inertia (even with a 10% accuracy) could help discriminate among various equations of state. We note, however, that whereas our results suggests that a measurement of the moment of inertia could discriminate between equations of state that are either stiff or soft at high density, the sensitivity to the density dependence of the symmetry energy appears to be weak—especially for models with a soft symmetry energy.

Although we find the total moment of inertia interesting, the main focus of this study was its crustal component I_{cr}. Several reasons prompted this choice. First, an analysis of pulsar glitches in the Vela pulsar suggests that at least 1.4% of the total moment of inertia must reside in the solid crust. This places significant constrains on the EOS. Second, the crust is thin and the density within it is low, so simple—yet fairly accurate—analytic expressions for I_{cr} exist. These indicate that the crustal moment of inertia depends sensitively on a fundamental observable: the transition pressure at the core-crust interface (P_t). Third, given the strong correlation between the core-crust transition density and the neutron skin thickness of ^{208}Pb, one expects a similar correlation to emerge in the case of P_t and I_{cr}. Finally, given that at the time of this writing the proposal of the second run for the Parity Radius Experiment (PREx) is underway, the prospects of constraining crustal properties with laboratory data appears imminent.

However, we found no correlation between the transition pressure P_t and the neutron skin thickness in ^{208}Pb. Whereas a robust correlation exists between R_n-R_p and various bulk properties of the EOS at the transition region—such as the baryon density, energy density, and proton fraction—no such correlation develops in the case of the transition pressure. And because of its sensitivity to the transition pressure, we conclude that the crustal moment of inertia will not be significantly constrained by a measurement of the neutron skin thickness

in ^{208}Pb. This represents the main conclusion of our work. We found the explanation for this behavior subtle and rooted on the observed correlation between the transition density ρ_t and R_n-R_p. As expected, the larger the value of R_n-R_p the stiffer the symmetry energy. That is, given a fixed value of the baryon density the resulting pressure increases with R_n-R_p. However, the transition pressure is obtained by evaluating the EOS—not at a fixed value of the density, but rather—at the *transition density*, which is inversely correlated to R_n-R_p. It is precisely the fact that ρ_t changes with R_n-R_p that destroys any correlation between P_t and R_n-R_p [see Fig. 4.4(b)]. Although at odds with some studies that support the existence of such a correlation [57, 58, 59, 60], our result appears consistent with a very recent analysis by Ducoin, Margueron, and Providencia [101].

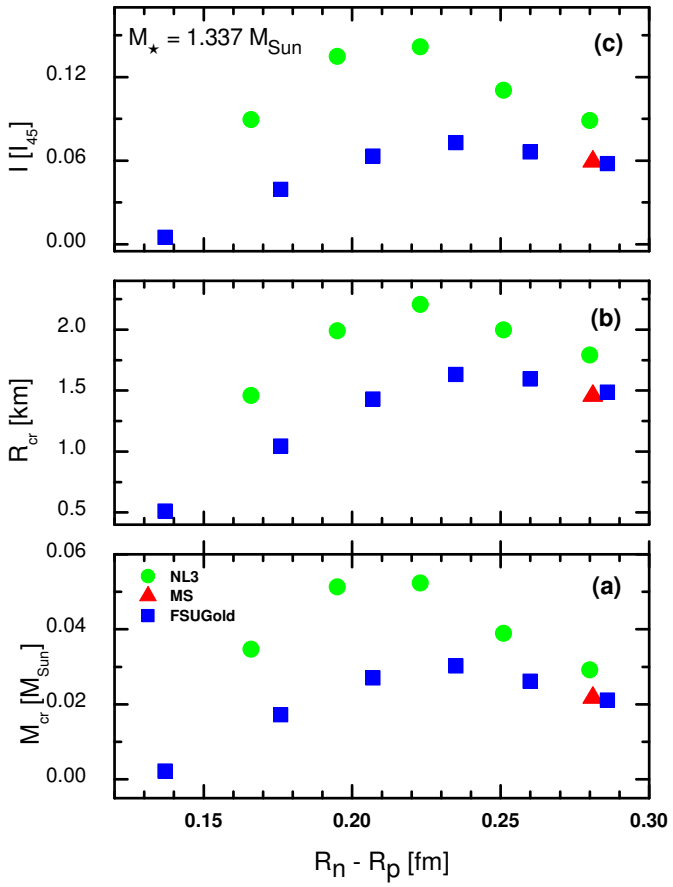

Figure 4.7: Crustal mass (a), crustal thickness (b), and crustal moment of inertia (c) as a function of the neutron skin thickness in ^{208}Pb for a 1.337 $M_{\odot}$ neutron star (J0737-3039 A). The various mean-field interactions are described in the text.

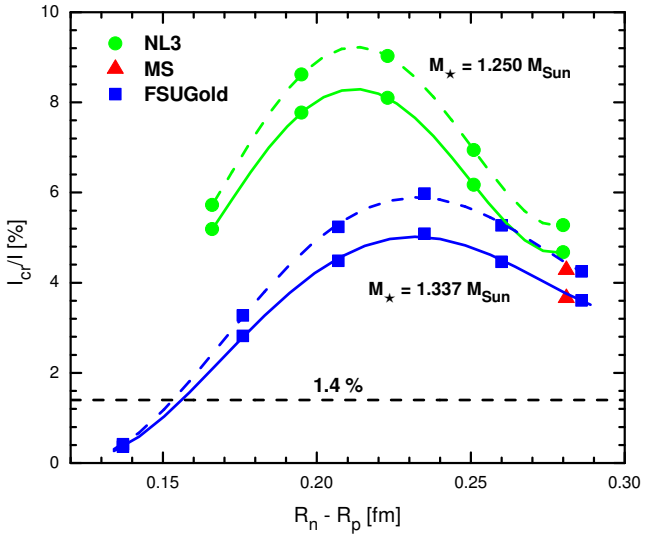

Figure 4.8: Fraction of the crustal moment of inertia as a function of the neutron skin thickness in ^{208}Pb for the binary pulsar J0737-3039 with masses of 1.337 $M_\odot$ (J0737-3039 A) and 1.25 $M_\odot$ (J0737-3039 B). The various mean-field interactions are described in the text.

CHAPTER 5

NEW RELATIVISTIC EFFECTIVE INTERACTION FOR NUCLEI, GIANT RESONANCES, AND NEUTRON STARS

5.1 Introduction

Recently Özel *et. al.* [11] reported a combined mass-radius measurement of three neutron stars, and subsequently determined the equation of state governing these neutron stars. The mass versus radius relationship of neutron stars is intimately connected to the equation of state of cold, neutron-rich matter. Indeed, an EOS is the sole ingredient that must be supplied to solve the equations of stellar structure (*i.e.*, the Tolman-Oppenheimer-Volkoff equations). Conversely, knowledge of the $M - R$ relation is sufficient to uniquely determine the equation of state of neutron-star matter [17]. As argued by Lindblom almost 20 years ago, the availability of such information—even from a single neutron star—will provide interesting information about the equation of state [17]. In particular, the equation of state determined by Ref. [11] is softer than those containing only nucleonic degrees of freedom. This conclusion is both very interesting and provocative. Viewed in this light, we compute the equation of state of neutron-star matter and the resulting $M - R$ relation using accurately-calibrated relativistic mean-field models. These models have been calibrated to the properties of infinite nuclear matter at saturation density [16], to the ground-state properties of finite nuclei [14, 97], or to both [15]. Unlike the former two, the latter parametrization predicts a significantly soft symmetry energy, a feature that appears consistent with the behavior of dilute neutron matter (see Ref. [96] and references therein). A detailed explanation of the role of the model parameters on the equation of state is given

in Chapters 4 and 6. We note, however, that none of the models considered in this work include exotic degrees of freedom, such as hyperons, meson (condensates), or quarks. Thus, we shall see that relative to the conclusions of Ref. [11] our results are mixed. On the one hand, the stellar radii predicted by the relativistic models are larger than observed, seemingly confirming that such equations of state are too stiff. On the other hand, the agreement between the predicted and observational EOS suggests the contrary.

Note that the simultaneous determination of both the mass and radius of a neutron star is very difficult. However, tremendous advances in X-ray astronomy have produced large amounts of high quality data that have allowed the simultaneous determination of both masses, radii, and the underlying equation of state [11, 12]. Unfortunately, neutron star radii inferred from X-ray observations of the luminosity and temperature are sensitive to models of the stellar atmosphere (see Ref. [65, 102] and references therein). Moreover, mass and radius determination from X-ray burst (as in Ref. [11]) may be hindered by systematic uncertainties [12]. For example Özel *et. al.* inferred very small stellar radii from their recent analysis of three X-ray bursts [11], while Steiner *et. al.* extracted neutron star radii significantly larger (of the order of 12 km) [12]. Still, we believe that such studies will eventually become instrumental in constraining the dense matter equation of state. In particular, the recent interpretation of X-ray observations by Steiner *et. al.* suggests that the FSUGold equation of state is slightly stiff at intermediate densities and soft at high densities. This in turn suggests that the FSUGold model predicts neutron star radii that are too large and a maximum neutron-star mass that is too small. This analysis is further confirmed—at least for the high density domain—by a recent two solar mass neutron-star measurement by Demorest *et. al* [13] using Shapiro time delay.

In response to the references above, in this chapter we will also introduce a new relativistic effective interaction that is simultaneously constrained by the properties of finite nuclei, their collective excitations, and neutron-star properties. By adjusting two of the empirical parameters of the theory, one can efficiently tune the neutron skin thickness of ^{208}Pb and the maximum neutron star mass. The new effective interaction is fitted to a neutron skin thickness in ^{208}Pb of only $R_n - R_p = 0.16$ fm and a moderately large maximum neutron star mass of 1.94 $M_\odot$. The maximum mass prediction of this new model is consistent with

the recent mass measurement by Ref. [13] ($M = 1.97 \pm 0.04\ M_{\odot}$), which was not yet known at the time of this research.

5.2 Current Uncertainties in the Relativistic Models of the Neutron-Star Matter Equation of State

The structure of neutron stars is sensitive to the equation of state of cold, fully catalyzed, neutron-rich matter over an enormous range of densities. As discussed in section 3.8, for the low-density outer crust we employ the equation of state of Baym, Pethick, and Sutherland [46]. At densities of about a third to a half of nuclear-matter saturation density, uniformity in the system is restored and for this (liquid-core) region we use an EOS derived from a representative set of accurately calibrated relativistic mean-field models [14, 15, 16, 61]. For the intermediate complex and exotic nuclear pasta regions we use a fairly accurate polytropic equations of state.

Accounting for most of the stellar radius and practically all of its mass, the liquid core of the neutron star is structurally the most important component of the star. Matter in the liquid core is assumed to be composed of neutrons, protons, electrons, and muons in chemical equilibrium. We reiterate that no exotic degrees of freedom are included in the models discussed. Both electrons and muons are treated as non-interacting relativistic Fermi gases. For the hadronic component, the equation of state is generated using accurately-calibrated relativistic models [14, 15, 16, 61]. These models include a nucleon field (ψ) interacting via standard Yukawa couplings to two isoscalar mesons (a scalar ϕ and a vector V_{μ}) and one vector-isovector meson ($\mathbf{b}_{\mu}$): $g_{\rm s}$, $g_{\rm v}$, and g_{ρ}. In addition to Yukawa couplings, the model is supplemented by non-linear meson interactions: κ for cubic, and λ for quartic scalar-isoscalar self-interactions, ζ for quartic vector-isoscalar self interaction, and $\Lambda_{\rm v}$ for the quartic mixed isoscalar-isovector interaction. The inclusion of scalar cubic and quartic self-interactions dates back to the late seventies [8] and is instrumental for softening the incompressibility coefficient of symmetric nuclear matter, as required to explain the excitation of the the nuclear breathing mode. Of particular interest and of critical importance to the present study are the vector self-interaction (ζ) and the isoscalar-isovector mixing term ($\Lambda_{\rm v}$).

Table 5.1: Parameter sets for a representative "extra-soft" RMF model discussed in the text. The units of parameter κ is given in MeV. The meson masses are the same as in the FSUGold model.

Model	g_s^2	g_v^2	g_ρ^2	κ	λ	ζ	Λ_v
XS	131.0059	258.1044	213.9596	0.0079	+0.04339	0.09	0.04

In the Fig. 4.2, using the three RMF models discussed in the text, the mass of the neutron star was given as a function of the central density (a), and as a function of its radius (b). This figure illustrates that the empirical parameter ζ provides an efficient tool to control the high-density component of the equation of state. While the RMF models with $\zeta = 0$ (such as NL3) predict the same observed properties at normal nuclear densities, yet they produce maximum neutron star masses that differ by almost one solar mass. The higher the value of ζ one gets the softer equation of state at high densities. The particular case of $\zeta = 0$ corresponds to the stiffest equation of state at high densities (Look at Fig. 4.1).

The isoscalar-isovector coupling constant Λ_v was introduced to modify the poorly known density dependence of the symmetry energy. We remind that the symmetry energy represents the energy cost involved in changing protons into neutrons (and vice-versa). To a good approximation, it is given by the difference in energy between pure neutron matter and symmetric nuclear matter. With only one isovector parameter (g_ρ) to adjust, relativistic mean-field models have traditionally predicted a *stiff* symmetry energy. The addition of Λ_v provides a simple—yet efficient and reliable—method of softening the symmetry energy without compromising the success of the model in reproducing well determined ground-state observables [15]. Indeed, whereas models with different values of Λ_v reproduce the same exact properties of symmetric nuclear matter, they yield vastly different predictions for both the neutron radii of heavy nuclei and for the radius of neutron stars [30, 78]. Given that the neutron-star radius is believed to be primarily controlled by the symmetry pressure at intermediate densities [3], the Parity Radius Experiment (PREx) at the Jefferson Laboratory will provide a unique laboratory constraint on a fundamental neutron-star property [85, 86].

In summary, the two empirical parameters ζ and Λ_v provide a highly economical and efficient control of the softness of the high-density component of equation of state and of

the symmetry pressure at intermediate densities, respectively—with the former primarily controlling the maximum neutron star mass (panel (a) of Fig. 4.2), and the latter the stellar radius (panel (b) of Fig. 4.2). Parameter sets for all the models employed in this work are listed in Table 2.1 and 2.2. In addition, as a representative set we have constructed an *"Extra Soft"* (XS) relativistic mean-field model constrained by the properties of symmetric nuclear matter at saturation density (*i.e.,* equilibrium density, binding energy per nucleon, and incompressibility coefficient). In regards to these properties, the model is indistinguishable from FSUGold (see Table 5.1). The only additional constraint imposed on the model is that its limiting mass be no smaller than 1.6 solar masses. We feel that lowering this limiting value any further may start conflicting with the observational data [3]. Although no exhaustive parameter search was conducted, we trust that the resulting *extra-soft* equation of state (as given in Table 5.1) is representative of the softness that may be achieved with present-day relativistic mean-field models. With such a soft model, neutron-star radii get significantly reduced indeed (see Fig. 5.1). For example, the neutron radius of a 1.4 $M_{\odot}$ neutron star is reduced by almost one kilometer relative to the FSUGold prediction (see Table 5.2) and by more than 1.5 km at its limiting mass of 1.6 $M_{\odot}$. Yet the minimum neutron-star radius of $R=10.41$ km predicted by the model remains outside the observational error bars.

In Fig. 5.1 we compare observational results for neutron star masses and radii against the model predictions. The very stiff behavior of the NL3 equation of state is immediately evident. With both empirical parameters ζ and $\Lambda_{\rm v}$ set equal to zero, it is not surprising that the NL3 model predicts neutron-star masses as large as 2.8 $M_{\odot}$ with very large radii. As compared to the observational data, the NL3 model suggests a radius for a 1.7 solar-mass neutron star that is about 6 km too large. Moreover, the NL3 equation of state is so stiff that gravity in a 2.8 $M_{\odot}$ neutron star can compress matter to only about four times normal nuclear density (see Table 5.2). All these, even when the model provides an excellent description of many laboratory observables.

As first suggested by Müller and Serot [16], adding a vector self-interaction (with $\zeta=0.06$) dramatically reduces the repulsion at high densities and ultimately the limiting neutron-star mass. As compared to the NL3 parameter set, the maximum neutron star mass predicted by Müller and Serot (MS) is reduced by almost one solar mass (see Fig. 5.1 and Table 5.2).

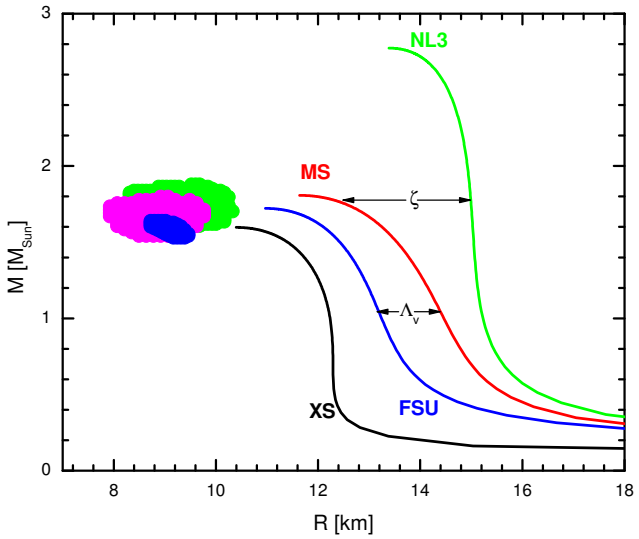

Figure 5.1: *Mass-vs-Radius* relation predicted by the four relativistic mean-field models discussed in the text. The observational data is for the three neutron stars reported in Ref. [11]. These neutron stars are in the binaries 4U 1608-52[103] (green), EXO 1745-248 [104] (magenta), and 4U 1820-30 [105] (blue).

Consistent with this softening is a significant increase in the compactness of the star. For example, for a neutron-star mass of about 1.8 $M_{\odot}$, NL3 predicts a stellar radius that is more than 3 kilometers larger than MS. Note, however, that the density dependence of the symmetry energy predicted by NL3 and MS is practically identical (see inset in Fig. 5.2). In particular, this is reflected in the identical prediction of 0.28 fm for the neutron-skin thickness of ^{208}Pb. This suggests that tuning the density dependence of the symmetry energy—via the addition of the isoscalar-isovector mixing term $\Lambda_{\rm v}$—may yield a further reduction in neutron-star radii [78], as suggested by observation.

Incorporating information on nuclear collective modes in the calibration procedure of the FSUGold model favors a non-zero value for $\Lambda_{\rm v}$ [15]. Further, it now seems that the resulting softening of the symmetry energy is consistent with the EOS of dilute neutron matter predicted by various microscopic approaches (see Refs. [90, 94, 99] and references therein). That the addition of $\Lambda_{\rm v}$ produces the intended effect can be appreciated in Fig. 5.1

Table 5.2: Predictions for the central baryon density, central pressure, mass, and radius of the limiting neutron star for the four models employed in the text. The last column lists predictions for the radius of a 1.4 solar-mass neutron star. The baryon density is given in fm^{-3}, the pressure in MeV fm^{-3}, the mass in solar masses, and the radii in kilometers.

Model	ρ_c	P	M	R	$R_{1.4}$
NL3	0.668	441.87	2.77	13.39	15.07
MS	1.040	311.73	1.81	11.64	13.78
FSU	1.155	347.20	1.72	10.97	12.66
XS	1.259	348.64	1.60	10.39	11.73

and Table 5.2. That is, although one has adopted the same value of ζ for both MS and FSUGold, their predictions for the radius of a *"canonical"* 1.4 solar-mass neutron star differ by more than one kilometer. Related to this fact is the significant smaller neutron-skin thickness of ^{208}Pb predicted by FSUGold (0.21 fm *vs* 0.28 fm). However, it appears that the combined softening of the EOS at high densities (through ζ) and of the symmetry pressure (through Λ_{v}) is insufficient to explain the observational data; the minimum stellar radius predicted by the FSUGold model is about 11 km, significantly larger than suggested by observation.

In an effort to describe the observational data, we have constructed an *"Extra Soft"* (XS) relativistic mean-field model constrained by the properties of symmetric nuclear matter at saturation density (*i.e.*, equilibrium density, binding energy per nucleon, and incompressibility coefficient). In regards to these properties, the model is indistinguishable from FSUGold. The only additional constraint imposed on the model is that its limiting mass be no smaller than 1.6 solar masses [106]. We feel that lowering this limiting value any further may start conflicting with the observational data [3]. Although no exhaustive parameter search was conducted, we trust that the resulting *extra-soft* equation of state (as given in Table 5.1) is representative of the softness that may be achieved with present-day relativistic mean-field models. With such a soft model, neutron-star radii get significantly reduced indeed (see Fig. 5.1). For example, the neutron radius of a 1.4 $M_{\odot}$ neutron star is reduced by almost one kilometer relative to the FSUGold prediction (see Table 5.2) and by more than 1.5 km

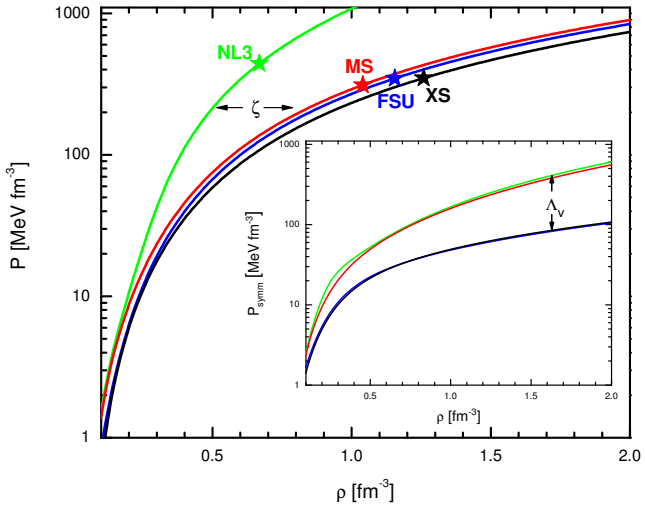

Figure 5.2: Equation of state (*Pressure vs baryon density* of neutron-star matter predicted by the four relativistic mean-field models discussed in the text as compared to the observational extraction [11]. The symbols (stars) indicate the central density and pressure of the maximum-mass neutron star. The inset shows the symmetry pressure, given as the pressure of pure neutron matter minus that of symmetric nuclear matter.

at its limiting mass of 1.6 $M_\odot$. Yet the minimum neutron-star radius of $R = 10.39$ km predicted by the model remains outside the observational error bars.

Do we then conclude that the results presented in Fig. 5.1 are indicative of relativistic equations of state that are too stiff? Do the observational results unambiguously called for a softer equation of state, as would be produced by exotic states of matter, such as meson condensates and/or quark matter? To answer this question we compare in Fig. 5.2 the various equations of state used to generate Fig. 5.1 against the values extracted from the observational data. The inset in the figure displays the symmetry pressure for the models under consideration. To a good approximation, the symmetry pressure can be taken as the difference of the pressure of pure neutron matter and that of the symmetric nuclear matter, $P_{\rm symm} \approx P_{\rm PNM} - P_{\rm SNM}$. The observed softening of the symmetry pressure between models is entirely due to $\Lambda_{\rm v}$. Note, however, that unlike the neutron-skin thickness of neutron-rich

nuclei, the radius of the neutron star is not uniquely constrained by the symmetry pressure at low to intermediate densities [78]. Thus models with similar symmetry pressures, may—and do—predict significantly different stellar radii. Contrary to the expectations generated by Fig. 5.1, most of the equations of state *are not too stiff*. Indeed, with the exception of NL3, the remaining equations of state appear, if anything, slightly *too soft* at the highest density. Based on these results—and these results alone—nucleonic equations of state do not seem to be in conflict with the observational data.

In summary, the *Mass-vs-Radius* relation of neutron stars was computed using equations of state derived from relativistic mean-field models. Although the models are calibrated in the vicinity of nuclear-matter saturation density, it is possible to tune their high-density behavior in a highly efficient and economical manner. In this study we have used two parameters to control the maximum neutron star mass and the stellar radius. As we compared our predictions to the observational data a conflict emerged. Whereas one could generate equations of state that are in agreement with observation, the predicted stellar radii are too large. This result is particularly intriguing given that *"inversion"* methods exist for extracting the equation of state of stellar matter directly from masses and radii of neutron stars [17]. Thus, one would expect that if the M-R predictions do not match observation, neither would the equations of state. Clearly, to reconcile these facts much work remains to be done in both the observational and theoretical fronts. And while the existence of exotic stars is very appealing, suggesting the downfall of the purely nucleonic equations of state may be premature.

5.3 The New Effective Interaction: IU-FSU

In this section we develop an effective interaction suitable for the calculation of the ground-state properties of finite nuclei, their collective response, and the structure of neutron stars [107]. Astrophysical predictions are notoriously difficult as they involve two large extrapolations away from the familiar landscape of stable nuclei. Whereas one involves isospin extrapolations from the domain of stable nuclei to the very neutron-rich systems present in neutron stars, the other one involves an extrapolation from the density of normal nuclei to the very high (and very low) densities that are encountered in neutron stars.

To reduce the uncertainties associated with these extrapolations we impose two additional constraints—one experimental and one observational—on the effective interaction. Specifically, we extend the standard protocol of fitting to the binding energies and charge radii of finite nuclei by demanding that the new effective interaction also reproduces: (a) the neutron radius of ^{208}Pb and (b) the maximum mass of a neutron star. We have selected these two quantities over other possible choices because they can be determined in a model independent manner from experiment and observation. In particular, fixing the neutron radius in ^{208}Pb reduces significantly the uncertainties associated with extrapolations in isospin. The proposed second run of the Lead Radius experiment (PREx) aims to determine the neutron radius of ^{208}Pb in a model independent fashion by using parity violating electron scattering [85, 86]. To reduce the uncertainty associated with extrapolations to high densities, we have selected to fix the maximum neutron star mass. At the time of this research, the maximum neutron star mass selected for the fit was at least equal to the largest—well measured—mass determined from observation [108]. A recent neutron-star mass measurement of $1.97 \pm 0.04\ M_{\odot}$ by Demorest *et. al* [13] has confirmed that the new proposed model indeed agrees with the latest observation.

In principle, other choices are possible to guide these extrapolations. For example, laboratory experiments with heavy ions have played a critical role in probing the nuclear equation of state. By tuning the energy of the colliding beams and the neutron-proton asymmetry, heavy-ion collisions probe vast regions of the phase diagram. In particular, isospin diffusion data may be used to constrain the density dependence of the symmetry energy [41, 109, 110]. This could be used instead of the neutron radius in ^{208}Pb. Moreover, experiments with very energetic heavy ions have compressed nuclear matter to densities in excess of four times nuclear matter saturation density [98]. The determination of the pressure of symmetric nuclear matter at these high densities may be used instead of the maximum neutron star mass. However, not only is the interpretation of heavy-ion data model dependent, but heavy-ion systems are much less neutron rich and often much hotter than neutron stars. This introduces large and uncontrolled uncertainties.

In the past, the correlation between the neutron skin of ^{208}Pb and the non-uniform solid crust of a neutron star has been studied [30]. For models with a stiff equation of state,

namely, one where the pressure increases rapidly with density, it is energetically unfavorable to separate uniform nuclear matter into regions of high and low densities. Thus, models with a stiff equation of state predict low transition densities from non-uniform to uniform neutron-rich matter. The neutron skin thickness in ^{208}Pb also depends on the equation of state of neutron-rich matter: the stiffer the equation of state the thicker the neutron skin. Thus, an inverse relationship was established: *the thicker the neutron skin of a heavy nucleus, the lower the transition from non-uniform to uniform neutron-rich matter (Look at Fig. 4.6)*. This represents one of the many examples that show the utility of constraining the neutron skin thickness in ^{208}Pb—and consequently the effective interaction—for astrophysical applications.

We have already discussed the existence of many relativistic effective interactions. For example, the NL3 interaction [14, 97] provides an excellent description of the binding energy and charge radii of many nuclei throughout the periodic table. When extrapolated to the neutron-star domain, the NL3 effective interaction predicts a very stiff equation of state that generates both large stellar radii and a large maximum neutron star mass. On the other hand, the FSUGold interaction [15] also provides a good description of closed shell nuclei, but predicts a significantly softer equation of state. Indeed, whereas NL3 predicts a maximum neutron star mass of 2.77 $M_{\odot}$, the FSU interaction predicts a limiting mass almost one full solar mass smaller (of 1.72 $M_{\odot}$). The softer equation of state emerges as one incorporates constraints from giant resonances and heavy-ion collisions. At present, we are not aware of any nuclear effective interaction that also incorporates astrophysical constraints in the calibration procedure. The aim of this study is therefore to obtain a new effective interaction that improves on both NL3 and FSUGold by incorporating some of the recent constraints suggested by Steiner, Lattimer, and Brown [12]. In particular, we will show that the EOS predicted by the new model generates a limiting neutron star mass intermediate between NL3 and FSUGold but stellar radii smaller than both.

Our starting point will be the relativistic effective-field theory of Ref. [16] supplemented with an isoscalar-isovector coupling as introduced in Ref. [30]. The interacting Lagrangian

density for this model is given by [16, 30]

$$\begin{aligned}\mathcal{L}_{\rm int} &= \bar{\psi}\left[g_{\rm s}\phi - \left(g_{\rm v}V_{\mu} + \frac{g_{\rho}}{2}\boldsymbol{\tau}\cdot\mathbf{b}_{\mu} + \frac{e}{2}(1+\tau_3)A_{\mu}\right)\gamma^{\mu}\right]\psi \\ &- \frac{\kappa}{3!}(g_{\rm s}\phi)^3 - \frac{\lambda}{4!}(g_{\rm s}\phi)^4 + \frac{\zeta}{4!}g_{\rm v}^4(V_{\mu}V^{\mu})^2 + \Lambda_{\rm v}g_{\rho}^2\,\mathbf{b}_{\mu}\cdot\mathbf{b}^{\mu}g_{\rm v}^2V_{\nu}V^{\nu}\,. \qquad (5.1)\end{aligned}$$

The model contains an isodoublet nucleon field (ψ) interacting via the exchange of two isoscalar mesons, the scalar sigma (ϕ) and the vector omega (V^{μ}), one isovector meson, the rho ($\mathbf{b}^{\mu}$), and the photon (A^{μ}). In addition to meson-nucleon interactions, the Lagrangian density includes scalar and vector self-interactions. (Note that while the original model allows for ρ-meson self-interactions [16], their phenomenological impact has been documented to be small so they will not be considered in this study). The scalar self-interaction is responsible for reducing the compression modulus of nuclear matter from the unrealistically large value of $K = 545$ MeV [7, 10] all the way down to about $K = 230$ MeV. This latter value appears to be consistent with measurements of the isoscalar giant monopole resonance (GMR) in ^{208}Pb [38, 111, 112, 113].

Omega-meson self-interactions, as described by the parameter ζ, soften the equation of state at high density and can be tuned to reproduce the maximum mass of a neutron star. Indeed, Müller and Serot found it was possible to build models with different values of ζ that reproduce the same observed properties at normal nuclear densities, yet produced maximum neutron star masses that differ by almost one solar mass [16]. In particular, models with $\zeta = 0$ predict large limiting masses of about 2.8 $M_{\odot}$—even for models with a soft symmetry energy. In contrast, the nonlinear coupling constant $\Lambda_{\rm v}$ was included to modify the density-dependence of the symmetry energy. Tuning $\Lambda_{\rm v}$ provides a simple and efficient method of softening the symmetry energy without compromising the success of the model in reproducing well determined ground-state observables [15]. Here we will adjust $\Lambda_{\rm v}$ by assuming a relatively small value for the neutron skin thickness of ^{208}Pb. Many properties of finite nuclei, such as the binding energies and charge radii of closed shell nuclei, are insensitive to the values of ζ and $\Lambda_{\rm v}$. Indeed, the NL3 effective interaction reproduces these observables without ever introducing these two empirical parameters. Our approach here is to accommodate newly proposed astrophysical constraints that suggest that, relative to the FSUGold interaction, the equation of state of stellar matter must be slightly softer at intermediate densities and stiffer at high densities [12].

The new effective interaction is generated by adopting the following procedure. We start from the FSUGold parameter set [15] as listed in Table 2.1 and Table 2.2. This parameter set reproduces ground-state properties and collective excitations of closed shell nuclei. However, this interaction has a relatively large value of $\zeta = 0.06$. This reduces the pressure at high densities and generates a relatively small neutron star maximum mass of 1.72 $M_{\odot}$. Note that, to date, the only terrestrial constraint on the high-density component of the EOS comes from energetic heavy-ion collisions [98]. The FSUGold equation of state fits these data comfortable within the errors. Yet, the reported errors are large enough to accommodate slightly stiffer equations of state. As we aim for an interaction with a somewhat larger maximum mass of about 2.0 $M_{\odot}$, we reduce the value of ζ from 0.06 to 0.03. Next, we refit the isoscalar parameters ($g_{\rm s}$, $g_{\rm v}$, κ, and λ) to maintain the saturation properties of symmetric nuclear matter at their FSUGold values, namely, a saturation density of 0.148 fm^{-3} (or a Fermi momentum of $k_{\rm F} = 1.30$ fm^{-1}), an energy per nucleon of $E/A = -16.30$ MeV, and an incompressibility coefficient of $K = 230$ MeV.

Table 5.3: Parameter set for the IU-FSU models discussed in the text. The parameter κ is given in the units of MeV. The meson masses $m_{\rm s}$, $m_{\rm v}$, and m_{ρ} are chosen to have the same values as in the FSUGold model. The nucleon mass has been fixed at $M = 939$ MeV.

Model	$g_{\rm s}^2$	$g_{\rm v}^2$	g_{ρ}^2	κ	λ	ζ	$\Lambda_{\rm v}$
IU-FSU	99.4266	169.8349	184.6877	3.3808	+0.000296	0.03	0.046

We then increase the isoscalar-isovector coupling constant $\Lambda_{\rm v}$ from its FSUGold value of 0.03 to 0.046. This change softens the density dependence of the symmetry energy and reduces the neutron radius in ^{208}Pb. We aim for a modest value of the neutron skin thickness in ^{208}Pb of about $R_n - R_p = 0.16$ fm. This value, although smaller as compared to other relativistic mean field models, is close to those predicted by many non-relativistic models. Note that when we change $\Lambda_{\rm v}$, we also change g_{ρ} in order to maintain the symmetry energy fixed at $\sim$26 MeV at a Fermi momentum of $k_{\rm F} = 1.15$ fm^{-1}. This procedure and the justification for it are described in detail in Ref. [30]. Increasing $\Lambda_{\rm v}$ in this fashion reduces the density dependence of the symmetry energy. This generates a symmetry energy at low densities that is *larger* than the one for FSUGold. As a result, protons near the surface of ^{208}Pb are

Table 5.4: Bulk parameters characterizing the behavior of infinite nuclear matter at saturation density ρ_0. The quantities ε_0 and K_0 represent the binding energy per nucleon and incompressibility coefficient of symmetric nuclear matter, whereas J, L, and $K_{\rm sym}$ represent the energy, slope, and the curvature of the symmetry energy at saturation density.

Model	ρ_0 (fm^{-3})	ε_0 (MeV)	K_0 (MeV)	J (MeV)	L (MeV)	$K_{\rm sym}$ (MeV)
NL3	0.1482	−16.24	271.5	37.28	118.2	+100.9
MS	0.1484	−15.75	250.0	35.00	102.4	−0.2
FSU	0.1484	−16.30	230.0	32.59	60.5	−51.3
IU-FSU	0.1546	−16.40	231.3	31.30	47.2	+28.5

pulled closer to the neutrons in an effort to minimize the neutron-proton asymmetry. This leads to an increase in the charge radius of ^{208}Pb. In order to maintain the charge radius in ^{208}Pb at its experimental value we must slightly increase the Fermi momentum of symmetric nuclear matter from 1.30 to 1.318 fm^{-1}. We then refit the parameters of the model to keep the other saturation properties of nuclear matter intact. Finally, the scalar coupling $g_{\rm s}$ is slightly tuned to improve the fit to the binding energies of closed shell nuclei. Note that we have not changed the scalar mass $m_{\rm s}$ from its FSUGold value.

The resulting parameter set—henceforth referred to as the *Indiana University-Florida State University (IU-FSU) interaction*—is listed in Table 5.3. The resulting bulk properties of infinite nuclear matter have been collected in Table 5.4. In addition, predictions for several ground-state properties of closed shell nuclei are listed in Table 5.5 and compared against other theoretical models and experiment (when available). Finally, using the Hartree code provided by Professor Piekarewicz, predictions for the charge and neutron densities of ^{208}Pb are displayed in Fig. 5.3. Whereas significant differences can be observed in the prediction of the neutron densities, the difference among the models is small for the charge density. Note that although the parameters of the model will eventually be determined from an accurate calibration procedure, the new model reproduces rather well the charge radii and binding energies of closed shell nuclei. However, the IU-FSU interaction predicts the rather modest value of $R_n - R_p = 0.16$ fm for the, as yet unknown, neutron skin thickness in ^{208}Pb.

Table 5.5: Experimental data for the binding energy per nucleon and charge radii for several doubly magic nuclei. Results are presented for the four models employed in the text alongside their predictions for the neutron skin thickness of these nuclei. Note that the MS model is not accurately-calibrated, while it predicts the correct charge radii, it underestimates the binding energy per nucleon.

Nucleus	Observable	Experiment	NL3	MS	FSU	IU-FSU
^{40}Ca	B/A (MeV)	8.55	8.54	7.61	8.54	8.53
	$R_{\rm ch}$ (fm)	3.45	3.46	3.44	3.42	3.41
	$R_n - R_p$ (fm)	—	−0.05	−0.05	−0.05	−0.05
^{48}Ca	B/A (MeV)	8.67	8.64	7.74	8.58	8.55
	$R_{\rm ch}$ (fm)	3.45	3.46	3.45	3.45	3.44
	$R_n - R_p$ (fm)	—	0.23	0.24	0.20	0.17
^{90}Zr	B/A (MeV)	8.71	8.68	7.86	8.67	8.67
	$R_{\rm ch}$ (fm)	4.26	4.26	4.25	4.25	4.23
	$R_n - R_p$ (fm)	—	0.11	0.11	0.09	0.07
^{132}Sn	B/A (MeV)	8.36	8.37	7.62	8.34	8.33
	$R_{\rm ch}$ (fm)	—	4.70	4.69	4.71	4.68
	$R_n - R_p$ (fm)	—	0.35	0.35	0.27	0.22
^{208}Pb	B/A (MeV)	7.87	7.88	7.17	7.89	7.89
	$R_{\rm ch}$ (fm)	5.50	5.51	5.50	5.52	5.48
	$R_n - R_p$ (fm)	—	0.28	0.28	0.21	0.16

5.4 Giant Resonances

At the time that the FSUGold effective interaction was calibrated, the only evidence in favor of a symmetry energy softer than NL3 came from nuclear collective excitations, particularly the mass dependence of the isoscalar giant monopole resonance (GMR). Whereas NL3—with an incompressibility coefficient of $K = 271$ MeV—was able to reproduce the centroid energy of the GMR in ^{208}Pb, it overestimated the GMR in ^{90}Zr. It was later confirmed that the success of the NL3 interaction in reproducing the breathing mode in ^{208}Pb was accidental, as it resulted from a combination of both a stiff EOS for symmetric nuclear matter (Panel (a) of Fig. 5.4) and a stiff symmetry energy [115] (Panel (b) of Fig. 5.4). Indeed, with a relatively large neutron-proton asymmetry of $\alpha \equiv (N - Z)/A = 0.212$, the GMR in ^{208}Pb probes the incompressibility of neutron-rich matter, rather than that of symmetric matter. Given that the incompressibility of neutron-rich matter softens with α [116], NL3 could reproduce the GMR in ^{208}Pb by cancelling its stiff incompressibility

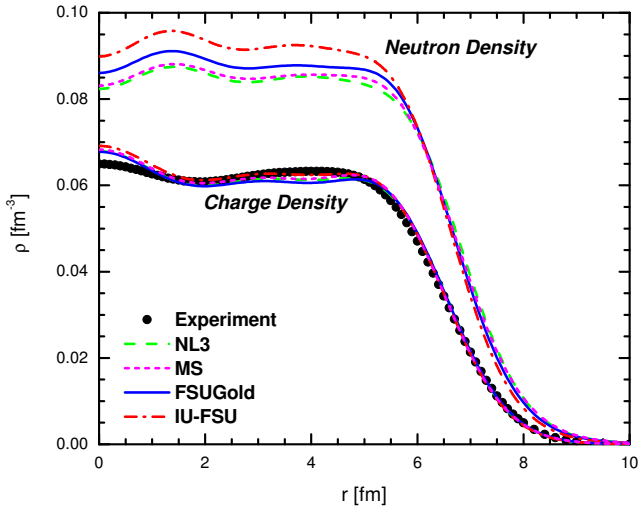

Figure 5.3: Model predictions for the charge and neutron densities of ^{208}Pb (The code was provided by Professor Piekarewicz). The experimental charge density is from Ref. [114].

coefficient K with a correspondingly stiff symmetry energy:

$$K_0(\alpha) = K_0 + K_\tau \alpha^2 + \mathcal{O}(\alpha^4) = K_0 + \left(K_{\rm sym} - 6L - \frac{Q_0}{K_0} L \right) \alpha^2 + \mathcal{O}(\alpha^4) \ , \tag{5.2}$$

where the expressions for K_0, Q_0, L, and $K_{\rm sym}$ were introduced in equations (2.48), (2.49), (2.56), and (2.57), respectively. This cancellation, however, is incomplete in ^{90}Zr because its nucleon asymmetry is almost twice as small as that of ^{208}Pb (See Table 5.6). Thus, to develop the FSU effective interaction Ref. [15] used the GMR in ^{90}Zr, rather than in ^{208}Pb, to fix the incompressibility coefficient of symmetric nuclear matter. Having fixed K, Ref. [15] used the GMR—and the isovector giant dipole resonance (IVGDR)—in ^{208}Pb to constrain the density dependence of the symmetry energy [15]. As we shall see below (see Table 5.7), the newly proposed IU-FSU effective interaction continues to reproduce the centroid energy of these three modes.

The distribution of both isoscalar monopole and isovector dipole strength were computed in a relativistic random-phase approximation (RPA). The first step in calculating the RPA response is the computation of the mean-field ground state in a self-consistent

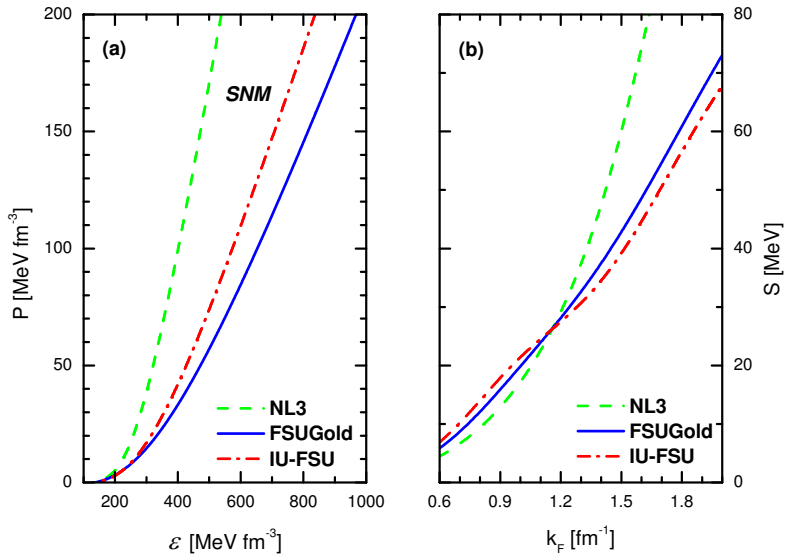

Figure 5.4: Equations of state for symmetric nuclear matter (a), and the symmetry energy as a function of baryon Fermi momentum (b) is given for the three models discussed in the text.

mean-field approximation (This part of the research requires a heavy numerical computations, and was performed by Professor Piekarewicz). Once self-consistency is achieved, three important pieces of information become available: (i) the single-particle energies of the occupied orbitals, (ii) their single-particle wave functions, and (iii) the self-consistent mean-field potential. This mean-field potential—without any modification—must then be used to generate the nucleon propagator; only then can one ensure the conservation of the vector current. The nucleon propagator, which is an essential building block of the uncorrelated polarization tensor, is computed non-spectrally to avoid any dependence on the artificial cutoffs and truncations that plague most spectral approaches. Moreover, a great merit of the non-spectral approach is that the continuum is treated exactly. Once the uncorrelated polarization insertion is computed, the correlated RPA polarization is obtained by iterating it to all orders with the consistent residual interaction. The distribution of strength is then obtained directly from the imaginary part of the polarization tensor. A detailed de-

Table 5.6: Incompressibility coefficients of the neutron-rich matter are given for the models discussed in the text. The asymmetry parameter $\alpha = 0$ corresponds to the SNM, $\alpha = 0.111$ to the nuclei of ^{90}Zr, and $\alpha = 0.212$ to the nuclei of ^{208}Pb.

Models	$K(\alpha = 0)$ (MeV)	$K(\alpha = 0.111)$ (MeV)	$K(\alpha = 0.212)$ (MeV)
NL3	271.5	262.9	240.2
FSUGold	230.0	226.6	217.6
IU-FSU	231.3	228.9	222.6

scription of the relativistic RPA approach may be found in Ref. [111, 117]. Results for the centroid energies of the giant monopole and dipole resonances are presented in Table 5.7 for the three effective interactions considered in the text. Unlike the NL3 model, the results obtained with both the FSUGold and the IU-FSU effective interactions are consistent with experiment.

Table 5.7: Centroid energies for the GMR in ^{208}Pb and ^{90}Zr, and the peak energy for the IVGDR in ^{208}Pb. Experimental data are extracted from Refs. [38] and [118].

Nucleus	Observable	Experiment	NL3	FSUGold	IU-FSU
^{208}Pb	GMR (MeV)	14.17 ± 0.28	14.32	14.04	14.17
^{90}Zr	GMR (MeV)	17.89 ± 0.20	18.62	17.98	17.87
^{208}Pb	IVGDR (MeV)	13.30 ± 0.10	12.70	13.07	13.24

5.5 Equation of State and Neutron Star Structure in the IU-FSU Model

5.5.1 Symmetric Nuclear and Pure Neutron Matter

Following standard mean-field practices, the energy density of asymmetric nuclear matter may be computed over all values of the asymmetry parameter, $\alpha = (\rho_n - \rho_p)/\rho$. The equation of state (pressure as a function of baryon density) for symmetric nuclear matter ($k_{\rm F}^p = k_{\rm F}^n$ and $R_0 \equiv g_\rho b_0 \equiv 0$) is displayed in Fig 5.5. By design, the FSUGold and IU-FSU interactions have (almost) the same incompressibility coefficient so they predict similar pressures at low to intermediate densities. However, at higher densities the IU-FSU interaction is stiffer because it has a smaller value of ζ as compared to the FSUGold interaction. To date, the only

terrestrial constraint on the high-density component of the EOS comes from energetic heavy-ion collisions. Both of these models predict equations of state that are consistent with the phenomenological flow analysis by Danielewicz, Lacey, and Lynch [98]. In contrast, the NL3 interaction, although enormously successful in reproducing ground-state properties of finite nuclei, predicts an equation of state that is significantly stiffer than the phenomenological extraction.

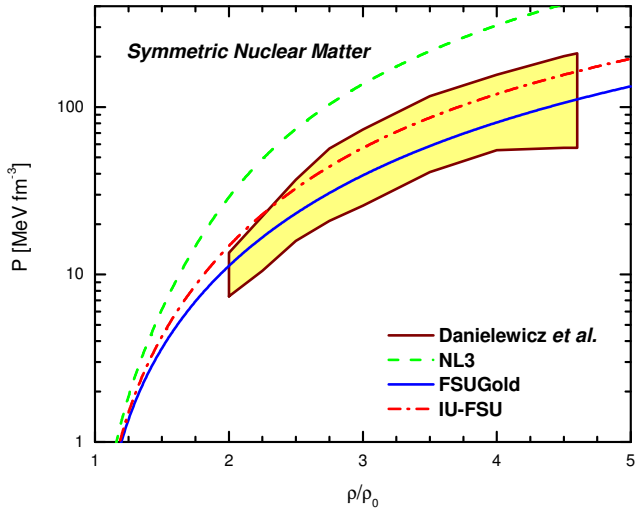

Figure 5.5: The equation of state—pressure P *vs* baryon density—of symmetric nuclear matter. Here ρ_0 is the density of nuclear matter at saturation and the shaded area represents the EOS extracted from the analysis of Ref. [98].

The equation of state of pure neutron matter (PNM) provides a powerful theoretical constraint on models of the effective interaction. By building on the universal behavior of dilute Fermi gases with an infinite scattering length, significant progress has been made in constraining the equation of state of pure neutron matter [90]. To date, a variety of models using different neutron-neutron interactions and a variety of many-body techniques have been employed to compute the EOS of dilute neutron matter (see Ref. [94] and references therein). In Fig. 5.6 we display the energy per particle of pure neutron matter for a variety of microscopic approaches [94] and for the three relativistic effective interaction discussed in the

text. In most relativistic descriptions the isovector interaction is modelled by the exchange of a single vector-isovector ("rho") meson with its (Yukawa) coupling to the nucleon tuned to reproduce the symmetry energy at saturation density. Invariably, such a simple prescription generates a stiff symmetry energy. In turn, this yields an EOS for dilute neutron matter that is inconsistent with the model-independent results of Schwenk and Pethick (denoted by the shaded area in Fig. 5.6). The FSUGold isovector interaction improves on NL3 by adding an isoscalar-isovector mixing term ($\Lambda_{\rm v}$) that softens the symmetry energy. Recall that such a softening is required to reproduce the centroid energies of various collective modes (see Table 5.7). Without any further adjustment, the FSUGolf interaction is also consistent with the theoretical constraints (see solid blue line). Finally, the IU-FSU interaction—with an additional softening relative to FSUGold—remains within the theoretical "error bars".

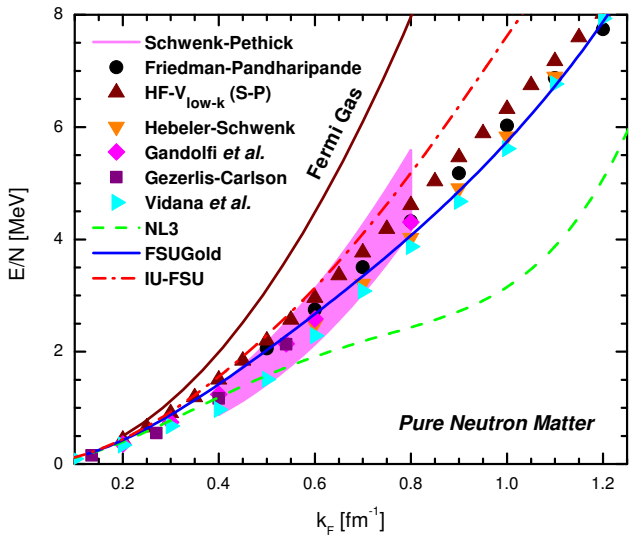

Figure 5.6: Energy per nucleon as a function of the Fermi momentum for pure neutron matter.

5.5.2 Neutron Star Matter

We conclude this section by computing the *mass-vs-radius* (M-R) relationship of neutron stars. Given that the structure of neutron stars is sensitive to the EOS over an enormous

range of densities, we must resort to various descriptions as discussed in Sections 3.8 and 5.2. For the non-uniform outer crust we employ the equation of state of Baym, Pethick, and Sutherland [46]. At densities of about a third of nuclear-matter saturation density, uniformity in the system is restored. For this (liquid-core) region we use an EOS generated from the relativistic models discussed in the text. Although significant progress has been made in simulating the exotic structure of the inner crust (*i.e.,* the region between the outer crust and the liquid core) a detailed equation of state is still missing in this region. Hence, we resort to a fairly accurate polytropic EOS to interpolate between the solid crust and the uniform liquid core [56, 74, 75, 76, 77]. The transition from the uniform liquid core to the solid crust is sensitive to the density dependence of the symmetry energy. The crust-to-core transition density ρ_t is obtained from an RPA stability analysis to determine the onset of the instability to small amplitude density oscillations [77]. With such an equation of state in hand, we can now proceed to integrate the Tolman-Oppenheimer-Volkoff equations to determine the structure of neutron stars.

In Fig. 5.7 we display predictions for the equation of state of stellar matter (*i.e.,* neutron-rich matter in beta equilibrium) for the three models discussed in the text, alongside the constraint extracted from Ref. [12]. For reference, also shown is the stiffest ($P = \mathcal{E}$) possible equation of state consistent with causality. As suggested in Ref. [12], the FSUGold interaction appears slightly stiff at intermediate densities and too soft at high densities. The IU-FSU interaction successfully corrects both of these problems. Note, however, that the observational EOS can accommodate even stiffer equations of state. We stress that, if required, this can be implemented rather easily by reducing even further the value of ζ.

In Fig. 5.8 we display predictions for the M-R relation and compare them against observational constraints extracted from the analyses of Refs. [11] and [12]. The very stiff behavior of the EOS predicted by NL3 is immediately ruled out by both observational constraints, although it comfortably predicts the recent maximum stellar mass measurement by [13]. In the case of the FSUGold effective interaction, we recently identified a conflict when compared with the analysis by Özel and collaborators (See Ref. [106] and Section 5.2). Whereas the FSUGold model seems to generate an EOS that is consistent with observation, the predicted stellar radii were simply too large. Relative to the analysis by Steiner Lattimer,

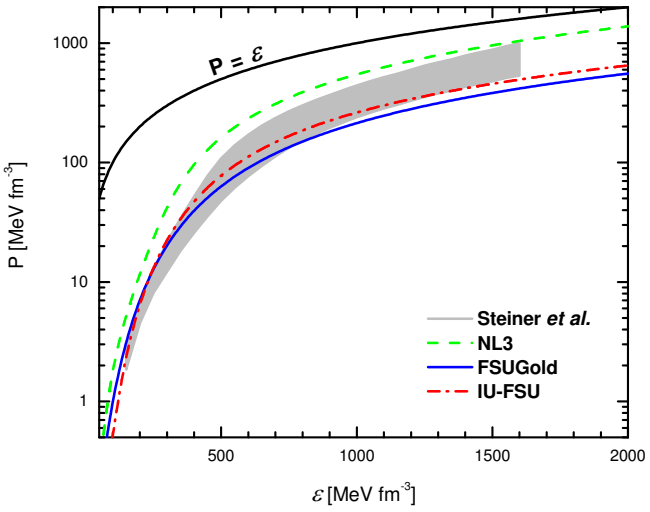

Figure 5.7: Equation of state—pressure *vs* energy density—of neutron-rich matter in beta equilibrium. The shaded region displays the observational constraint extracted from Ref. [12]. The solid black line ($P = \mathcal{E}$) denotes the stiffest possible equation of state consistent with causality.

and Brown [12], the FSU predictions overestimate the stellar radius—although not as much as suggested by [11]—but underestimates the maximum neutron star mass. The IU-FSU interaction, with a softer EOS at intermediate densities and a stiffer one at high densities, is motivated in response to these findings. Indeed, the IU-FSU interaction predicts a maximum stellar mass of 1.94 $M_\odot$ and a stellar radius of $R = 12.49$ km for a 1.4 $M_\odot$ neutron star (see Table 5.8). These predictions are consistent with the 2σ values extracted from X-ray observations by Steiner, Lattimer, and Brown [12]. However, they are well outside the limits extracted by Özel and collaborators [11]. Given that such extractions depend critically on the models used to simulate X-ray bursts, much work remains to be done to reconcile these two analyses. We close this section by listing in Table 5.8 predictions for several important neutron-star properties. In addition to the properties already discussed (such as masses and radii), the table includes the minimum proton fraction and the minimum density required for the onset of the direct Urca process and the minimum stellar mass that may cool down

by the direct Urca process. Note that small neutron star radii and enhanced cooling are generally regarded as good indicators of a possible phase transition in the stellar core.

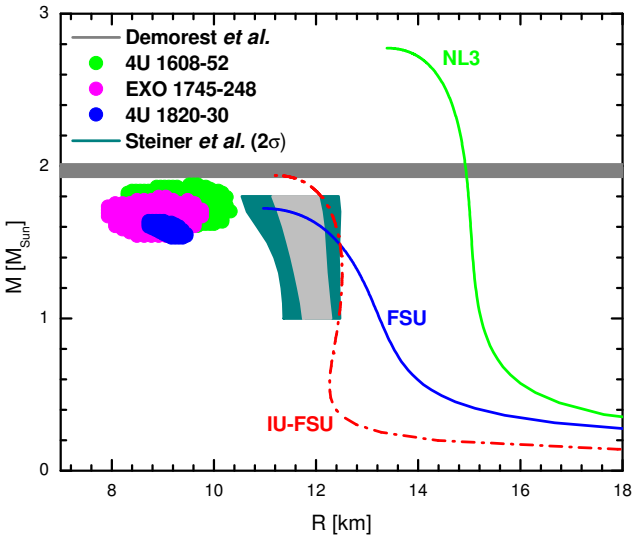

Figure 5.8: *Mass-vs-Radius* relation predicted by the three relativistic mean-field models discussed in the text. The observational data that suggest very small stellar radii represent 1σ confidence contours for the three neutron stars reported in Ref. [11]. The two shaded areas that suggest larger radii are 1σ and 2σ contours extracted from the analysis of Ref. [12]. The recent maximum stellar mass measurement of Ref. [13] without radius constraint is also supplemented.

5.6 Conclusions

The structure of neutron stars depends sensitively on the equation of state of neutron-rich matter in beta equilibrium. As such, nuclear effective interactions play a critical role in astrophysical applications. Given the large extrapolations in isospin and density that are required to compute the EOS, it is imperative to constrain the effective interaction. Motivated by two recent analyses that have provided simultaneous mass and radius information on neutron stars [11, 12], we have introduced a new effective interaction constrained by the ground state properties of finite nuclei, their collective excitations, the properties of both

Table 5.8: Predictions for several neutron-star observables. The various quantities are as follows: ρ_t is the transition density from non-uniform to uniform neutron-rich matter, R is the radius of a 1.4 solar-mass neutron star, $M_{\rm max}$ is the maximum mass, $R_{\rm max}$ is the corresponding radius for the maximum mass, $\rho_{\rm Urca}$ is the threshold density for the direct Urca process, and $M_{\rm Urca}$ is the minimum mass neutron star that may cool down by the direct Urca process.

Observable	NL3	FSUGold	IU-FSU
ρ_t (fm^{-3})	0.052	0.076	0.087
R (km)	15.07	12.66	12.50
$M_{\rm max}(M_\odot)$	2.774	1.722	1.939
$R_{\rm max}$ (km)	13.39	10.97	11.19
$\rho_{\rm Urca}$ (fm^{-3})	0.205	0.467	0.613
$Y_{p\rm Urca}$	0.130	0.137	0.138
$M_{\rm Urca}(M_\odot)$	0.839	1.301	1.772

dilute and dense matter, and the structure of neutron stars. Thus, experimental, theoretical, and observational constraints have all been incorporated into the calibration procedure.

Following the conclusions of Ref. [12]—that suggest that the accurately calibrated FSUGold effective interaction is slightly stiff at intermediate densities but soft at high densities—we have used two empirical parameters to correct these shortcomings. The new effective interaction—dubbed *"IU-FSU"*—softens the EOS at intermediate densities by reducing the neutron skin thickness of ^{208}Pb and stiffens the EOS at high density by increasing the maximum neutron star mass relative to the FSUGold predictions.

Existing relativistic mean-field interactions are flexible enough to reproduce, not only the charge density and binding energy of closed shell nuclei, but also the neutron skin thickness of ^{208}Pb and the maximum neutron star mass [32, 106]. In particular, the density dependence of the symmetry energy is highly sensitive to the empirical parameter $\Lambda_{\rm v}$. Thus, an increase in the value of $\Lambda_{\rm v}$ softens the EOS at intermediate densities and generates a neutron skin thickness in ^{208}Pb of only R_n–R_p=0.16 fm. For comparison, the NL3 and FSUGold effective interactions predict significantly larger neutron skins: 0.28 fm and 0.21 fm, respectively. To stiffen the EOS at high densities we rely on the empirical parameter ζ [16, 32, 106]. Including ζ may be used to change the maximum neutron star mass by almost one solar mass without adversely affecting the bulk properties of nuclear matter around saturation density. Relative

to the FSUGold model, the new IU-FSU interaction increases the maximum neutron star mass from 1.72 $M_{\odot}$ to 1.94 $M_{\odot}$.

As more accurate data become available, the coupling constants of the theory may need to be re-adjusted. The calibration procedure outlined here can accomplish this task rapidly and efficiently. Ultimately, however, one would rely on an *accurate* calibration procedure to determine the best-fit parameters of the theory and to obtain correlations among the various observables. Nevertheless, as it stands now the new IU-FSU relativistic effective interaction reproduces: (a) the binding energies and charge radii of closed-shell nuclei, (b) various nuclear giant (monopole and dipole) resonances, (c) the low-density behavior of pure neutron matter, (d) the high-density behavior of symmetric nuclear matter, and (e) the mass-radius relation of neutron stars.

CHAPTER 6

ON THE ACCURATE CALIBRATION OF RMF MODELS: CORRELATING OBSERVABLES AND PROVIDING MEANINGFUL THEORETICAL UNCERTAINTIES

6.1 Introduction

The need to provide meaningful uncertainties in theoretical predictions of physical observables is a theme that is gaining significant momentum among the scientific community. Indeed, the search for a microscopic theory that both predicts and provides well-quantified theoretical uncertainties is one the founding pillars of the successful UNEDF collaboration [119]. Moreover, as recently articulated in an editorial published in the Physical Review A [120], theoretical predictions submitted for publication are now expected to be accompanied by meaningful uncertainty estimates. The need for *"theoretical error bars"* becomes particularly critical whenever models calibrated in certain domain are used to extrapolate into uncharted regions.

Although firmly rooted in QCD, computing both the nucleon-nucleon (NN) interaction and the properties of nuclei in terms of the underlying quark and gluon constituents remains a daunting task. Hence, rather than relying strictly on QCD, one uses the properties of QCD (such as chiral symmetry and relevant energy scales) as a guide to construct phenomenological interactions using nucleons and mesons as the fundamental degrees of freedom. However, QCD has little to say about the strength of the underlying model parameters which must then be constrained from experimental data. For example, deuteron properties along with two-body scattering data are used to build a nucleon-nucleon interaction that may then be

used (supplemented with a phenomenological three-body force) to compute *ab-initio* the properties of light nuclei. Attempting ab-initio calculations of the properties of medium-to-heavy nuclei remains well beyond the scope of the most powerful computers to date. In this case one must bring to bear the full power of density functional theory (DFT). Following the seminal work by Kohn and collaborators [121], DFT shifts the focus from the complicated many-body wave-function to the much simple one-body density. Moreover, Kohn and Sham have shown how the one-body density may be obtained from a variational problem that reduces to the solution of a set of mean-field-like (*"Kohn-Sham"*) equations [122]. The form of the Kohn-Sham potential is in general reminiscent of the underlying (bare) NN potential. However, the constants that parametrize the Kohn-Sham potential are directly fitted to many-body observables (such as masses and charge radii) rather than two-body data. In this manner the complicated dynamics originating from exchange and correlation effects get implicitly encoded in the empirical constants. Yet regardless of whether the effective interaction is fitted to two-nucleon or to many-body data—the determination of the model parameters often relies on the optimization of a quality measure.

In this contribution we focus on density functional theory and follow the standard protocol of determining the model parameters through a χ^2-minimization procedure. This procedure is implemented by: (a) selecting a set of accurately measured ground-state observables and (b) demanding that the differences between these observables and the predictions of the model be minimized. Note that in the present framework a model consists of both a set of parameters and a χ^2-measure. In general, modifying the χ^2-measure (*e.g.*, by adding observables) results in a change in the model parameters. Traditionally, once the χ^2-minimum has been found one proceeds to validate the model against observables not included in the quality fit. Nuclear collective excitations are a potentially *"safe"* testing arena for the model as they represent the *small oscillations* around the variational ground state. But what happens when the model must be extrapolated to regions of large isospin imbalance and high density as in the interior of neutron stars? Clearly, without reliable theoretical uncertainties it is difficult to assess the predictions of the model. To remedy this situation we propose to study the *small oscillations* around the χ^2-minimum—rather than the minimum itself. As we shall see, such a statistical analysis—inspired by the recent study

reported in Ref. [123]—provides access to a wealth of information that remains hidden if one gets trapped in the χ^2-minimum. Among the critical questions that we will be able to answer is how fast does the χ^2-measure deteriorate as one moves away from the minimum. Should additional observables be added to the χ^2-measure to better constrain the model? And if such observables are hard to determine are there others that may be more readily accessible and provide similar constraints? A particularly topical example that illustrates such a synergy is the correlation between the neutron-skin thickness and electric dipole polarizability of neutron-rich nuclei [123, 124]. A detailed analysis of such correlation—which involves a systematic study of the isovector dipole response—is beyond the scope of this initial study and will become the subject of a forthcoming publication. Yet the study of correlations among observables sensitive to the poorly-determined density dependence of the symmetry energy will become a recurring theme throughout this contribution.

This chapter has been organized as follows. In Sec. 6.2 we develop the necessary formalism to implement the correlation analysis. This section is divided in two parts: (a) a discussion on the structure of a class of relativistic mean-field models and (b) a complete derivation of the statistical formalism required to perform the covariance analysis. In Sec. 6.3 two simple examples are used to illustrate the power of the formalism. This exercise culminates with the estimation of meaningful theoretical error bars and correlation coefficients. Our conclusions and outlook are presented in Sec. 6.4.

6.2 Formalism

In this section we develop the formalism required to implement the correlation analysis. First, in Sec. 6.2.1 we introduce a fairly general class of relativistic mean-field models that are rooted in effective-field-theory concepts, such as naturalness and power counting. Second, in Sec. 6.2.2 we present a self-contained derivation of the ideas and formulas required to implement the covariance analysis.

6.2.1 Relativistic Mean-Field Models

Relativistic mean-field models traditionally include an isodoublet nucleon field (ψ) interacting via the exchange of two isoscalar mesons (a scalar ϕ and a vector V^μ), one vector-

isovector meson (b^μ), and the photon (A^μ) [10, 16, 29]. The non-interacting Lagrangian density for such a model may be written as follows:

$$\begin{aligned}\mathcal{L}_0 = {} & \bar{\psi}\left(i\gamma^\mu\partial_\mu - M\right)\psi + \frac{1}{2}\partial_\mu\phi\,\partial^\mu\phi - \frac{1}{2}m_{\rm s}^2\phi^2 \\ & - \frac{1}{4}V^{\mu\nu}V_{\mu\nu} + \frac{1}{2}m_{\rm v}^2V^\mu V_\mu - \frac{1}{4}\mathbf{b}^{\mu\nu}\cdot\mathbf{b}_{\mu\nu} + \frac{1}{2}m_\rho^2\,\mathbf{b}^\mu\cdot\mathbf{b}_\mu - \frac{1}{4}F^{\mu\nu}F_{\mu\nu}\ , \end{aligned} \tag{6.1}$$

where $V_{\mu\nu}$, $\mathbf{b}_{\mu\nu}$, and $F_{\mu\nu}$ are the isoscalar, isovector, and electromagnetic field tensors, respectively. That is,

$$V_{\mu\nu} = \partial_\mu V_\nu - \partial_\nu V_\mu\ , \tag{6.2a}$$

$$\mathbf{b}_{\mu\nu} = \partial_\mu \mathbf{b}_\nu - \partial_\nu \mathbf{b}_\mu\ , \tag{6.2b}$$

$$F_{\mu\nu} = \partial_\mu A_\nu - \partial_\nu A_\mu\ . \tag{6.2c}$$

The four constants M, $m_{\rm s}$, $m_{\rm v}$, and m_ρ represent the nucleon and meson masses and may be treated (if wished) as empirical parameters. Often, however, $m_{\rm s}$ is determined from an accurate calibration procedure. The interacting Lagrangian density has evolved significantly over the years and now incorporates a variety of meson self-interacting terms that are designed to improve the quality of the model. Following ideas developed in Ref. [16] we write the interacting Lagrangian density in the following form:

$$\mathcal{L}_{\rm int} = \bar{\psi}\left[g_{\rm s}\phi - \Big(g_{\rm v}V_\mu + \frac{g_\rho}{2}\boldsymbol{\tau}\cdot\mathbf{b}_\mu + \frac{e}{2}(1+\tau_3)A_\mu\Big)\gamma^\mu\right]\psi - U(\phi, V_\mu, \mathbf{b}_\mu)\ . \tag{6.3}$$

In addition to the standard Yukawa interactions, the Lagrangian is supplemented with an effective potential $U(\phi, V_\mu, \mathbf{b}_\mu)$ consisting of non-linear meson interactions that serve to simulate the complicated dynamics that lies beyond the realm of the mean-field theory. Indeed, by fitting the various coupling constants directly to nuclear properties—rather than to two-nucleon data—the complicated dynamics originating from nucleon exchange, short-range effects, and many-body correlations gets implicitly encoded in a small number of parameters. For the purpose of the present discussion we introduce explicitly all non-linear terms up to fourth-order in the meson fields. That is,

$$\begin{aligned} U(\phi, V^\mu, \mathbf{b}^\mu) = {} & \frac{\kappa}{3!}\Phi^3 + \frac{\lambda}{4!}\Phi^4 - \frac{\zeta}{4!}\Big(W_\mu W^\mu\Big)^2 - \Lambda_{\rm v}\Big(W_\nu W^\nu\Big)\Big(\mathbf{B}_\mu\cdot\mathbf{B}^\mu\Big) - \frac{\xi}{4!}\Big(\mathbf{B}_\mu\cdot\mathbf{B}^\mu\Big)^2 \\ & + \kappa_0\Phi W_\mu W^\mu + \kappa_1\Phi\mathbf{B}_\mu\cdot\mathbf{B}^\mu + \lambda_0\Phi^2 W_\mu W^\mu + \lambda_1\Phi^2\mathbf{B}_\mu\cdot\mathbf{B}^\mu \\ & - \Lambda'_{\rm v}\Big(W_\mu W_\nu\Big)\Big(\mathbf{B}^\mu\cdot\mathbf{B}^\nu\Big) + \ldots \end{aligned} \tag{6.4}$$

where the following definitions have been introduced: $\Phi \equiv g_{\rm s}\phi$, $W_\mu \equiv g_{\rm v}V_\mu$, and $\mathbf{B}_\mu \equiv g_\rho \mathbf{b}_\mu$. Given that the present analysis will be restricted to the study of uniform nuclear matter, terms proportional to the derivatives of the meson fields have not been included. As it stands, the relativistic model contains 14 undetermined parameters (1 meson mass, 3 Yukawa couplings, and 10 meson self-interaction terms). Note that if one incorporates the occasionally-used scalar-isovector δ-meson [125, 126], then 9 additional parameters must be included to this order (1 Yukawa coupling, and 8 meson self-interaction terms). That is,

$$\begin{aligned}\mathcal{L}_{\rm int,\delta} &= \bar{\psi}\left[\frac{1}{2}\boldsymbol{\tau}\cdot\mathbf{D}\right]\psi - \kappa_0'\mathbf{D}\cdot\mathbf{B}^\mu W_\mu - \kappa_1'\Phi\mathbf{D}\cdot\mathbf{D} - \frac{\lambda'}{4!}\left(\mathbf{D}\cdot\mathbf{D}\right)^2 - \lambda_0'\Phi^2\left(\mathbf{D}\cdot\mathbf{D}\right) \\ &- \lambda_1'\left(\mathbf{D}\cdot\mathbf{D}\right)W_\mu W^\mu - \lambda_2'\left(\mathbf{D}\cdot\mathbf{D}\right)\mathbf{B}_\mu\cdot\mathbf{B}^\mu - \lambda_3'\left(\mathbf{D}\cdot\mathbf{B}_\mu\right)\left(\mathbf{D}\cdot\mathbf{B}^\mu\right) + \Lambda_{\rm v}''\Phi\left(\mathbf{D}\cdot\mathbf{B}^\mu\right)W_\mu\ ,\end{aligned} \tag{6.5}$$

where $\mathbf{D} \equiv g_\delta\boldsymbol{\delta}$ have been introduced.

A model with 14—or 23—parameters goes significantly beyond the early relativistic models that were able to reproduce the saturation point of symmetric nuclear matter as well as various ground-state observables with only a handful of parameters (a single meson mass and three Yukawa couplings) [7, 10, 127]. Although fairly successful, those early models suffered from a major drawback: an unrealistically large incompressibility coefficient. Such a problem was successfully solved by Boguta and Bodmer with the introduction of cubic and quartic scalar meson self-interactions [8]. Remarkably, using only these six parameters $(m_{\rm s}, g_{\rm s}, g_{\rm v}, g_\rho, \kappa, \lambda)$ it is possible to reproduce a host of ground-state properties of finite nuclei (both spherical and deformed) throughout the periodic table [14, 97]. And by adding two additional parameters (ζ and $\Lambda_{\rm v}$) the success of the model can be extended to the realm of nuclear collective excitations and neutron-star properties [15, 30, 99, 107].

Given that the existent database of both laboratory and observational data appears to be accurately described by an 8-parameter model, is there any compelling reason to include 6—or 15—additional parameters? And if so, what criteria does one use to constrain these remaining parameters? A meaningful criterion used to construct an effective Lagrangian for nuclear-physics calculations has been proposed by Furnstahl, Serot, and Tang based on the concept of *"naive dimensional analysis"* and *"naturalness"* [128, 129]. The basic idea behind naturalness is that once the *dimensionful* meson fields (having units of mass) have been properly scaled using strong-interaction mass scales, the remaining *dimensionless*

coefficients of the effective Lagrangian should all be *"natural"*; that is, neither too small nor too large [128, 130]. Such an approach is both useful and powerful as it allows an organizational scheme based on an expansion in powers of the meson fields. Terms in the effective Lagrangian with a large number of meson fields will then be suppressed by a large strong-interaction mass scale. In this regard the assumption of naturalness is essential as the suppression from the large mass scale should not be compensated by large, *i.e.*, unnatural, coefficients. It was by invoking the concept of naturalness that we were able to truncate the effective potential $U(\phi, V^{\mu}, \mathbf{b}^{\mu})$ beyond quartic terms in the meson fields.

Although we have justified the truncation of the effective Lagrangian invoking naturalness, we are not aware of an additional organizational principle that may be used *a-priori* to limit further the form of $U(\phi, V^{\mu}, \mathbf{b}^{\mu})$. This implies that *all* model parameters must be retained, as it is unnatural to set some coefficients arbitrarily to zero without a compelling symmetry argument [131]. In principle then, all model parameters must be retained and subsequently determined from a fit to empirical data. In practice, however, many successful theoretical models—such as NL3 [14, 97] and FSUGold [15]—arbitrarily set some of these parameters to zero. The *"justification"* behind these fairly ad-hoc procedure is that whereas the neglected terms are of the same order in a power-counting scheme, the full set of parameters is poorly determined by existing data, so ignoring a subset model parameters does not compromise the quality of the fit [16, 128].

An important goal of this chapter is to investigate correlations among the parameters of the model and whether additional physical observables could remove such correlations. To do so we follow the standard protocol of determining the model parameters through a χ^2 minimization procedure. Traditionally, this procedure is implemented by selecting a set of accurately measured ground-state observables for a variety of nuclei and then demanding that the differences between the observables and the predictions of the model be minimized. Once this is done, the success of the model may be gauged by computing observables not included in the fit. However, it is often difficult to assess the uncertainty in the predictions of the model. To address this deficiency we propose to study the *small oscillations* around the minimum—rather than the minimum itself. Such a study—inspired by the recent statistical analysis presented in Ref. [123]—provides access to a wealth of information that, in turn,

enables one to specify meaningful theoretical error bars as well as to explore correlations among model parameters and calculated observables.

Although the following discussion is framed in the context of an underlying χ^2-measure, our arguments are general as they merely rely on the existence of a (local) minimum (or an extremum). As in any small-oscillations problem, deviations of the χ^2-measure from its minimum value are controlled by a symmetric $F \times F$ matrix, where F represents the total number of model parameters. Being symmetric, such a matrix may be brought into a diagonal form by means of an orthogonal transformation. The outcome of such a diagonalization procedure is a set of F eigenvalues and F eigenvectors. When a point in parameter space is expanded in terms of these eigenvectors, the deviations of the χ^2-measure from its minimum value take the form of a system of F *uncoupled harmonic oscillators*—with the eigenvalues playing the role of the F spring constants. The spring constants may be *"stiff"* or *"soft"* depending on whether the curvature around the minimum is steep or shallow, respectively. As one explores the parameter landscape along a stiff direction—and thus along a particular linear combination of model parameters—a rapid worsening of the χ^2-measure ensues, suggesting that the fitting protocol is robust enough to constrain this particular linear combination. Conversely, no significant deterioration in the quality of the fit is observed as one moves along a soft direction. In this case the χ^2-minimum is of little significance as scores of parameter sets (*i.e.,* models) of nearly equal quality may be generated. This situation derives from the lack of certain critical observables in the χ^2-measure. As we shall see, the particular linear combination of model parameters defining the soft direction often provides enough hints to identify the missing observable(s). Moreover, through this sort of analysis one may establish correlations among observables that are particularly sensitive to such soft directions. This is important as certain observables may be easier to measure than others. A particular topical case is that of the neutron-skin thickness in ^{208}Pb and the electric dipole polarizability [123, 124, 132].

6.2.2 Linear Regression and Covariance Analysis

As discussed earlier, relativistic models of nuclear structure are characterized by a number of model parameters, such as masses, Yukawa couplings, and non-linear meson coupling constants. Following the notation of Ref. [123], we denote a point in such a parameter space

by $\mathbf{p} = (p_1, \ldots, p_F)$, where F is the total number of model parameters. In principle, each value of $\mathbf{p}$ represents a model. In practice, of course, one is ordinarily interested in the *"best model"* as defined by a quality measure. To do so, the model parameters are often calibrated to a well-determined set of ground-state properties of finite nuclei (such as masses and charge radii) that is supplemented by a few bulk properties of infinite nuclear matter (such as the binding energy, incompressibility coefficient, and symmetry energy at saturation density). Once the model parameters and the group of observables have been selected, the optimal parameter set is determined via a least-squares fit to the following χ^2 quality measure:

$$\chi^2(\mathbf{p}) = \sum_{n=1}^{N} \left(\frac{\mathcal{O}_n^{(\mathrm{th})}(\mathbf{p}) - \mathcal{O}_n^{(\mathrm{exp})}}{\Delta \mathcal{O}_n} \right)^2 . \tag{6.6}$$

Here N (often much larger than F) denotes the total number of selected observables whereas "th" and "exp" stand for the theoretical prediction and experimental measurement, respectively. Further, every observable is weighted by a factor of $(\Delta \mathcal{O}_n)^{-1}$ that is (customarily) associated with the accuracy of the measurement.

We assume that—through a numerical procedure that is not of particular relevance to this work—an accurately-calibrated model $\mathbf{p}_0$ has been found. This implies that all first derivatives of χ^2 vanish at $\mathbf{p}_0$. That is,

$$\frac{\partial \chi^2(\mathbf{p})}{\partial p_i}\Big|_{\mathbf{p}=\mathbf{p}_0} \equiv \partial_i \chi^2(\mathbf{p}_0) = 0 \quad (\text{for } i = 1, \ldots, F) . \tag{6.7}$$

The existence of the minimum (as opposed to a maximum or saddle point) also implies that a particular set of F second derivatives (to be defined shortly) must all be positive. Approaches based on a least-squares fit to a χ^2-measure often culminate with the identification of the optimal parametrization $\mathbf{p}_0$. The predictive power of the model may then be appraised by computing observables that were not included in the fitting protocol. Less often, however, least-squares-fit approaches are used to evaluate the *"uniqueness"* of the model. In other words, how fast does the χ^2-measure deteriorate as one moves away from $\mathbf{p}_0$? Clearly, if the minimum is relatively flat (at least along one direction), then there will be little (or no) deterioration in the quality of the fit. Through a statistical analysis, we will be able to obtain a physically reasonable domain of parameters. We implement such analysis by studying the small oscillations around the χ^2-minimum. As a bonus, we will be able to

uncover correlations among observables and attach meaningful theoretical error bars to the theoretical predictions [123]. To start, we expand the χ^2-measure around the optimal $\mathbf{p}_0$ model. That is,

$$\chi^2(\mathbf{p}) = \chi^2(\mathbf{p}_0) + \frac{1}{2}\sum_{i,j=1}^{F}(\mathbf{p}-\mathbf{p}_0)_i(\mathbf{p}-\mathbf{p}_0)_j\partial_i\partial_j\chi^2(\mathbf{p}_0) + \dots \tag{6.8}$$

For convenience, we quantify the departure from the minimum by defining scaled, dimensionless variables

$$x_i \equiv \frac{(\mathbf{p}-\mathbf{p}_0)_i}{(\mathbf{p}_0)_i}\ . \tag{6.9}$$

In terms of these scaled variable, the quadratic deviations of the χ^2-measure from its minimum value take the following compact form:

$$\chi^2(\mathbf{p}) - \chi^2(\mathbf{p}_0) \equiv \Delta\chi^2(\mathbf{x}) = \mathbf{x}^T\hat{\mathcal{M}}\,\mathbf{x}\ , \tag{6.10}$$

where $\mathbf{x}$ is a column vector of dimension F, $\mathbf{x}^T$ is the corresponding transpose (row) vector, and $\hat{\mathcal{M}}$ is the *symmetric* $F\times F$ matrix of second derivatives defined by

$$\mathcal{M}_{ij} = \frac{1}{2}\left(\frac{\partial\chi^2}{\partial x_i\partial x_j}\right)_{\mathbf{x}=0} = \frac{1}{2}(\mathbf{p}_0)_i(\mathbf{p}_0)_j\partial_i\partial_j\chi^2(\mathbf{p}_0)\ . \tag{6.11}$$

Being symmetric, the matrix $\hat{\mathcal{M}}$ can be brought to a diagonal form by means of an orthogonal (change-of-basis) transformation. Denoting by $\hat{\mathcal{A}}$ the orthogonal matrix whose columns are composed of the normalized eigenvectors and by $\hat{\mathcal{D}} = \mathrm{diag}(\lambda_1,\dots,\lambda_F)$ the *diagonal* matrix of eigenvalues, the following relation holds true: $\hat{\mathcal{M}} = \hat{\mathcal{A}}\hat{\mathcal{D}}\hat{\mathcal{A}}^T$. By inserting this relation into Eq. (6.10), we obtain the following simple and illuminating expression:

$$\Delta\chi^2(\mathbf{x}) = \mathbf{x}^T\left(\hat{\mathcal{A}}\hat{\mathcal{D}}\hat{\mathcal{A}}^T\right)\mathbf{x} = \boldsymbol{\xi}^T\hat{\mathcal{D}}\boldsymbol{\xi} = \sum_{i=1}^{F}\lambda_i\xi_i^2\ . \tag{6.12}$$

Here the vector $\boldsymbol{\xi} = \hat{\mathcal{A}}^T\mathbf{x}$ represents a point in parameter space expressed, not in terms of the original model parameters $(g_{\rm s}, g_{\rm v}, \dots)$ but rather, in terms of the new (*"rotated"*) basis. As previously advertised, the deviations of the χ^2-measure from its minimum value have been parametrized in terms of F uncoupled harmonic oscillators—with the eigenvalues playing the role of the spring constants. In this way, each eigenvalue controls the deterioration in the quality of the fit as one moves along a direction defined by its corresponding eigenvector.

A *"soft"* direction—characterized by a small eigenvalue and thus little deterioration in the χ^2 measure—involves a particular linear combination of model parameters that is poorly constrained by the choice of observables included in the least-squares fit. By isolating such linear combination(s) one can identify what kind of observables (*e.g.*, isovector observables) should be added to the χ^2-measure to better constrain the theoretical model. Moreover, one may also explore correlations among various observables (*e.g.*, neutron-skin thickness and dipole polarizability) thereby facilitating the experimental extraction of some of these critical observables. This could be done by either refining existing experimental measurements or by designing brand new ones.

A concept of fundamental importance to the correlation analysis is the *covariance* between two observables A and B, denoted by $\mathrm{cov}(A,B)$ [133]. Assuming that $(\mathbf{x}^{(1)},\ldots,\mathbf{x}^{(M)})$ represent M points (or models) in the neighborhood of the optimal model $\mathbf{x}^{(0)}=\mathbf{0}$, the covariance between A and B is defined as:

$$\mathrm{cov}(A,B)=\frac{1}{M}\sum_{m=1}^{M}\Big[\Big(A^{(m)}-\langle A\rangle\Big)\Big(B^{(m)}-\langle B\rangle\Big)\Big]=\langle AB\rangle\ -\langle A\rangle\langle B\rangle\ , \tag{6.13}$$

where $A^{(m)}\equiv A(\mathbf{x}^{(m)})$ and "$\langle\,\rangle$" denotes a statistical average. From the above definition the *correlation coefficient*—often called the Pearson product-moment correlation coefficient—now follows:

$$\rho(A,B)=\frac{\mathrm{cov}(A,B)}{\sqrt{\mathrm{var}(A)\mathrm{var}(B)}}\ , \tag{6.14}$$

where the *variance* of A is simply given by $\mathrm{var}(A)\equiv\mathrm{cov}(A,A)$. Note that two observables are said to be fully correlated if $\rho(A,B)=1$, fully anti-correlated if $\rho(A,B)=-1$, and uncorrelated if $\rho(A,B)=0$. If one expands the deviation of both observables from their average value, then cov(A, B) may be written as

$$\mathrm{cov}(A,B)=\sum_{i,j=1}^{F}\frac{\partial A}{\partial x_i}\left[\frac{1}{M}\sum_{m=1}^{M}x_i^{(m)}x_j^{(m)}\right]\frac{\partial B}{\partial x_j}\equiv\sum_{i,j=1}^{F}\frac{\partial A}{\partial x_i}C_{ij}\frac{\partial B}{\partial x_j}\ , \tag{6.15}$$

where both derivatives are evaluated at the minimum ($\mathbf{x}^{(0)}=\mathbf{0}$) and the *covariance matrix* C_{ij} has been introduced [133]. In order to continue, it is critical to decide how should the M points be generated. A particularly convenient choice is to assume that these M points (or models) are distributed according to the quality measure $\chi^2(\mathbf{x})$. That is, we assume a

probability distribution $\phi(\mathbf{x})$ given by

$$\phi(\mathbf{x}) = \exp\left[-\frac{1}{2}\Delta\chi^2(\mathbf{x})\right] = \exp\left(-\frac{1}{2}\mathbf{x}^T\hat{\mathcal{M}}\,\mathbf{x}\right) \ . \tag{6.16}$$

The covariance matrix may then be written as follows:

$$C_{ij} = \frac{\int x_i x_j \phi(\mathbf{x}) d\mathbf{x}}{\int \phi(\mathbf{x}) d\mathbf{x}} = \frac{1}{Z(0)}\left[\frac{\partial^2 Z(\mathbf{J})}{\partial J_i \partial J_j}\right]_{\mathbf{J}=\mathbf{0}} \ , \tag{6.17}$$

where we have defined the *"partition"* function $Z(\mathbf{J})$ as

$$Z(\mathbf{J}) = \int \phi(\mathbf{x}) e^{\mathbf{J}\cdot\mathbf{x}} d\mathbf{x} = \int \exp\left(-\frac{1}{2}\mathbf{x}^T\hat{\mathcal{M}}\,\mathbf{x} + \mathbf{J}\cdot\mathbf{x}\right) d\mathbf{x} \ . \tag{6.18}$$

The above gaussian integrals may be readily evaluated by completing the square. That is, let us shift the variable $\mathbf{x}$ to $\mathbf{y} + \hat{\mathcal{M}}^{-1}$, so that the integration measure is not altered:

$$d\mathbf{x} = d(\mathbf{y} + \hat{\mathcal{M}}^{-1}\mathbf{J}) = d\mathbf{y} \ . \tag{6.19}$$

Then the exponential factor can be rearranged as

$$\begin{aligned} -\frac{1}{2}\mathbf{x}^T\hat{\mathcal{M}}\,\mathbf{x} + \mathbf{J}\cdot\mathbf{x} \ &= \ -\frac{1}{2}\left(\mathbf{y}^T\hat{\mathcal{M}}\,\mathbf{y} + 2\mathbf{J}\cdot\mathbf{y} + \mathbf{J}^T\hat{\mathcal{M}}^{-1}\,\mathbf{J}\right) + \\ &+ \ \mathbf{J}\cdot\mathbf{y} + \mathbf{J}^T\hat{\mathcal{M}}^{-1}\,\mathbf{J} = -\frac{1}{2}\mathbf{y}^T\hat{\mathcal{M}}\,\mathbf{y} + \frac{1}{2}\mathbf{J}^T\hat{\mathcal{M}}^{-1}\,\mathbf{J} \ . \end{aligned} \tag{6.20}$$

Finally, one obtains

$$Z(\mathbf{J}) = Z(0)\exp\left(\frac{1}{2}\mathbf{J}^T\hat{\mathcal{M}}^{-1}\,\mathbf{J}\right) \equiv Z(0)e^{W(\mathbf{J})} \ . \tag{6.21}$$

Hence, under the assumption that the model parameters are generated according to the χ^2-measure, the covariance matrix becomes equal to the inverse of the matrix of second derivatives of χ^2. That is,

$$C_{ij} = \frac{1}{Z(0)}\left[\frac{\partial^2 Z(\mathbf{J})}{\partial J_i \partial J_j}\right]_{\mathbf{J}=\mathbf{0}} = \frac{\partial^2 W(\mathbf{J})}{\partial J_i \partial J_j} = (\mathcal{M}^{-1})_{ij} \tag{6.22}$$

Finally then, we arrive at a form for the covariance of two observables that is both simple and easy to compute:

$$\mathrm{cov}(A,B) = \sum_{i,j=1}^{F} \frac{\partial A}{\partial x_i}(\hat{\mathcal{M}}^{-1})_{ij}\frac{\partial B}{\partial x_j} = \sum_{i=1}^{F} \frac{\partial A}{\partial \xi_i}\lambda_i^{-1}\frac{\partial B}{\partial \xi_i} \ . \tag{6.23}$$

The last term in the previous expression is particularly illuminating. Consider, for example, the case of a very soft direction in the χ^2-measure, namely, an eigenvector of $\hat{\mathcal{M}}$ (say $\boldsymbol{\xi}_i$) with a very small eigenvalue (say $\lambda_i^{-1} \gg 1$). Such a situation routinely emerges in RMF models whenever two or more isovector parameters are included in the Lagrangian density but only masses and charge—not neutron—radii are used to define the χ^2-measure. Having identified a soft direction, one could then search for an observable A (*e.g.,* the neutron-skin thickness in ^{208}Pb) that is particularly sensitive to such a soft direction (as indicated by $\partial A/\partial \xi_i \gg 1$). Adding such an observable to the χ^2-measure will stiffen the formerly soft direction, thereby improving the predictive power of the model. Moreover, if A is difficult to measure, one could search for alternative observables that are strongly correlated to A. Although some of these notions have been heuristically implemented for some time, the statistical analysis discussed here provides a quantitative measure of the correlation between observables [123].

6.3 Results

In this section we provide two simple examples that illustrate the ideas presented in the previous sections. Here terms such as *"unique"* and *"predictive"* will be used to characterize a model. We regard a model as being unique if *all* the eigenvalues of $\hat{\mathcal{M}}$ are large (*i.e.,* $\lambda_i \gg 1$ for all i). A model is predictive if it can successfully account for physical observables not included in the χ^2-measure. Note that a model has been defined here as consisting of both an underlying Lagrangian density (or effective interaction) and a set of physical observables defining the χ^2-measure.

6.3.1 Example 1: Linear Walecka Model

We start this section by discussing the linear Walecka model as an example of a model that is unique but not predictive. The Lagrangian density for this case is simple as it only contains two coupling constants [7, 10]. That is,

$$\mathcal{L}_{\rm int} = g_{\rm s}\bar{\psi}\psi\phi - g_{\rm v}\bar{\psi}\gamma^{\mu}\psi V_{\mu} \; . \tag{6.24}$$

The Walecka model is perhaps the simplest model that can account—at the mean-field level—for the saturation of symmetric nuclear matter. Indeed, it is the saturation density

and the energy per nucleon at saturation that are typically used to calibrate the two parameters of the model. To make this simple model slightly less trivial we determine the two parameters of the model by minimizing a quality measure χ^2 defined in terms of three *"observables"*: (i) the saturation density ρ_0, (ii) the energy per nucleon at saturation ε_0, and (iii) the effective Dirac mass M_0^*. Central values and uncertainties for these three quantities are given as follows:

$$\rho_0 = (0.155 \pm 0.01)\ \text{fm}^{-3}\ , \tag{6.25a}$$

$$\varepsilon_0 = (-16 \pm 1)\ \text{MeV}\ , \tag{6.25b}$$

$$M_0^* = (0.6 \pm 0.1)\ M\ . \tag{6.25c}$$

Using standard numerical techniques, a minimum value for the χ^2-measure of $\chi_0^2 = 0.34145$ is obtained at

$$g_{\text{s}}^2 = \ \ 93.62647\ , \tag{6.26a}$$

$$g_{\text{v}}^2 = 180.48347\ . \tag{6.26b}$$

Having computed the minimum value of the quality measure, we now examine its behavior around the minimum. This is implemented by diagonalizing the symmetric matrix of second derivatives $\hat{\mathcal{M}}$ [see Eq. (6.11)]. The outcome of such a diagonalization procedure is the diagonal matrix of eigenvalues $\hat{\mathcal{D}}$ and the orthogonal matrix of normalized eigenvectors $\hat{\mathcal{A}}$. That is,

$$\hat{\mathcal{D}} = \text{diag}(\lambda_1, \lambda_2) = \text{diag}(7.4399 \times 10^4, 8.3195 \times 10^1)\ , \tag{6.27a}$$

$$\hat{\mathcal{A}} = \begin{pmatrix} \cos\theta & \sin\theta \\ -\sin\theta & \cos\theta \end{pmatrix} = \begin{pmatrix} 0.74691 & 0.66492 \\ -0.66492 & 0.74691 \end{pmatrix}\ . \tag{6.27b}$$

It is evident that both eigenvalues are very large. This indicates that both directions in parameter space are stiff and consequently the quality measure ($\Delta\chi^2 = \lambda_1\xi_1^2 + \lambda_2\xi_2^2$) will deteriorate rapidly as one moves away from the χ^2-minimum. Note that λ_1 is significantly larger than λ_2; this is to be expected. When probing the parameter landscape along the first direction (i.e., $\xi_2 = 0$) the scalar and vector coupling constants move *"out-of-phase"* (see the first column of the matrix $\hat{\mathcal{A}}$). For example, the scalar attraction would get larger at the same time that the vector repulsion would get smaller. This would yield a significant

increase in the binding energy per particle and consequently a drastic deterioration in the χ^2-measure. Recall that large and *cancelling* scalar and vector potentials are the hallmark of relativistic mean-field models.

To quantify the extent by which the linear Walecka model is unique, we now proceed to compute the variance in the coupling constants using Eq. (6.23). We obtain

$$\sigma_{\rm s}^2 = \left(\hat{\mathcal{M}}^{-1}\right)_{11} = \lambda_1^{-1}\cos^2\theta + \lambda_2^{-1}\sin^2\theta = 5.3217\times10^{-3}\ , \tag{6.28a}$$

$$\sigma_{\rm v}^2 = \left(\hat{\mathcal{M}}^{-1}\right)_{22} = \lambda_1^{-1}\sin^2\theta + \lambda_2^{-1}\cos^2\theta = 6.7116\times10^{-3}\ . \tag{6.28b}$$

In turn, this translates into the following uncertainties in the optimal values of the coupling constants:

$$g_{\rm s}^2 = \ \ 93.62647\,(1\pm\sigma_{\rm s}) = \ \ 93.62647 \pm 6.83008\ , \tag{6.29a}$$

$$g_{\rm v}^2 = 180.48347\,(1\pm\sigma_{\rm v}) = 180.48347 \pm 14.78596\ . \tag{6.29b}$$

We conclude that the uncertainties in the model parameters—and thus in most of the predictions of the model—are of the order of 5-to-10 percent. In principle, the model uncertainties could be reduced by refining the experimental database [see Eq. (6.25)]. The great merit of the present statistical approach is that one may systematically explore the extent by which the experimental measurement must be refined in order to achieve the desired theoretical accuracy. Note that the theoretical uncertainties are dominated by the *smallest* eigenvalue of $\hat{\mathcal{M}}$ [see Eq. (6.28)]. Thus, assessing the uniqueness of the model by varying each model-parameter individually (*e.g*, first $g_{\rm s}^2$ and then $g_{\rm v}^2$) is misleading and ill advised. It is misleading because in doing so the quality measure will in general be dominated by the *largest* eigenvalue [see Eq. (6.12)]. Yet it is the lowest eigenvalue that determines the uniqueness of the model.

Carrying out the covariance analysis further, we now proceed to compute correlation coefficients between model parameters and observables [see Eqs. (6.14) and (6.23)]. In estimating uncertainties in the model parameters one concentrates on the diagonal elements of the (inverse) matrix of second derivatives [see Eq. (6.28)]. Information on the correlation between model parameters is, however, stored in the off-diagonal elements. For example,

the correlation coefficient between g_s^2 and g_v^2 is given by

$$\rho(g_s^2, g_v^2) = \frac{\left(\hat{\mathcal{M}}^{-1}\right)_{12}}{\sqrt{\left(\hat{\mathcal{M}}^{-1}\right)_{11}\left(\hat{\mathcal{M}}^{-1}\right)_{22}}} = 0.9977 \,. \tag{6.30}$$

The strong (positive) correlation between g_s^2 and g_v^2 is easily understood. Given that configurations in parameter space are distributed according to the χ^2-measure, model parameters in which g_s^2 and g_v^2 move out-of-phase are strongly suppressed, as they are controlled by the largest eigenvalue λ_1. As a result, an overwhelming number of configurations are generated with g_s^2 and g_v^2 moving in phase, thereby leading to a large positive correlation. Correlation coefficients between various isoscalar observables have been tabulated in Table 6.1. Given that the correlation coefficients are sensitive to the first derivatives of the observables along all (eigen)directions [see Eq. (6.23)], we have listed them for completeness in Table 6.2. We observe that all observables display a much larger sensitivity to the stiff direction than to the soft one. This could (and does) lead to sensitive cancellations since the large derivatives compensate for the small value of λ_1^{-1}. Indeed, the correlation between the saturation density and the binding energy at saturation is very small. On the other hand, the incompressibility coefficient appears to be strongly correlated to the binding energy. This behavior is also displayed in graphical form in Fig. 6.1 where predictions for the various observables were generated with model parameters distributed according to $\phi(\mathbf{x})$ [see Eq. (6.16)]. Note that the *covariance ellipsoids* in Fig. 6.1 were generated by selecting those model parameters that satisfy $\Delta\chi^2 \leq 1$.

Table 6.1: Correlation coefficients between isoscalar observables in the linear Walecka model.

	ε_0	ρ_0	K_0	M_0^*
ε_0	+1.0000	−0.0036	−0.9998	+0.8867
ρ_0	−0.0036	+1.0000	−0.0174	+0.4591
K_0	−0.9998	−0.0174	+1.0000	+0.8962
$M_0^\star$	+0.8867	+0.4591	+0.8962	+1.0000

Based on the previous statistical analysis it appears that the linear Walecka model is unique (at least at the $5-10\%$ level). But is the linear Walecka model predictive? To test

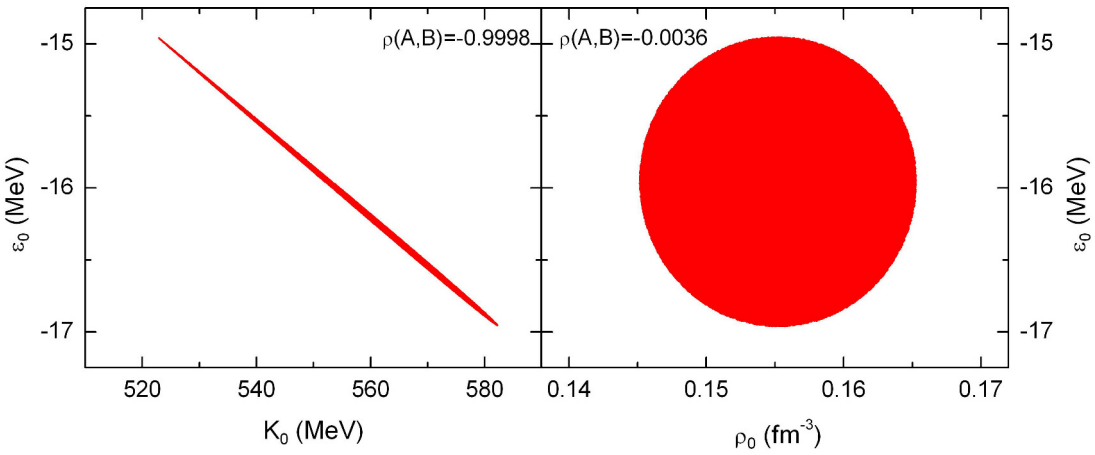

Figure 6.1: Predictions from the linear Walecka models for the saturation density, binding energy, and incompressibility coefficient at saturation. Model parameters were generated according to the distribution $\exp(-\Delta\chi^2/2)$. Both of the covariance ellipsoids were generated by limiting the models to the region $\Delta\chi^2 \leq 1$.

Table 6.2: First derivatives of the *scaled* observables (*i.e.*, observable scaled to its value at the χ^2-minimum) as a function of ξ_1 and ξ_2 evaluated at the χ^2-minimum; see Eq. (6.23).

	$\partial\xi_1$	$\partial\xi_2$
$\partial\varepsilon_0$	-1.6698×10^{1}	-1.1716×10^{-1}
$\partial\rho_0$	3.6619	-5.7333×10^{-1}
∂K_0	1.4261×10^{1}	1.1055×10^{-1}
∂M_0^*	-3.2349	-8.8817×10^{-2}

the predictability of the model we focus on two physical observables that were not included in the χ^2-measure, namely, the incompressibility coefficient K_0 and the symmetry energy J. We obtain—with properly computed theoretical errors—the following results:

$$K_0 = (552.537 \pm 29.655)\ \text{MeV}\ , \tag{6.31a}$$

$$J = (19.775 \pm 0.683)\ \text{MeV}\ . \tag{6.31b}$$

Both predictions, even after theoretical errors have been incorporated, differ significantly from the presently acceptable values of $K_0 \approx (240 \pm 20)\,\text{MeV}$ and $J \approx (32 \pm 2)\,\text{MeV}$. This conclusion should hardly come as a surprise. After all, the predominant role played by the

model parameters κ and λ in softening the incompressibility coefficient and g_ρ in stiffening the symmetry energy have been known for a long time. What is relevant from the present statistical analysis is that we have established quantitatively that the linear Walecka model fails because its prediction for K_0 differs from the experimental value by more than 10 standard deviations. We must then conclude that whereas the linear Walecka is (fairly) unique, it is not predictive. We now proceed to discuss a particular extension of the Walecka model that is highly predictive but not unique: the non-linear FSUGold model.

6.3.2 Example 2: Non-linear FSUGold Model

Modern relativistic models of nuclear structure have evolved significantly since the early days of the linear Walecka model. In the present example we focus on the FSUGold parameter set [15] that is defined by an interacting Lagrangian density of the following form:

$$\begin{aligned} \mathcal{L}_{\rm int} &= \bar{\psi}\left[g_{\rm s}\phi - \Big(g_{\rm v}V_\mu + \frac{g_\rho}{2}\boldsymbol{\tau}\cdot\mathbf{b}_\mu + \frac{e}{2}(1+\tau_3)A_\mu\Big)\gamma^\mu\right]\psi \\ &- \frac{\kappa}{3!}\Phi^3 - \frac{\lambda}{4!}\Phi^4 + \frac{\zeta}{4!}\Big(W_\mu W^\mu\Big)^2 + \Lambda_{\rm v}\Big(W_\nu W^\nu\Big)\Big(\mathbf{B}_\mu\cdot\mathbf{B}^\mu\Big)\,. \end{aligned} \tag{6.32}$$

Modifications to the linear Walecka model are motivated by the availability of an ever increasing database of high-quality data. For example, the two non-linear scalar terms κ and λ induce a significant softening of the compression modulus of nuclear matter relative to the original Walecka model [7, 8, 10]. This is demanded by measurement of the giant monopole resonance in medium to heavy nuclei [38]. Further, omega-meson self-interactions, as described by the parameter ζ, also serve to soften the equation of state of symmetric nuclear matter but at much higher densities. Indeed, by tuning the value of ζ it is possible to produce maximum neutron star masses that differ by almost one solar mass while maintaining the saturation properties of nuclear matter intact [16]. Such a softening appears consistent with the dynamics of high-density matter as probed by energetic heavy-ion collisions [98]. Finally, $\Lambda_{\rm v}$ induces isoscalar-isovector mixing and is responsible for modifying the poorly-constrained density dependence of the symmetry energy [30, 78]. In particular, a softening of the symmetry energy induced by $\Lambda_{\rm v}$ appears consistent with the distribution of both isoscalar monopole and isovector dipole strength in medium to heavy nuclei [15, 39, 117]. In summary, FSUGold is a fairly successful RMF model that has been validated against

theoretical, experimental, and observational constraints [99]. Note that as additional laboratory and observational data become available (notably the recent report of a 2-solar mass neutron star [13]) refinements to the model my be required [107]. For now, however, we will be content with using the FSUGold model to study the small oscillations around the minimum.

As mentioned earlier, a model should be understood as a combination of an interacting Lagrangian density and a quality measure. We define the χ^2-measure in terms of the following set of observables generated directly from the FSUGold parameter set:

$$\rho_0 = 0.1484 \text{ fm}^{-3} , \tag{6.33a}$$

$$\varepsilon_0 = -16.30 \text{ MeV} , \tag{6.33b}$$

$$\varepsilon(2\rho_0) = -5.887 \text{ MeV} , \tag{6.33c}$$

$$K_0 = 230.0 \text{ MeV} , \tag{6.33d}$$

$$M_0^* = 0.6100 \; M , \tag{6.33e}$$

$$\tilde{J} = 26.00 \text{ MeV} , \tag{6.33f}$$

$$L = 60.52 \text{ MeV} , \tag{6.33g}$$

$$M_{\max} = 1.722 \; M_\odot . \tag{6.33h}$$

Note that in all cases a 2% uncertainty is attached to all observables—except in the case of the slope of the symmetry energy L where the significant larger value of 20% is assumed. This reflects our poor understanding of the density dependence of the symmetry energy. Also note that $\tilde{J}$ represents the value of the symmetry energy at a sub-saturation density of $\rho \approx 0.1\,\text{fm}^{-3}$—a density at which the theoretical uncertainties are minimized [100]. Finally, notwithstanding the Demorest *et al.* result [13], the maximum neutron star mass is fixed at $M_{\max} = 1.722\, M_\odot$. Given that a theoretical model is used to generate the various observables, a much larger database could be used to define the χ^2-measure, if desired. By construction, a very small value for the χ^2-measure is obtained at the FSUGold minimum. We now proceed to explore the wealth of information available as one studies deviations around this minimum value. As in the previous section, the symmetric matrix of second derivatives $\hat{\mathcal{M}}$

(now a 7×7 matrix) may be diagonalized by means of an orthogonal transformation. The diagonal matrix of eigenvalues $\hat{\mathcal{D}}$ and the matrix of eigenvectors $\hat{\mathcal{A}}$ are given by

$$\hat{\mathcal{D}} = \mathrm{diag}(1.2826\times10^{6}, 1.5305\times10^{4}, 4.2472\times10^{2}, 3.2113\times10^{2}, 1.2692\times10^{2}, 6.9619, 3.7690)\ , \tag{6.34a}$$

$$\hat{\mathcal{A}} = \begin{pmatrix} -7.4967\times10^{-1} & -2.3685\times10^{-1} & 3.0853\times10^{-1} & 1.2931\times10^{-1} & -5.1254\times10^{-1} & -8.5089\times10^{-2} & 6.8417\times10^{-3} \\ 6.5682\times10^{-1} & -1.5751\times10^{-1} & 3.6654\times10^{-1} & 1.6504\times10^{-1} & -6.0281\times10^{-1} & -1.3685\times10^{-1} & 8.5353\times10^{-3} \\ -1.5331\times10^{-4} & 3.1315\times10^{-3} & -7.0050\times10^{-1} & 6.8701\times10^{-2} & -3.9206\times10^{-1} & -3.3843\times10^{-2} & 5.9137\times10^{-1} \\ 3.8535\times10^{-2} & -2.8770\times10^{-1} & -2.4254\times10^{-2} & 4.7416\times10^{-1} & 4.3796\times10^{-2} & 8.2968\times10^{-1} & -5.7643\times10^{-3} \\ 3.9417\times10^{-2} & -6.8525\times10^{-1} & -1.3772\times10^{-1} & 3.8776\times10^{-1} & 3.5428\times10^{-1} & -4.8376\times10^{-1} & 2.6431\times10^{-3} \\ -5.9458\times10^{-2} & 6.0558\times10^{-1} & 5.4897\times10^{-2} & 7.5689\times10^{-1} & 6.8021\times10^{-2} & -2.2175\times10^{-1} & 6.2795\times10^{-3} \\ 1.2995\times10^{-4} & -3.1465\times10^{-3} & 5.0714\times10^{-1} & -5.7010\times10^{-2} & 2.9691\times10^{-1} & 3.6238\times10^{-2} & 8.0628\times10^{-1} \end{pmatrix}\ . \tag{6.34b}$$

Note that the scaled parameters of the model are associated to the original coupling constants as follows:

$$\{x_1, x_2, x_3, x_4, x_5, x_6, x_7\} \rightarrow \{g_{\rm s}^2, g_{\rm v}^2, g_\rho^2, \kappa, \lambda, \zeta, \Lambda_{\rm v}\}\ . \tag{6.35}$$

We observe that the stiffest direction is dominated by two isoscalar parameters and represents—as in the case of the linear Walecka model—an out-of-phase oscillation between the scalar attraction and the vector repulsion. Given that in RMF models the cancellation between the scalar attraction and the vector repulsion is so delicate, any out-of-phase motion yields a significant change in the binding energy per nucleon and a correspondingly dramatic increase in the quality measure. The second stiffest direction also involves exclusively isoscalar parameters and is dominated by the quartic scalar (λ) and vector (ζ) couplings—and to a lesser extent by the cubic term (κ). This linear combination of parameters is largely constrained by the incompressibility coefficient K_0 and the maximum neutron-star mass $M_{\rm max}$. Although the determination of the maximum neutron-star mass to a 2% accuracy presents a significant observational challenge, our statistical analysis suggests that such a determination would strongly constrain the equation of state from saturation density up to neutron-star densities. The third stiffest direction (with still a fairly large eigenvalue of $\lambda_3 \approx 425$) is dominated by the two isovector parameters g_ρ^2 and $\Lambda_{\rm v}$. For this particular *"mode"* both parameters oscillate out of phase. This behavior can be readily understood by recalling the expression for the symmetry energy [78]:

$$E_{\rm sym}(\rho) = \frac{k_F^2}{6E_F^*} + \frac{g_\rho^2\rho}{8m_\rho^{*2}}\ , \quad \left(m_\rho^{*2} \equiv m_\rho^2 + 2\Lambda_{\rm v} g_\rho^2 W_0^2\right)\ . \tag{6.36}$$

In order for the symmetry energy $\tilde{J}$ to remain fixed, then both g_ρ^2 and $\Lambda_{\rm v}$ must move in phase. If they move out of phase, then the symmetry energy can not be kept at this value

and the quality measure deteriorates. By the same token, the in-phase motion of g_ρ^2 and $\Lambda_{\rm v}$ is very poorly constrained—as evinced by the last and softest direction. And it is only because the slope of the symmetry energy L was assumed to be somehow constrained (at the 20% level) that a positive eigenvalue was even obtained. Note that one of the main goals of the successfully commissioned Lead Radius experiment (PREx) at the Jefferson Laboratory is to constrain the density dependence of the symmetry energy (*i.e.*, L) by accurately measuring the neutron radius of ^{208}Pb [85, 86]. The next to last eigenvalue ($\lambda_6 \approx 7$) is also relatively small. This suggest that the out-of-phase motion of the two non-linear scalar couplings (κ and λ) is poorly constrained by the nuclear-matter observables defining the quality measure. Perhaps supplementing the quality measure with finite-nuclei observables will help ameliorate this problem. Work along these lines is currently in progress.

We now proceed to estimate theoretical uncertainties as well as to compute correlation coefficients for both the model parameters and the physical observables. We start by computing theoretical uncertainties (*i.e.*, variances) for the model parameters. These are given by [see Eq. (6.23)]

$$\sigma_i^2 = \left(\hat{\mathcal{M}}^{-1}\right)_{ii} = \left(\hat{\mathcal{A}}\hat{\mathcal{D}}^{-1}\hat{\mathcal{A}}^T\right)_{ii} = \sum_{j=1}^{7} \mathcal{A}_{ij}^2 \lambda_j^{-1} \,, \tag{6.37}$$

and result in the following theoretical uncertainties for the model parameters:

$$g_{\rm s}^2 = 112.19955 \pm 6.54468 \;\; [5.833\%] \,, \tag{6.38a}$$

$$g_{\rm v}^2 = 204.54694 \pm 15.81183 \;\; [7.730\%] \,, \tag{6.38b}$$

$$g_\rho^2 = 138.47011 \pm 42.75427 \;\; [30.876\%] \,, \tag{6.38c}$$

$$\kappa = 1.42033 \pm 0.44827 \;\; [31.561\%] \,, \tag{6.38d}$$

$$\lambda = 0.02376 \pm 0.00445 \;\; [18.748\%] \,, \tag{6.38e}$$

$$\zeta = 0.06000 \pm 0.0057 \;\; [9.447\%] \,, \tag{6.38f}$$

$$\Lambda_{\rm v} = 0.03000 \pm 0.01251 \;\; [41.711\%] \,. \tag{6.38g}$$

We observe that three out of the five isoscalar parameters, namely, $g_{\rm s}^2$, $g_{\rm v}^2$, and ζ, are relatively well constrained (at the $\lesssim 10\%$ level). Whereas $g_{\rm s}^2$ and $g_{\rm v}^2$ are well determined by the saturation properties of symmetric nuclear matter, it is the maximum neutron-star mass

that constrains ζ. Yet the remaining two isoscalar parameters (κ and λ) are poorly determined. This is particularly true in the case of κ which displays a large ($\approx$30%) uncertainty. As alluded earlier, these large uncertainties develop because the out-of-phase motion of κ and λ—as controlled by the relatively soft sixth eigenvector—is poorly constrained. Given that the in-phase motion of the two isovector parameters (g_ρ^2 and $\Lambda_{\rm v}$) is controlled by the softest of eigenvectors, the theoretical uncertainties in these parameters is also fairly large ($\approx$30% and $\approx$40%, respectively). However, whereas the reason for the latter is associated with the large error bars assigned to L, we are unaware at this time on how to better constrain κ and λ. Perhaps supplementing the quality measure with information on various nuclear compressional modes may help resolve this issue. Plans to do so in the near future are under consideration.

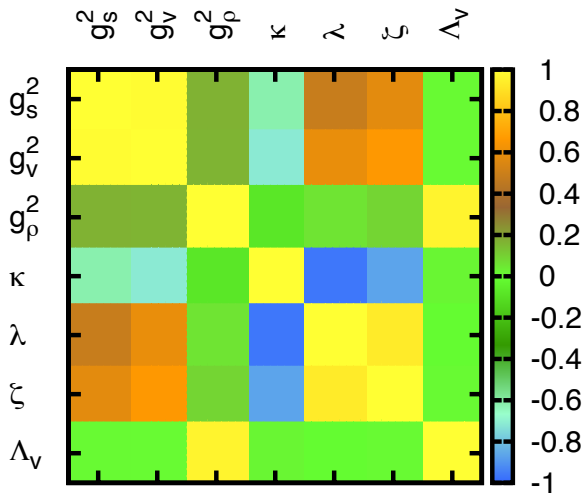

Figure 6.2: Color-coded plot of the 21 independent correlation coefficients between the 7 model parameters of the FSUGold effective interaction.

We have computed correlation coefficients between all 21 distinct pairs of model parameters and have displayed them in graphical (color-coded) form in Fig. 6.2. As depicted in the figure, the strongest correlations are between $g_{\rm s}^2$ and $g_{\rm v}^2$ (0.988), g_ρ^2 and $\Lambda_{\rm v}$ (0.967), and κ and λ (-0.962). As alluded in the case of the simpler linear Walecka model, the correlations

are dominated by the *softest directions*; in this case the sixth and seventh eigenvectors. Given that for these two eigenvectors $g_{\rm s}^2$ and $g_{\rm v}^2$ as well as g_ρ^2 and $\Lambda_{\rm v}$ move in phase whereas κ and λ move out of phase, the observed correlations ensue. In other words, the three largest eigenvalues strongly suppress the generation of model parameters with $g_{\rm s}^2$ and $g_{\rm v}^2$ moving out of phase, κ and λ in phase, and g_ρ^2 and $\Lambda_{\rm v}$ out of phase, respectively. Note then, that the distribution of isovector parameters g_ρ^2 and $\Lambda_{\rm v}$ is generated in such a way that the symmetry energy at sub-saturation density $\tilde{J}$ remains fixed at 26 MeV (at least within a 2% uncertainty). This quantitative fact validates our heuristic approach—already employed numerous times—to correlate isovector observables (see Refs. [96, 124, 134] and references therein).

We now extend the covariance analysis to the case of physical observables. To do so, we must supply the relevant *"matrix"* of first derivatives [see Eq. (6.23)]. For completeness we list the first derivatives in tabular form in Tables 6.3 and 6.4. Note that in the case of the model parameters the corresponding matrix of first derivatives is the matrix of eigenvectors $\hat{\mathcal{A}}$. The derivatives encapsulate the sensitivity of the various observables to changes along the different eigenvectors. For example, whereas isoscalar observables (such as $\varepsilon_0, \rho_0, K_0$) are insensitive to changes along the mostly isovector seventh eigenvector, both L and the neutron-skin thickness of ^{208}Pb, $R_n - R_p$, display a fairly large sensitivity.

Table 6.3: First derivatives of the *scaled* observables (*i.e.*, observable scaled to its value at the χ^2-minimum) as a function of ξ_i at the χ^2-minimum; see Eq. (6.23).

	$\partial\xi_1$	$\partial\xi_2$	$\partial\xi_3$	$\partial\xi_4$
$\partial\varepsilon_0$	$1.0551\times10^{+1}$	-7.1882×10^{-1}	-2.9433×10^{-2}	4.9029×10^{-2}
$\partial\rho_0$	-2.2472	1.3904	-9.8868×10^{-4}	2.2220×10^{-1}
∂K_0	-7.4792	1.3890	-3.6799×10^{-2}	-1.8808×10^{-1}
∂M^*	1.1505	-5.5581×10^{-1}	-1.0614×10^{-1}	-8.3170×10^{-2}
$\partial\tilde{J}$	-2.7862×10^{-1}	6.5586×10^{-2}	-3.9136×10^{-1}	2.5698×10^{-2}
∂J	-1.6811	9.4897×10^{-1}	-3.2446×10^{-1}	1.7826×10^{-1}
∂L	-1.8759	1.1812	1.5849×10^{-2}	2.6611×10^{-1}
$\partial(R_n-R_p)$	7.0224	9.6188×10^{-2}	-2.3362×10^{-1}	1.9804×10^{-1}
$\partial R_{1.0}$	9.9947×10^{-1}	-3.1989×10^{-1}	-1.6534×10^{-2}	-6.5939×10^{-2}
$\partial R_{1.4}$	5.0300×10^{-1}	-3.0884×10^{-1}	9.3778×10^{-3}	-1.1119×10^{-1}
$\partial M_{\rm max}$	-2.7675×10^{-1}	-1.4882×10^{-1}	3.1173×10^{-2}	-1.6394×10^{-1}

Table 6.4: First derivatives of the *scaled* observables (*i.e.*, observable scaled to its value at the χ^2-minimum) as a function of ξ_i at the χ^2-minimum; see Eq. (6.23).

	$\partial\xi_5$	$\partial\xi_6$	$\partial\xi_7$
$\partial\varepsilon_0$	5.1626×10^{-2}	-1.7025×10^{-2}	-7.7009×10^{-4}
$\partial\rho_0$	5.3440×10^{-2}	1.8998×10^{-2}	1.5875×10^{-3}
∂K_0	4.8215×10^{-2}	-2.1691×10^{-2}	-3.0813×10^{-4}
∂M^*	1.6492×10^{-1}	1.2614×10^{-2}	-2.7701×10^{-3}
$\partial\tilde{J}$	-6.8299×10^{-2}	6.0862×10^{-4}	6.2323×10^{-4}
∂J	-3.6792×10^{-2}	6.2151×10^{-3}	-8.4827×10^{-2}
∂L	-1.0180×10^{-1}	-2.2526×10^{-2}	-3.8593×10^{-1}
$\partial(R_n-R_p)$	-2.5651×10^{-2}	-1.9368×10^{-2}	-3.4167×10^{-1}
$\partial R_{1.0}$	-4.5197×10^{-2}	-4.5964×10^{-3}	-3.9800×10^{-2}
$\partial R_{1.4}$	-6.3792×10^{-2}	3.1016×10^{-3}	-2.6571×10^{-2}
$\partial M_{\rm max}$	-6.8790×10^{-2}	3.4817×10^{-2}	-2.4367×10^{-3}

Given the enormous interest in constraining the density dependence of the symmetry energy, we estimate theoretical uncertainties on three—mostly isovector—observables. These are the symmetry energy at saturation density J, the neutron-skin thickness of ^{208}Pb, and the radius ($R_{1.4}$) of a $M = 1.4M_\odot$ neutron star. Recall that it was $\tilde{J}$ (not J) that was included in the definition of the quality measure. We obtain,

$$J = (32.593 \pm 1.574)\,\text{MeV} \quad [4.830\%]\,, \tag{6.39a}$$

$$R_n - R_p = (0.207 \pm 0.037)\,\text{fm} \quad [17.698\%]\,, \tag{6.39b}$$

$$R_{1.4} = (11.890 \pm 0.194)\,\text{km} \quad [1.631\%]\,. \tag{6.39c}$$

We now comment on each of these cases individually. Before we do so, however, note that correlation coefficients for 11 observables (*i.e.*, 55 independent pairs) are depicted in a color-coded format in Fig. 6.3. First, the central value of J along with its theoretical uncertainty may be easily understood by invoking a first-order expansion for the symmetry energy $\tilde{J}$ at sub-saturation density ($\tilde{\rho}_0 \approx 0.103\,\text{fm}^{-3}$) in terms of J and L [116]. That is,

$$J = \tilde{J} + xL + \ldots \approx (32.208 \pm 1.346)\,\text{MeV}\,, \quad x = \frac{1}{3}\left(1 - \frac{\tilde{\rho}_0}{\rho_0}\right) \approx 0.103\,, \tag{6.40}$$

where the errors were added in quadrature. So although J is strongly correlated to L (with a correlation coefficient of 0.922) the error in the former is significantly smaller than the

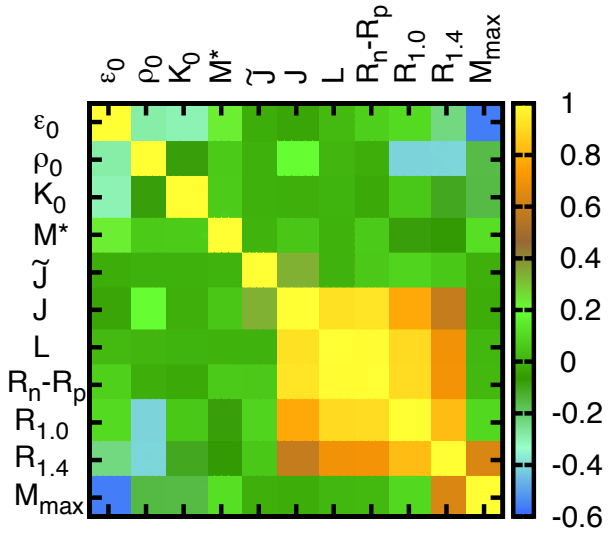

Figure 6.3: Color-coded plot of the 55 independent correlation coefficients between 11 physical observables as computed with the FSUGold effective interaction.

latter because of the small value of x. Second, for the neutron-skin thickness of ^{208}Pb we find a theoretical error comparable to the one assumed for L and a correlation coefficient between the two observables of almost one (0.995). Such a strong correlation is consistent with two recent studies that employ a large number of accurately-calibrated relativistic and non-relativistic interactions to uncover the correlation [55, 135]. Also consistent with these studies, specifically with Ref. [55], is the fact that the proposed 1% measurement of the neutron radius of ^{208}Pb by the PREx collaboration [85, 86] may not be able to place a significant constrain on L. For example, our covariance analysis suggests that the 20% uncertainty assumed for L translates into a theoretical error in the neutron skin of 0.037 fm—or about a 0.7% uncertainty in the neutron radius of ^{208}Pb. Conversely, if L is to be determined to within 10% (*i.e.*, $L \approx 60 \pm 6$ MeV) then the neutron skin must be constrained to about 0.018 fm so the neutron radius must be measured with close to a 0.3% accuracy—a fairly daunting task. Finally, we obtain a very small theoretical uncertainty for the radius of a 1.4 solar-mass neutron star and a correlation coefficient between L and $R_{1.4}$ (or $R_n - R_p$ and $R_{1.4}$) of 0.811. Although the radius of the neutron star is sensitive to the

density dependence of the symmetry energy [136], $R_{1.4}$ can not be uniquely constrained by a measurement of $R_n - R_p$ because whereas the latter depends on the symmetry energy at (or below) saturation density, the former is also sensitive to the equation of state at higher densities [78]. Note that a far better correlation coefficient of 0.942 is obtained between L and the radius of a 1.0 solar-mass neutron star. Regardless (with all things being equal) knowledge of the slope of the symmetry energy to a 20% accuracy significantly constrains the stellar radius.

6.4 Conclusions

The demand for theoretical predictions that include meaningful and reliable uncertainties is increasing. Such a sentiment has been articulated in a recent publication by the editors of the Physical Review A [120]. The need to quantify model uncertainties in an area such as theoretical nuclear physics is particularly urgent as models that are fitted to experimental data are then used to extrapolate to the extremes of temperature, density, isospin asymmetry, and angular momentum. Inspired by some of the central ideas developed in Ref. [123], a systematic statistical approach was applied to a class of relativistic mean-field models. The aim of this statistical analysis was twofold. First, to attach meaningful and reliable theoretical uncertainties to both the model parameters as well as to the predicted observables. Second, to quantify the degree of correlation between physical observables.

Modern relativistic mean-field models have evolved considerably since the early days of the linear Walecka model. Based on certain shortcoming of the Walecka model—most notably the inability to reproduce the incompressibility coefficient of symmetric nuclear matter—the Lagrangian density was augmented by non-linear cubic and quartic scalar-meson terms. However, based on modern effective-field-theory tenets, such as naturalness and power counting, a consistent Lagrangian density should include all terms up to fourth order in the meson fields. But in doing so, how should one constrain the large number of model parameters? In principle, one should follow the standard protocol of determining all model parameters through a χ^2-minimization procedure. In practice, however, many successful theoretical approaches arbitrarily set some of the model parameters to zero. The argument behind this fairly ad-hoc procedure is that the full set of parameters is poorly

determined by existing data, so ignoring a subset model parameters does not compromise the quality of the fit.

A covariance analysis such as the one implemented here should be able to clarify in a quantitative fashion the precise meaning of a *"poorly determined set of parameters"*. To do so, one should focus—not on the minimum of the χ^2-measure but rather—on its behavior around the minimum. As in any small-oscillations problem, the deviations around the minimum are controlled by a symmetric matrix of second derivatives that may be used to extract theoretical error bars and to compute correlation coefficients among physical observables. However, to access the wealth of information available in the covariance analysis we took it a step further and diagonalized the matrix of second derivatives. Upon diagonalization, the deviations of the χ^2-measure from the minimum are parametrized in terms of a collection of *"uncoupled harmonic oscillators"*. By doing so, one could readily identify stiff and soft modes in parameter space, namely, eigenvectors characterized by either large or small eigenvalues, respectively.

We now summarize some of the most important lessons learned. First, a stiff direction represents a particular linear combination of model parameters that is well constrained by the set of physical observables included in the χ^2-measure. By the same token, a soft direction suggests that additional physical observables are required to further constrain the model. Second, given that model parameters around the minimum are distributed according to the χ^2-measure, the soft directions dominate the correlation analysis. Finally, testing whether a model is well constrained by individually varying its parameters—rather than by varying them coherently as suggested by the structure of the eigenvectors—may be misleading. To illustrate these findings we used two relatively simple, yet illuminating, examples: (a) the linear Walecka model and (b) the FSUGold parametrization. Note that ultimately we aim to implement the covariance analysis with a χ^2-measure defined by a consistent Lagrangian density.

A particularly clear example of a stiff direction was represented by the out-of-phase motion of the scalar $g_{\rm s}$ and vector $g_{\rm v}$ coupling constants in the linear Walecka model. Indeed, increasing the scalar attraction while at the same time reducing the vector repulsion leads to a significant increase in the binding energy per nucleon and, thus, in a significant de-

terioration of the χ^2-measure. The in-phase motion of $g_{\rm s}$ and $g_{\rm v}$, however, is not as well constrained (the ratio of the two eigenvalues is about 1000). Therefore, configurations in parameter space generated by the χ^2-measure were dominated by pairs of coupling constants that were in phase, thereby resulting in a correlation coefficient between $g_{\rm s}$ and $g_{\rm v}$ that was, as expected, large and positive. Note, however, that if $g_{\rm s}$ and $g_{\rm v}$ were varied individually, one would erroneously conclude that the model is much better constrained than it really is—since changes in the χ^2-measure would be dominated by the largest eigenvalue.

In our second example we considered the accurately-calibrated FSUGold interaction with an isovector interaction determined by two parameters (g_ρ and $\Lambda_{\rm v}$). We found the out-of-phase motion of g_ρ and $\Lambda_{\rm v}$ to be strongly constrained by the value of the symmetry energy at a density of about 0.1 fm. However, our poor knowledge of the density dependence of the symmetry energy left the in-phase motion of $g_{\rm v}$ and $\Lambda_{\rm v}$ largely unconstrained. Effectively then, correlations in the isovector sector were induced by the in-phase motion of g_ρ and $\Lambda_{\rm v}$—subject to the constraint that the symmetry energy at $\rho\approx 0.1$ fm remains intact. This procedure validates the heuristic approach that we have used for some time to estimate correlations among isovector observables. Yet a benefit of the present analysis is that one can precisely quantify the theoretical errors as well as the correlation among observables. For example, we concluded that if the slope of the symmetry energy is to be determined with a 10% uncertainty, then the neutron-skin thickness of ^{208}Pb should be measured with a 0.3% accuracy. This more stringent limit seems to agree with the conclusions of Ref. [55].

In the future we aim to apply the covariance analysis discussed here to the construction of a relativistic density functional that will include all terms up to fourth order in the meson fields. Moreover, we plan to calibrate the χ^2-measure using various properties of finite nuclei and neutron stars. In addition, we reiterate a point made in Ref. [123] that the methodology used in this work should be applicable to any problem where model parameters are determined from optimizing a quality measure.

CHAPTER 7

SUMMARY

In this chapter, we summarize the most important results obtained in this dissertation work.

1. An overview of the relativistic mean-field theories is given. The equation of state and several expressions for the properties of the infinite nuclear matter are obtained in the relativistic mean-field approximation. The results are applied to symmetric, asymmetric and pure neutron matter.

2. A detailed survey of neutron star structure calculations is given. It has been discussed in detail how to make strong connections between neutron-star and nuclear observables as they share the same equation of state.

3. An algorithm for how to enforce the beta equilibrium conditions in the neutron star equation of state is presented. Scaling of parameters is very important in numerical calculations. An example of scaling of parameters is shown for the case of the neutron star structure calculations.

4. The mechanism of the cooling of neutron stars through the direct Urca process has been discussed. The analytical expression and numerical solutions for the threshold proton fraction is presented.

5. The sensitivity of stellar moments of inertia to the neutron-star matter equation of state is examined using accurately-calibrated relativistic mean-field models. The results are presented in the slow-rotation approximation for the case of binary pulsar PSR J0737-3039. This sensitivity is probed by tuning both the density dependence of the symmetry energy and the high density component of the equation of state, properties that are at present poorly constrained by existing laboratory data. Our results indicate that knowledge of the pulsar moment of inertia with a 10% accuracy could tightly constrain the equations of state. This suggests that a measurement of the moment of inertia could help discriminate between equations of state that are either stiff

or soft at high density. However the sensitivity of the moment of inertia to the density dependence of the symmetry energy appears to be weak. This is revealed especially for models with a soft symmetry energy.

6. An important component of neutron star calculations, the crustal moment of inertia, is discussed in detail. An analytical expression for the fraction of the moment of inertia contained in the solid crust has been obtained. Our results show that the crustal moment of inertia reveals a high sensitivity to the transition pressure at the core-crust interface. This may suggest the existence of a strong correlation between the density dependence of the symmetry energy and the crustal moment of inertia. However, no correlation was found. We concluded that constraining the density dependence of the symmetry energy—through, for example, the measurement of the neutron skin thickness in ^{208}Pb—will place no significant bound on either the transition pressure or the crustal moment of inertia.

7. Motivated by recent astrophysical measurements of the pressure of cold matter above nuclear-matter saturation density [11], we computed the equation of state of neutron star matter using accurately calibrated relativistic mean-field models. We showed that although these models are calibrated near the nuclear-matter saturation density, it is possible to tune their high-density behavior in a highly efficient and economical manner with just two parameters. We found the predictions of these models to be in fairly good agreement with the measured equation of state. Yet, it is shown that the mass-vs-radius relations predicted by these same models display radii that are consistently larger than some of the observations.

8. We have introduced a new relativistic effective interaction that is simultaneously constrained by the properties of finite nuclei, their collective excitations, and neutron-star properties. By adjusting two of the empirical parameters of the theory, we have efficiently tuned the neutron skin thickness of ^{208}Pb and the maximum mass of a neutron star. The procedure is illustrated in response to the recent interpretation of X-ray observations by Steiner, Lattimer, and Brown [12] that suggests that the FSUGold effective interaction predicts neutron star radii that are too large and a maximum stellar mass that is too small. The new effective interaction is fitted to a neutron skin thickness in ^{208}Pb of only $R_{\rm n} - R_{\rm p} = 0.16$ fm and a moderately large maximum neutron star mass of 1.94 $M_{\rm Sun}$.

9. The following are the achievements of the new IU-FSU interactions. In addition to the properties of nuclear matter, this relativistic effective interaction reproduces:

   a) The binding energies and charge radii of closed-shell nuclei;

b) Various nuclear giant (monopole and dipole) resonances;

c) The low-density behavior of pure neutron matter;

d) The high-density behavior of symmetric nuclear matter;

e) The mass-radius relation of neutron stars;

g) The consistent limiting mass of a neutron star.

10. Theoretical uncertainties in the predictions of relativistic mean-field models are estimated using a chi-square minimization procedure that is implemented by studying small oscillations around the chi-square minimum. By diagonalizing the matrix of second derivatives, one gains access to a wealth of information—in the form of powerful correlations—that would normally remain hidden. The power of the covariance analysis is illustrated by using two relativistic mean-field models: (a) the original linear Walecka model and (b) the accurately calibrated FSUGold parametrization.

11. In addition to providing meaningful theoretical uncertainties for both model parameters and predicted observables, the covariance analysis establishes robust correlations between physical observables. In particular, we showed that whereas the correlation coefficient between the slope of the symmetry energy and the neutron-skin thickness of Lead is indeed very large, a 1% measurement of the neutron radius of Lead may only be able to constrain the slope of the symmetry energy to about 30%.

APPENDIX A

ANALYTICAL DERIVATION OF THE CRUSTAL MOMENT OF INERTIA

In this appendix we describe the necessary steps used to obtain the expression for the crustal moment of inertia given in Eq. (3.23). Given that the uniform liquid core accounts for most of the stellar mass and that the "fluid" in the crust behave non-relativistically, the following three approximations are assumed valid in the solid crust [3]:

$$M(r) \approx M(R) = M \ , \tag{A.1a}$$

$$P(r) \ll \mathcal{E}(r) \ , \tag{A.1b}$$

$$4\pi r^3 P(r) \ll M(r) = M \ . \tag{A.1c}$$

Under these assumptions the equations for stellar structure simplify considerably. For example, Eq. (3.13) for the metric $\nu(r)$ reduces to

$$\nu(r) = \frac{1}{2}\ln\left(1 - \frac{R_s}{R}\right) - \frac{1}{2}R_s \int_r^R \frac{dx}{x^2 - xR_s} = \frac{1}{2}\ln\left(1 - \frac{R_s}{r}\right) \ , \tag{A.2}$$

where $R_s \equiv 2GM$ is the Schwarzschild radius of the star. Similarly, in the crustal region the TOV-equation [Eq. (3.9)] becomes equal to

$$\frac{dP(r)}{dr} = -\frac{GM\mathcal{E}(r)}{r^2\Big(1 - R_s/r\Big)} = -\frac{R_s\mathcal{E}(r)}{2r^2\Big(1 - R_s/r\Big)} \ . \tag{A.3}$$

If not for the (important) general-relativistic correction $(1 - R_s/r)^{-1}$, this expression would be identical to the equation of hydrostatic equilibrium in the purely Newtonian limit. Finally, the effective frequency $\bar{\omega}$ is approximated by its value at $r = R$. That is,

$$\frac{\bar{\omega}(r)}{\Omega} \approx \frac{\bar{\omega}(R)}{\Omega} = \left[1 - \left(\frac{R_s}{R}\right)\left(\frac{I}{MR^2}\right)\right] \ , \tag{A.4}$$

where we have made use of Eqs. (3.16b) and (3.17).

Using the above simplified expressions valid in the stellar crust, one obtains the following approximation for the crustal moment of inertia [1, 3, 56]:

$$I_{cr} = \frac{8\pi}{3}\left[1-\left(\frac{R_s}{R}\right)\left(\frac{I}{MR^2}\right)\right]\int_{R_t}^{R} r^4 \frac{\mathcal{E}(r)}{1-R_s/r}dr$$
$$= \frac{16\pi}{3R_s}\left[1-\left(\frac{R_s}{R}\right)\left(\frac{I}{MR^2}\right)\right]\int_{0}^{P_t} r^6 dP\ . \tag{A.5}$$

where the last line follows from using the simplified TOV equation [see Eq. (A.3)]. To perform the above integral we need an equation of state to compute the pressure profile $P=P(r)$ in the crust. As suggested in Refs. [1, 56], a polytropic equation of state of index $\gamma=4/3$ will be adopted for the crust. That is,

$$P(\mathcal{E}) = K\mathcal{E}^{\gamma} = K\mathcal{E}^{4/3}\ , \tag{A.6}$$

where K is a constant.

Using such a simple—yet fairly accurate—EOS enables one to solve the TOV equation exactly. To do so, we first introduce the following scaling variables:

$$x \equiv r/R_s\ ; \quad p \equiv P/P_t\ ; \quad \epsilon \equiv \mathcal{E}/\mathcal{E}_t\ , \tag{A.7}$$

where $P_t \equiv P(R_t)$ and $\mathcal{E}_t \equiv \mathcal{E}(R_t)$ are the pressure and energy density at the crust-core interface, with R_t the transition (or core) radius. In terms of these scaling variables, the TOV-equation in the crust [Eq. (A.3)] takes the following simple form:

$$\xi\frac{dp}{dx} = -\frac{p^{1/\gamma}}{x(x-1)}\ , \tag{A.8}$$

where the small parameter $\xi \equiv 2P_t/\mathcal{E}_t$ (of the order of a few percent) has been introduced. The above equation can now be integrated subject to the boundary condition $x=x_t=R_t/R_s$ at $p=1$. We obtain

$$x(p) = \left(1-\left(1-x_t^{-1}\right)\exp\left[-\frac{\xi}{\alpha}\left(p^{\alpha}-1\right)\right]\right)^{-1} \tag{A.9}$$
$$\approx x_t\left[1+(1-x_t)(p^{\alpha}-1)\frac{\xi}{\alpha}+\ldots\right]\ , \tag{A.10}$$

where $\alpha=(\gamma-1)/\gamma=1/4$ and the second line provides an approximation that is correct to first order in ξ. Although the integral appearing in Eq. (A.5) can now be performed

using standard numerical techniques, we prefer to provide an analytic expression for it by expanding the integrand in powers of the small parameter ξ. And although the results presented here are correct only to first-order in ξ, analytic expressions can be developed to arbitrary order. We obtain for an arbitrary power n

$$\int_0^1 x^n(p)dp = x_t^n \left[1 + \frac{n}{1+\alpha}(x_t - 1)\xi + \ldots\right] = x_t^n \left[1 + \frac{4n}{5}(x_t - 1)\xi + \ldots\right] . \tag{A.11}$$

Substituting the above expression into Eq. (A.5) we obtain the following analytic expression for the crustal moment of inertia to first order in $P_t/\mathcal{E}_t$:

$$I_{cr} \approx \frac{16\pi}{3}\frac{R_t^6 P_t}{R_s}\left[1 - \left(\frac{R_s}{R}\right)\left(\frac{I}{MR^2}\right)\right]\left[1 + \frac{48}{5}(R_t/R_s - 1)(P_t/\mathcal{E}_t) + \ldots\right] . \tag{A.12}$$

Taking steps closely analogous to the ones followed for the crustal moment of inertia, the fraction of the stellar mass contained in the solid crust may be written as

$$M_{cr} = 4\pi \int_{R_t}^{R} r^2 \mathcal{E}(r)dr \approx 8\pi R_s^3 P_t \int_0^1 \Big(x^4(p) - x^3(p)\Big)dp . \tag{A.13}$$

The integral can now be easily performed with the aid of Eq. (A.11). We obtain

$$M_{cr} \approx 8\pi R_t^3 P_t (R_t/R_s - 1)\left[1 + \frac{32}{5}(R_t/R_s - 3/4)(P_t/\mathcal{E}_t) + \ldots\right] . \tag{A.14}$$

APPENDIX B

THE ROLE OF THE δ-MESON IN THE ASYMMETRIC NUCLEAR MATTER

B.1 Interacting Lagrangian and the Equation of State

In this Appendix we study the role of the scalar-isovector δ-meson in the RMF theories and its impact on the symmetry energy. The δ-meson contribution in the effective interacting Lagrangian is introduced in a minimal way, through the linear Yukawa coupling to nucleon fields [137, 138]. The non-interacting Lagrangian for such a model is given by

$$\begin{aligned}\mathcal{L}_0 = {} & \bar{\psi}\left(i\gamma^\mu\partial_\mu - M\right)\psi + \frac{1}{2}\partial_\mu\phi\,\partial^\mu\phi - \frac{1}{2}m_{\rm s}^2\phi^2 + \frac{1}{2}\partial_\mu\boldsymbol{\delta}\cdot\partial^\mu\boldsymbol{\delta} - \frac{1}{2}m_\delta^2\boldsymbol{\delta}\cdot\boldsymbol{\delta} \\ & - \frac{1}{4}V^{\mu\nu}V_{\mu\nu} + \frac{1}{2}m_{\rm v}^2V^\mu V_\mu - \frac{1}{4}\mathbf{b}^{\mu\nu}\cdot\mathbf{b}_{\mu\nu} + \frac{1}{2}m_\rho^2\,\mathbf{b}^\mu\cdot\mathbf{b}_\mu - \frac{1}{4}F^{\mu\nu}F_{\mu\nu}\,, \end{aligned} \tag{B.1}$$

where $m_\delta = 980$ MeV. The interacting Lagrangian differs from the one of the FSUGold by an additional Yukawa coupling due to scalar-isovector exchange:

$$\begin{aligned}\mathcal{L}_{\rm int} = {} & \bar{\psi}\left[\left(g_{\rm s}\phi + g_\delta\frac{\boldsymbol{\tau}}{2}\cdot\boldsymbol{\delta}\right) - \left(g_{\rm v}V_\mu + \frac{g_\rho}{2}\boldsymbol{\tau}\cdot\mathbf{b}_\mu + \frac{e}{2}(1+\tau_3)A_\mu\right)\gamma^\mu\right]\psi \\ & - \frac{\kappa}{3!}\left(g_{\rm s}\phi\right)^3 - \frac{\lambda}{4!}\left(g_{\rm s}\phi\right)^4 + \frac{\zeta}{4!}\left(g_{\rm v}^2V_\mu V^\mu\right)^2 + \Lambda_{\rm v}\left(g_{\rm v}^2V_\nu V^\nu\right)\left(g_\rho^2\mathbf{b}_\mu\cdot\mathbf{b}^\mu\right)\,. \end{aligned} \tag{B.2}$$

The equations of motion for meson fields can be easily derived:

$$\left(\partial_\mu\partial^\mu + m_{\rm s}^2\right)\phi = g_{\rm s}\bar{\psi}\psi - \frac{\kappa}{2}g_{\rm s}^3\phi^2 - \frac{\lambda}{6}g_{\rm s}^4\phi^3\,, \tag{B.3a}$$

$$\left(\partial_\mu\partial^\mu + m_\delta^2\right)\boldsymbol{\delta} = g_\delta\bar{\psi}\frac{\boldsymbol{\tau}}{2}\psi\,, \tag{B.3b}$$

$$\partial_\mu V^{\mu\nu} + m_{\rm v}^2V^\nu = g_{\rm v}\bar{\psi}\gamma^\nu\psi - \frac{\zeta}{6}g_{\rm v}^4(V_\mu V^\mu)V^\nu - 2\Lambda_{\rm v}\left(g_\rho^2\mathbf{b}_\mu\cdot\mathbf{b}^\mu\right)g_{\rm v}^2V^\nu\,, \tag{B.3c}$$

$$\partial_\mu\mathbf{b}^{\mu\nu} + m_\rho^2\mathbf{b}^\nu = g_\rho\bar{\psi}\left(\frac{\boldsymbol{\tau}}{2}\gamma^\nu\right)\psi - 2\Lambda_{\rm v}\left(g_{\rm v}^2V_\mu\cdot V^\mu\right)g_\rho^2\mathbf{b}^\nu\,. \tag{B.3d}$$

In the absence of photon field, one can also derive the Dirac equation for the nucleons field:

$$\left[\gamma^{\mu}\left(i\partial_{\mu}-g_{\rm v}V_{\mu}-g_{\rho}\frac{\boldsymbol{\tau}}{2}\cdot\mathbf{b}_{\mu}\right)-\left(M-g_{\rm s}\phi-g_{\delta}\frac{\boldsymbol{\tau}}{2}\cdot\boldsymbol{\delta}\right)\right]\psi=0\,. \tag{B.4}$$

In the mean-field ground state the baryon sources are replaced by their normal ordered expectation values:

$$\bar{\psi}\mathbf{1}\psi\rightarrow\langle:\bar{\psi}\mathbf{1}\psi:\rangle=\rho_{\rm s}=\rho_{\rm s,p}+\rho_{\rm s,n}\ , \tag{B.5a}$$

$$\bar{\psi}\tau_a\psi\rightarrow\langle:\bar{\psi}\tau_a\psi:\rangle=\delta_{a3}\rho_{3,\rm s}=\rho_{\rm s,p}-\rho_{\rm s,n}\ , \tag{B.5b}$$

$$\bar{\psi}\gamma^{\mu}\psi\rightarrow\langle:\bar{\psi}\gamma^{\mu}\psi:\rangle=\delta^{\mu0}\rho_{\rm v}=\delta^{\mu0}\left(\rho_{\rm v,p}+\rho_{\rm v,n}\right)\ , \tag{B.5c}$$

$$\bar{\psi}\gamma^{\mu}\tau_a\psi\rightarrow\langle:\bar{\psi}\gamma^{\mu}\tau_a\psi:\rangle=\delta^{\mu0}\delta_{a3}\rho_{3,\rm v}=\delta^{\mu0}\delta_{a3}\left(\rho_{\rm v,p}-\rho_{\rm v,n}\right)\ . \tag{B.5d}$$

Introducing $\Phi\equiv g_{\rm s}\phi$, $D\equiv g_{\delta}\boldsymbol{\delta}$, $W^{\mu}\equiv g_{\rm v}V^{\mu}$, and $\mathbf{B}^{\mu}\equiv\mathbf{g}_{\rho}\mathbf{b}^{\mu}$ we can rewrite the equations of motion for meson fields:

$$\frac{1}{c_{\rm s}^2}\Phi_0+\frac{\kappa}{2}\Phi_0^2+\frac{\lambda}{6}\Phi_0^3=\rho_{\rm s}\ , \tag{B.6a}$$

$$\frac{1}{c_{\delta}^2}D_0=\frac{\rho_{3,\rm s}}{2}\ , \tag{B.6b}$$

$$\frac{1}{c_{\rm v}^2}W_0+2\Lambda_{\rm v}R_0^2W_0+\frac{\zeta}{6}W_0^3=\rho_{\rm v}\ , \tag{B.6c}$$

$$\frac{1}{c_{\rho}^2}R_0+2\Lambda_v W_0^2R_0=\frac{1}{2}\rho_{3,\rm v}\ . \tag{B.6d}$$

The Dirac equation for protons and neutrons can be written separately:

$$\left[i\gamma^{\mu}\partial_{\mu}-\gamma^0W_0-\frac{1}{2}\gamma^0B_0-\left(M-\Phi_0-\frac{1}{2}D_0\right)\right]\psi_{\rm p}=0\,, \tag{B.7a}$$

$$\left[i\gamma^{\mu}\partial_{\mu}-\gamma^0W_0+\frac{1}{2}\gamma^0B_0-\left(M-\Phi_0+\frac{1}{2}D_0\right)\right]\psi_{\rm n}=0\,. \tag{B.7b}$$

Note that the effective proton and neutron masses are no more the same due to the presence of δ-meson. Following the mean-field technique we can write the energy-momentum tensor in the RMF:

$$\begin{aligned}(T_{\mu\nu})_{\rm RMF}=i\bar{\psi}\gamma_{\mu}\partial_{\nu}\psi-g_{\mu\nu}\Big[&-\frac{1}{2c_{\rm s}^2}\Phi_0^2-\frac{1}{2c_{\delta}^2}D_0^2+\frac{1}{2c_{\rm v}^2}W_0^2+\frac{1}{2c_{\rho}^2}B_0^2-\\&-\frac{\kappa}{6}\Phi_0^3-\frac{\lambda}{24}\Phi_0^4+\frac{\zeta}{24}W_0^4+\Lambda_{\rm v}W_0^2B_0^2\Big]\,.\end{aligned} \tag{B.8}$$

The energy density of the system can be easily derived following standard mean-field calculations:

$$\mathcal{E} = \frac{1}{\pi^2}\int_0^{k_{\rm F}^p} k^2 E_{\rm p}^*\, dk + \frac{1}{\pi^2}\int_0^{k_{\rm F}^n} k^2 E_{\rm n}^*\, dk + W_0\rho_{\rm v} + \frac{1}{2}B_0\rho_{3,\rm v} + U(\Phi_0, D_0, W_0, B_0)\ , \quad \text{(B.9)}$$

where $E_{\rm i}^* = \sqrt{k^2 + M_{\rm i}^{*2}}$, $M_{\rm p}^* = M - \Phi_0 - \frac{1}{2}D_0$, $M_{\rm n}^* = M - \Phi_0 + \frac{1}{2}D_0$, $k_{\rm F}^p(k_{\rm F}^n)$ is the proton (neutron) Fermi momentum, and $U(\Phi_0, D_0, W_0, B_0)$ is given by the following expression:

$$\begin{aligned} U(\Phi_0, D_0, W_0, B_0) = {} & \frac{1}{2c_{\rm s}^2}\Phi_0^2 + \frac{\kappa}{3!}\Phi_0^3 + \frac{\lambda}{4!}\Phi_0^4 + \frac{1}{2c_\delta^2}D_0^2 \\ & - \frac{1}{2c_{\rm v}^2}W_0^2 - \frac{\zeta}{4!}W_0^4 - \frac{1}{2c_\rho^2}B_0^2 - \Lambda_{\rm v}W_0^2B_0^2\ . \end{aligned} \quad \text{(B.10)}$$

Similarly, the pressure of the system can be obtained as:

$$P = \frac{1}{3\pi^2}\int_0^{k_{\rm F}^p} \frac{k^4}{E_{\rm p}^*}\, dk + \frac{1}{3\pi^2}\int_0^{k_{\rm F}^n} \frac{k^4}{E_{\rm n}^*}\, dk - U(\Phi_0, D_0, W_0, B_0)\ , \quad \text{(B.11)}$$

B.2 Derivation of the Symmetry Energy

The symmetry energy is defined from the expansion of the energy per nucleon $E(\rho_{\rm v}, \alpha)$ in terms of the asymmetry parameter, $\alpha = (\rho_{\rm p,v} - \rho_{\rm n,v})/(\rho_{\rm p,v} + \rho_{\rm n,v})$:

$$E(\rho_{\rm v}, \alpha) \equiv \frac{\mathcal{E}(\rho_{\rm v}, \alpha)}{\rho_{\rm v}} = E(\rho_{\rm v}) + S(\rho_{\rm v})\alpha^2 + \mathcal{O}(\alpha^4)\ . \quad \text{(B.12)}$$

For $\alpha = \epsilon \ll 1$, we can write the expression of the symmetry energy as:

$$S(\rho_{\rm v}) = \frac{\mathcal{E}(\rho_{\rm v}, \alpha) - \mathcal{E}(\rho_{\rm v})}{\rho_{\rm v}\alpha^2}\ . \quad \text{(B.13)}$$

From the definition of the asymmetry parameter one can rearrange the proton and the neutron vector densities and Fermi momentums as

$$\rho_{\rm p,v} = \frac{1}{2}\rho_{\rm v}(1-\alpha)\ , \qquad k_{\rm F}^{\rm p} = (1-\alpha)^{1/3}k_{\rm F}\ , \quad \text{(B.14)}$$

$$\rho_{\rm n,v} = \frac{1}{2}\rho_{\rm v}(1+\alpha)\ , \qquad k_{\rm F}^{\rm n} = (1+\alpha)^{1/3}k_{\rm F}\ . \quad \text{(B.15)}$$

Moreover, $\rho_{3,\rm v} = -\alpha\rho_{\rm v}$. Substituting this last expression in the Eqn. (B.6d) we find that in the lowest order in α

$$B_0(\alpha) = \alpha B_0^0 + \mathcal{O}(\alpha^2)\ , \quad \text{(B.16)}$$

where we have assumed $W_0(\alpha) = W_0^0 + \mathcal{O}(\alpha)$. Substituting this result in the Eqn. (B.6c) we find that to the lowest order in α

$$W_0(\alpha) = W_0^0 + \alpha^2 W_0^1 + \mathcal{O}(\alpha^3) \ . \tag{B.17}$$

This result was expected as isoscalars treat protons and neutrons equally. However, isovector fields distinguish the nucleons, and thus result in the asymmetry between them. Therefore, in general, for small α one can expand each field as:

$$\Phi_0 = \Phi_0^0 + \alpha^2 \Phi_0^1 + \mathcal{O}(\alpha^4) \ , \tag{B.18a}$$

$$D_0 = \alpha_0 D_0^0 + \mathcal{O}(\alpha^3) \ , \tag{B.18b}$$

$$W_0 = W_0^0 + \alpha^2 W_0^1 + \mathcal{O}(\alpha^4) \ , \tag{B.18c}$$

$$B_0 = \alpha_0 B_0 + \mathcal{O}(\alpha^3) \ . \tag{B.18d}$$

Now we can calculate each term in the expression of the energy density $\mathcal{E}(\rho_{\rm v}, \alpha)$ for small α using the expansions above. After some tedious but straightforward algebra we arrive at the expression for the symmetry energy

$$S(\rho_{\rm v}) = \frac{k_{\rm F}^2}{6E_{\rm F}^*} + \frac{1}{8}c_\rho^2 \frac{\rho_{\rm v}}{1 + 2\Lambda_{\rm v} c_\rho^2 W_0^2} - \frac{1}{8}c_\delta^2 \frac{\rho_{\rm v} M^{*2}}{E_{\rm F}^{*2}\left[1 + c_\delta^2 A(k_{\rm F}, M^*)\right]} \ , \tag{B.19}$$

where

$$A(k_{\rm F}, M^*) \equiv \frac{1}{2\pi^3}\int_0^{k_{\rm F}} d^3k \frac{k^2}{E^{*3}} = \frac{3}{4}\left(\frac{\rho_{\rm s}}{M^*} - \frac{\rho_{\rm v}}{E_{\rm F}^*}\right) \ , \tag{B.20}$$

$$\rho_{\rm s} = \frac{M^*}{\pi^2}\left[k_{\rm F}E_{\rm F}^* - M^{*2}\ln\left(\frac{k_{\rm F} + E_{\rm F}^*}{M^*}\right)\right] \ , \tag{B.21}$$

and $M^* = M - \Phi_0$, $E_{\rm F}^* = \sqrt{k_{\rm F}^2 + M^{*2}}$.

The expression above shows that the inclusion of the δ-meson reduces the value of the symmetry energy. In order to maintain the value of the symmetry energy at its current experimental value (for example, at $\tilde{J} = 26.0$ MeV), one needs to compensate this reduction by increasing the value of the coupling constant c_ρ^2. At low densities both the scalar and vector interactions play an important role. However at high densities the scalar meson fields saturate, while the sole behavior of the equation of state at high densities are regulated by the vector interactions. Therefore, including δ-meson interaction in a minimal way will stiffen the equation of state at high densities, and thus result in the typical radii of neutron stars that are larger then those that do not incorporate δ-mesons.

REFERENCES

[1] J. M. Lattimer and M. Prakash, *Astrophys. J.* **550**, 426 (2001)

[2] J. M. Lattimer and M. Prakash, *Science* **304**, 536 (2004)

[3] J. M. Lattimer and M. Prakash, *Phys. Rept.* **442**, 109 (2007)

[4] P. Haensel, A. Y. Potekhin, and D. G. Yakovlev, *Neuton Stars 1: Equation of State and Structure*, Springer (2007)

[5] E. Witten, *Phys. Rev. D* **30**, 272 (1984)

[6] E. Fahri and R. L. Jaffe, *Phys. Rev. D* **30**, 2379 (1984)

[7] J. D. Walecka, *Ann. Phys.* **83**, 491 (1974)

[8] J. Boguta and A. R., Bodmer, *Nucl. Phys. A* **292**, 413 (1977)

[9] B. D. Serot, *Phys. Lett. B* **86**, 146 (1979); B. D. Serot, *Phys. Lett. B* **87**, 403 (E) (1979)

[10] B. D. Serot and J. D. Walecka, *Adv. Nucl. Phys.* **16**, 1 (1986)

[11] F. Özel, G. Baym, and T. Güver, *Phys. Rev. D* **82**, 101301, (2010)

[12] A. W. Steiner, J. M. Lattimer, and E. F. Brown, *Astrophys. J.* **722**, 33, (2010)

[13] P. Demorest, T. Pennucci, S. Ransom, M. Roberts, and J. Hessels, *Nature* **467**, 1081 (2010)

[14] G. A. Lalazissis, J. König, and P. Ring, *Phys. Rev. C* **55**, 540 (1997)

[15] B. G. Todd-Rutel and J. Piekarewicz, *Phys. Rev. Lett.* **95**, 122501 (2005)

[16] H. Muller and B. D. Serot, *Nucl. Phys. A* **606**, 508 (1996)

[17] L. Lindblom, *Astrophys. J.* **398**, 569 (1992)

[18] M. Burgay *et al.*, *Nature* **426**, 531 (2003)

[19] A. G. Lyne *et al.*, *Science* **303**, 1153 (2004)

[20] N. K. Glendenning, *Compact Stars*, Springer-Verlag, New York, (2000)

[21] R. C. Tolman, *Physical Review* **55** (4), 364

[22] J. R. Oppenheimer, and G. M. Volkoff, *Physical Review* **55** (4), 374 (1939)

[23] M. H. Johnson and E. Teller, *Physical Review* **98**, 783 (1955)

[24] H. P. Duerr, *Physical Review* **103**, 469 (1956)

[25] R. J. Furnstahl, C. E. Price, and G. E. Walker, *Phys. Rev. C* **36**, 2590 (1987)

[26] R. J. Furnstahl and C. E. Price, *Phys. Rev. C* **40**, 1398 (1989)

[27] Y. K. Gambhir, P. Ring, and A. Thimet, *Ann. Phys.* **198**, 132 (1990)

[28] B. D. Serot, *Rep. Prog. Phys.* **55**, 1855 (1992)

[29] B. D. Serot and J. D. Walecka, *Int. J. Mod. Phys. E* **6**, 515 (1997)

[30] C. J. Horowitz and J. Piekarewicz, *Phys. Rev. Lett.* **86**, 5647 (2001)

[31] J. D. Walecka, *Theoretical Nuclear and Subnuclear Physics*, Second Edition, Imperial College Press, (2000)

[32] F. J. Fattoyev and J. Piekarewicz, *Phys. Rev. C* **82**, 025810 (2010)

[33] B. G. Todd and J. Piekarewicz, *Phys. Rev. C* **67**, 044317 (2003)

[34] S. Weinberg, *Gravitation and Cosmology*, Wiley, New York (1972)

[35] P. Haensel, M. Proszynski, and M. Kutschera, *Astronomy and Astrophysics* **102**, 299 (1981)

[36] P. Möller, J. R. Nix, W. D. Myers, and W. J. Swiatecki, *Atomic Data and Nuclear Data Tables* **59**, 185 (1995)

[37] W. D. Myers and W. D. Swiatecki, *Phys. Rev. C* **57**, 3020 (1998)

[38] D. H. Youngblood, H. L. Clark, and Y. W. Lui, *Physical Review Letters* **82**, 691 (1999)

[39] J. Piekarewicz, *Phys. Rev. C* **69** 041301, (2004)

[40] B.-A. Li, L.W. Chen, and C. M. Ko, *Physics Reports* **464**, 113 (2008)

[41] M. B. Tsang et al., *Physical Review Letters* **102(12)**, 122701 (2009)

[42] H. H. Wolter et al., *Progress in Particle and Nuclear Physics* **62**, 402 (2009)

[43] Z. Xiao, B. A. Li, L. W. Chen, G. C. Yong, and M. Zhang, *Physical Review Letters* **102(6)**, 062502 (2009)

[44] L. W. Chen, *Sci.China G* **52**, 1494 (2009)

[45] A. Hewish, S. J. Bell, J. D. H. Pilkington, P. F. Scott, and R. A. Collins, *Nature* **217**, 709 (1968)

[46] G. Baym, C. Pethick, and P. Sutherland, *Astrophys. J.*, **170**, 299 (1971)

[47] X. Roca-Maza and J. Piekarewicz, *Phys. Rev. C* **78**, 025807 (2008)

[48] J. Piekarewicz, *AIP Conf. Proc.* **1128**, 144, (2009)

[49] D. G. Ravenhall, C. J. Pethick, and J. R. Wilson, *Phys. Rev. Lett.* **50**, 2066 (1983).

[50] M. Hashimoto, H. Seki, and M. Yamada, *Prog. Theor. Phys.* **71**, 320 (1984)

[51] F. Weber *Pulsars as Astrophysical Laboratories for Nuclear and Particle Physics*, Institute of Physics Publishing, Bristol, UK,)1999)

[52] J. B. Hartle, *Astrophys. J.*, **150**, 1005 (1967)

[53] J. B. Hartle and K. S. Thorne, *Astrophys. J.*, **153**, 807 (1968)

[54] L. D. Landau and E. M. Lifshitz, *The Classical Theory of Fields*, Pergamon, Oxford, (1971)

[55] X. Roca-Maza, M. Centelles, X. Vinas, and M. Warda, *Phys. Rev. Lett.* **106**, 252501 (2011)

[56] B. Link, R. I. Epstein, and J. M. Lattimer, *Phys. Rev. Lett.* **83**, 3362 (1999)

[57] J. Xu, L.-W. Chen, B.-A. Li, and H.-R. Ma, *Phys. Rev. C* **79**, 035802 (2009)

[58] J. Xu, L.-W. Chen, B.-A. Li, and H.-R. Ma, *Astrophys. J.* **697**, 1549 (2009)

[59] C. C. Moustakidis, T. Niksic, G. A. Lalazissis, D. Vretenar, and P. Ring, *Phys. Rev. C* **81**, 065803 (2010)

[60] A. Worley, P. G. Krastev, and B.-A. Li, 0801.1653, (2008)

[61] C. P. Lorenz, D. G. Ravenhall, and C. J. Pethick, *Phys. Rev. Lett.* **70**, 379 (1993)

[62] D. G. Ravenhall and C. J. Pethick, *Astrophys. J.* **424**, 846 (1994)

[63] J. Cottam, F. Paerels, and M. Mendez, *Nature* **420**, 51 (2002)

[64] L. Sidoli, A. N. Parmar, T. Oosterbroek, *Astron. Astrophys.* **429**, 291 (2005)

[65] V. Suleimanov, J. Poutanen, M. Revnivtsev, and K. Werner, *arXiv* 1004.4871, (2010)

[66] C. B. Jackson, J. Taruna, S. L. Pouliot, B. W. Ellison, D. D. Lee, J. Piekarewicz, *Eur. J. Phys.* **26**, 695 (2005)

[67] J. M. Lattimer, C. J. Pethick, M. Prakash, P. Haensel, *Phys. Rev. Lett.* **66**, 2701 (1991)

[68] B. Jegerlehner, F. Neubig, and G. Raffelt, *Phys Rev D* **54**, 1194 (1996)

[69] W. Becker (ed), *Neutron Stars and Pulsars*, Springer-Verlag, (2009)

[70] C. J. Horowitz and J. Piekarewicz, *Phys. Rev. C* **66**, 055803 (2002)

[71] P. Slane, D. J. Helfund, and S. S. Murray, arXiv: astro-ph/0204151 (2002)

[72] G. G. Pavlov, O. Y. Kargaltsev, D. Sanwal, and G. P. Garmire, *Astophys. J.* **554**, L189 (2001)

[73] J. P. Halpern and F. Y. H. Wang, *Astrophys. J.* **477**, 905 (1997)

[74] C. J. Horowitz, M. A. Perez-Garcia, and J. Piekarewicz, *Phys. Rev. C* **69**, 045804 (2004)

[75] C. J. Horowitz, M. A. Perez-Garcia, J. Carriere, D. K. Berry, and J. Piekarewicz, *Phys. Rev. C* **70**, 065806 (2004)

[76] C. J. Horowitz, M. A. Perez-Garcia, D. K. Berry, and J. Piekarewicz, *Phys. Rev. C* **72**, 035801 (2005)

[77] J. Carriere, C. J. Horowitz, and J. Piekarewicz, *Astrophys. J.* **593**, 463 (2003)

[78] C. J. Horowitz and J. Piekarewicz, *Phys. Rev. C* **64**, 062802 (2001)

[79] R. A. Hulse and J. H. Taylor, *Astrophys. J.* **195**, L51 (1975)

[80] I. A. Morrison, T. W. Baumgarte, S. L. Shapiro, and V. R. Pandharipande, *Astrophys. J.* **617**, L135 (2004)

[81] J. M. Lattimer and B. F. Schutz, *Astrophys. J.* **629**, 979 (2005)

[82] M. Bejger, T. Bulik, and P. Haensel, *Mon. Not. Roy. Astron. Soc.* **364**, 635 (2005)

[83] G. Lavagetto, I. Bombaci, A. D'Ai', I. Vidana, and N. R. Robba, arXiv:astro-ph/0612061, (2006)

[84] L. Iorio, *New Astron.* **14**, 40 (2008)

[85] C. J. Horowitz, S. J. Pollock, P. A. Souder, and R. Michaels, *Phys. Rev. C* **63**, 025501 (2001)

[86] K. Kumar, R. Michaels, P. A. Souder, and G. M. Urciuoli, URL http://hallaweb.jlab.org/parity/prex (2005)

[87] G. A. Baker, *Phys. Rev. C* **60**, 054311 (1999)

[88] H. Heiselberg, *Phys. Rev. A* **63**, 043606 (2002)

[89] J. Carlson, S.-Y. Chang, V. R. Pandharipande, and K. E. Schmidt, *Phys. Rev. Lett.* **91**, 050401 (2003)

[90] A. Schwenk and C. J. Pethick, *Phys. Rev. Lett.* **95**, 160401 (2005)

[91] Y. Nishida and D. T. Son, *Phys. Rev. Lett.* **97**, 050403 (2006)

[92] S. Gandolfi, A. Y. Illarionov, S. Fantoni, F. Pederiva, and K. E. Schmidt, *Phys. Rev. Lett.* **101**, 132501 (2008)

[93] I. Vidana, C. Providencia, A. Polls, and A. Rios, *Phys. Rev. C* **80**, 045806 (2009)

[94] A. Gezerlis and J. Carlson *Phys. Rev. C* **81**, 025803 (2010)

[95] K. Hebeler and A. Schwenk, *Phys. Rev. C* **82**, 014314 (2010)

[96] J. Piekarewicz, *J. Phys. G* **37**, 064038 (2010)

[97] G. A. Lalazissis, S. Raman, and P. Ring, *At. Data Nucl. Data Tables* **71**, 1 (1999)

[98] P. Danielewicz, R. Lacey, and W. G. Lynch, *Science* **298**, 1592 (2002)

[99] J. Piekarewicz, *Phys. Rev. C* **76**, 064310 (2007).

[100] R. J. Furnstahl, *Nucl. Phys. A* **706**, 85 (2002)

[101] C. Ducoin, J. Margueron, and C. Providencia, *Europhys. Lett.* **91**, 32001 (2010)

[102] V. Suleimanov, A. Y. Potekhin, and K. Werner, *Adv. Space Res.* **45**, 92 (2010)

[103] T. Güver, F. Özel, A. Cabrera-Lavers, and P. Wroblewski, *Astrophys. J.* **712**, 964 (2010)

[104] F. Özel, T. Güver, and D. Psaltis, *Astrophys. J.* **693**, 1775 (2009)

[105] T. Güver, P. Wroblewski, L. Camarota, and F. Özel *Astrophys. J.* **719**, 1807 (2010)

[106] F. J. Fattoyev and J. Piekarewicz, *Phys. Rev. C* **82**, 025805 (2010)

[107] F. J. Fattoyev, C. J. Horowitz, J. Piekarewicz, and G. Shen *Phys. Rev. C* **82**, 055803 (2010)

[108] P. C. C. Freire, *AIP Conf. Proc.* **983**, 459 (2008)

[109] M. B. Tsang et al., *Phys. Rev. Lett.* **92**, 062701 (2004)

[110] D. V. Shetty, S. J. Yennello, and G. A. Souliotis, *Phys. Rev. C* **75**, 034602(2007)

[111] J. Piekarewicz, *Phys. Rev. C* **64**, 024307 (2001)

[112] J. Piekarewicz, *Phys. Rev. C* **66**, 034305 (2002)

[113] G. Colò, N. Van Giai, J. Meyer, K. Bennaceur, and P. Bonche, *Phys. Rev. C* **70**, 024307 (2004)

[114] H. De Vries, C. W. De Jager, and C. De Vries, *Atom. Data Nucl. Data Tabl.* **36**, 495 (1987)

[115] J. Piekarewicz, *Phys. Rev. C* **69**, 041301 (2004)

[116] J. Piekarewicz and M. Centelles, *Phys. Rev. C* **79**, 054311 (2009)

[117] J. Piekarewicz, *Phys. Rev. C* **62**, 051304 (2000)

[118] J. Ritman and *et al.*, *Phys. Rev. Lett.* **70**, 533 (1993)

[119] *Building a universal nuclear energy density functional*, (UNEDF Collaboration), URL http://unedf.org

[120] The Editors, *Phys. Rev. A* **83**, 040001 (2011)

[121] W. Kohn, *Rev. Mod. Phys.* **71**, 1253 (1999)

[122] W. Kohn and L. J. Sham, *Phys. Rev.* **140**, A1133 (1965)

[123] W. Kohn and L. J. Sham, *Phys. Rev.* **140**, A1133 (1965)

[124] J. Piekarewicz, *Phys. Rev. C* **83**, 034319 (2011)

[125] B. Liu, V. Greco, V. Baran, M. Colonna, and M. Di Toro, Phys. Rev. C65, 045201 (2002)

[126] V. Baran, M. Colonna, V. Greco, and M. Di Toro, Phys. Rept. 410, 335 (2005)

[127] C. J. Horowitz and B. D. Serot, *Nucl. Phys. A* **368**, 503 (1981)

[128] R. J. Furnstahl, B. D. Serot, and H.-B. Tang, *Nucl. Phys. A* **615**, 441 (1997)

[129] R. J. Furnstahl, B. D. Serot, and H.-B. Tang, *Nucl. Phys. A* **618**, 446 (1997)

[130] B. Agrawal, *Phys. Rev. C* **81**, 034323 (2010)

[131] R. J. Furnstahl, B. D. Serot, and H.-B. Tang, *Nucl. Phys. A* **598**, 539 (1996)

[132] A. Tamii *et al.*, *Phys. Rev. Lett.* **107**, 062502 (2011)

[133] S. Brandt, *Data Analysis: Statistical and Computational Methods for Scientists and Engineers*, 3rd Ed., Springer, New York, (1999)

[134] J. Piekarewicz, *Phys. Rev. C* **76**, 031301 (2007)

[135] M. Centelles, X. Roca-Maza, X. Vinas, and M. Warda, *Phys. Rev. Lett.* **102**, 122502 (2009)

[136] A. W. Steiner, M. Prakash, J. M. Lattimer, and P. J. Ellis, *Phys. Rept.* **411**, 325 (2005)

[137] B. Liu, V. Greco, V. Baran, M. Colonna, M. Di Toro, *Phys. Rev. C* **65**, 045201 (2002)

[138] V. Greco, M. Colonna, M. Di Toro, F. Matera, *Phys. Rev. C* **67**, 015203 (2003)

BIOGRAPHICAL SKETCH

Farrooh Fattoyev was born on February 11, 1982 in the Sariasiya district, Surkhandarya province of the Republic of Uzbekistan. In 1998, he was admitted to the Physics Department of the Samarkand State University (SamSU), where he received his B.Sc. in Physics with honours (*summa cam laude*). As a winner of the *Al-Beruni State Scholarship* (2001), he was directly admitted to the Department of Theoretical Physics, National University of Uzbekistan, (NUUz) for graduate studies. For his masters thesis he worked on the electrodynamics of compact objects under the guidance of Prof. Bobomurat Ahmedov. He graduated from NUUz in 2004 with a M.Sc. diploma in theoretical physics with honours, for his thesis "Quasi-stationary Electromagnetic Effects in Gravitational Field".

From September of 2004 to October of 2005 he worked at the Institute of Nuclear Physics as a research assistant in the research team engaged in the theoretical studies of general relativity, relativistic astrophysics, and cosmology. From January of 2005 to March of 2005, he visited the Inter-University Center for Astronomy and Astrophysics (IUCAA), Pune, India for scientific collaboration. At IUCAA he worked on String Cosmology with Prof. M. Sami, and on general relativity with Prof. N. Dadhich.

In 2005, he was offered a scholarship by the International Centre for Theoretical Physics (ICTP), Trieste, Italy to continue his studies in the advanced masters program (*Laurea Magistralis*) initiated between the ICTP and the University of Trieste. For this masters thesis, he worked with Prof. Paolo Creminelli on the "Generalized Slow-Roll Approach in Inflation". He successfully completed his advanced master degree in theoretical physics in 2007 from the University of Trieste.

In 2007, he enrolled in the PhD program at the Florida State University. In September of 2008, he joined the Theoretical Nuclear Physics group to work under the supervision of Prof. Jorge Piekarewicz. His research involved the study of the equation of state of nuclear

matter in the relativistic mean-field theories. In Fall 2011, he successfully defended his dissertation titled "Sensitivity of Neutron Star Properties to the Equation of State". His interest is in testing the nuclear equation of state in the extreme region of densities and isospin asymmetries using the existing experimental and observational data. Currently, he has accepted a postdoctoral research associate position at Texas A&M University-Commerce.

Publications

1. **F. J. Fattoyev** and J. Piekarewicz, *Accurate calibration of relativistic mean-field models: correlating observables and providing meaningful theoretical uncertainties*, ***Phys. Rev. C***, (*submitted*)

2. **F. J. Fattoyev**, C. J. Horowitz, J. Piekarewicz and G. Shen, *Relativistic Effective Interaction for Nuclei, Giant Resonances, and Neutron Stars*, ***Phys. Rev. C***, **82**, 055803, 2010.

3. **F. J. Fattoyev** and J. Piekarewicz, *Sensitivity of the Moment of Inertia of Neutron Stars to the Equation of State of Neutron-Rich Matter*, ***Phys. Rev. C***, **82**, 025810, 2010.

4. **F. J. Fattoyev** and J. Piekarewicz, *Relativistic Models of Neutron-star Equation of State*, ***Phys. Rev. C***, **82**, 025805, 2010.

5. B. J. Ahmedov and **F. J. Fattoyev**, *Magnetic Fields of Spherical Compact Stars in Braneworld*, ***Phys. Rev. D***, **78**, Issue 4, 047501, 2008.

6. B. J. Ahmedov and **F. J. Fattoyev**, *Quasi-stationary electromagnetic effects in conductors and super-conductors in Schwarzschild space-time*, ***Int. J. Mod. Phys. D***, V. 14, No 5, 817, 2005.